

EFFECT OF THERMAL RADIATION ON HYBRID NANOFLUID FLOW OVER A CURVED STRETCHING SURFACE

By

FIRZA UMER



NATIONAL UNIVERSITY OF MODERN LANGUAGES

ISLAMABAD

June, 2024

EFFECT OF THERMAL RADIATION ON HYBRID NANOFLUID FLOW OVER A CURVED STRETCHING SURFACE

By

FIRZA UMER

MS Mathematics, National University of Modern Languages Islamabad, 2024

A THESIS SUBMITTED IN PARTIAL FULFILMENT OF
THE REQUIREMENTS FOR THE DEGREE OF

MASTER OF SCIENCE
In Mathematics

To

FACULTY OF ENGINEERING & COMPUTING



NATIONAL UNIVERSITY OF MODERN LANGUAGES ISLAMABAD

© Firza Umer, 2024



THESIS AND DEFENSE APPROVAL FORM

The undersigned certify that they have read the following thesis, examined the defense, are satisfied with overall exam performance, and recommend the thesis to the Faculty of Engineering and Computing for acceptance.

Thesis Title: Effect of Thermal Radiation on Hybrid Nanofluid Flow over a Curved Stretching Surface

Submitted By: Firza Umer

Registration #: 52 MS/Math/S22

Master of Science in Mathematics (MS Math)
Title of the Degree

Mathematics
Name of Discipline

Dr. Anum Naseem
Name of Research Supervisor

Signature of Research Supervisor

Dr. Sadia Riaz
Name of HOD (MATH)

Signature of HOD (MATH)

Dr. Noman Malik
Name of Dean (FEC)

Signature of Dean (FEC)

DATE: 7th June, 2024

AUTHOR'S DECLARATION

I Firza Umer

Daughter of Umer Farooq Azam

Registration # 52 MS/MATH/S22

Discipline Mathematics

Candidate of **Master of Science in Mathematics (MS Math)** at the National University of Modern Languages do hereby declare that the thesis **Effect of Thermal Radiation on Hybrid Nanofluid Flow over a Curved Stretching Surface** submitted by me in partial fulfillment of MS Mathematics degree, is my original work, and has not been submitted or published earlier. I also solemnly declare that it shall not, in future, be submitted by me for obtaining any other degree from this or any other university or institution. I also understand that if evidence of plagiarism is found in my thesis/dissertation at any stage, even after the award of a degree, the work may be cancelled and the degree revoked.

Signature of Candidate

Firza Umer
Name of Candidate

7th June, 2024

Date

ABSTRACT

Title: Effect of Thermal Radiation on Hybrid Nanofluid Flow over a Curved Stretching Surface.

The analysis of heat transfer characteristics of thermally radiative hybrid nanofluids over an exponentially curved surface proves essential for engineering and industrial applications like in polymer processing, materials science, mechanical engineering and aerospace engineering, all of which involve intricate geometry. A number of researchers have delved into the subject of MHD boundary layer flow over a curved stretching surface in light of the expanding technical significance of magnetohydrodynamic (MHD) phenomenon. The current study is based on steady, two dimensional, laminar flow of an electrically conducting, viscous and incompressible fluid flowing over an exponentially curved stretching surface with inclusion of viscous dissipation, thermal radiation and multiple shape factors. The considered hybrid nanofluid is comprised up of two nanoparticles, aluminum oxide and copper, and water is serving as the base fluid. The flow is induced by the curved surface's exponential stretching features. The Darcy Forchheimer effect is utilized to influence the momentum analysis. The governing equations for the hybrid nanofluid flow model are highly complicated coupled system of equations. Mathematical modeling is employed in order to transform the physical system into a set of partial differential equations, which are subsequently simplified as a system of nonlinear ordinary differential equations by employing appropriate similarity variables. The amended non-dimensional momentum and energy equations give the numerical solutions using the bvp4c MATLAB built in solver. The results are displayed in the form of graphs that investigate how different physical parameters influence the velocity profile, temperature profile, local Nusselt number and skin friction coefficient. It is observed that in contrast to magnetic parameter behavior, the velocity profile of a hybrid nanofluid rises with curvature parameter values. Meanwhile, it has been determined that the temperature profile improves for enhancing values of the thermal radiation parameter, Eckert number and the magnetic parameter. The highest thermal conductivity is observed in blade-shaped nanoparticles in most of the cases, whereas brick-shaped nanoparticles have the least.

TABLE OF CONTENTS

CHAPTER	TITLE	PAGE
	AUTHOR'S DECLARATION	ii
	ABSTRACT	iii
	TABLE OF CONTENTS	iv
	LIST OF TABLES	vii
	LIST OF FIGURES	viii
	LIST OF ABBREVIATIONS	x
	LIST OF SYMBOLS	xi
	ACKNOWLEDGEMENT	xiv
	DEDICATION	xv
1	INTRODUCTION	1
	Overview	1
	1.1 Hybrid Nanofluid	1
	1.2 Magnetohydrodynamics	2
	1.3 Thermal Radiation	3
	1.4 Viscous dissipation	4
	1.5 Thesis Organization	5
2	LITERATURE REVIEW	7
	2.1 Hybrid Nanofluid	7
	2.2 Magnetohydrodynamics	8
	2.3 Thermal Radiation	10
	2.4 Viscous Dissipation	11
3	FUNDAMENTAL CONCEPTS AND BASIC LAWS	14
	3.1 Fluid Mechanics	14

3.2	Newtonian and Non Newtonian Fluid	14
3.3	Types of Flow	15
3.3.1	Laminar and Turbulent flow	15
3.3.2	Steady and Unsteady Flow	15
3.3.3	Incompressible and Compressible Flow	16
3.4	Some Thermo-Physical Properties of Fluid	16
3.4.1	Density	16
3.4.2	Pressure	16
3.4.3	Shear Stress	17
3.4.4	Normal Stress	17
3.4.5	Dynamic Viscosity	17
3.4.6	Kinematic Viscosity	18
3.5	Newton Law of Viscosity	18
3.6	Specific Heat	18
3.7	Thermal Conductivity	19
3.8	Thermal Diffusivity	19
3.9	Radiative Heat Flux	19
3.10	Dimensionless Number	20
3.10.1	Prandtl Number	20
3.10.2	Reynolds Number	20
3.10.3	Nusselt Number	20
3.10.4	Skin Friction Coefficient	21
3.10.5	Eckert Number	21
3.11	Some Basic Laws	21
3.11.1	Continuity Equation	21
3.11.2	Momentum Equation	22
3.11.3	Energy Equation	22
3.12	MATLAB bvp4c	23

4	DARCY FORCHHEIMER FLOW OF HYBRID NANOFUID ACROSS A CURVED STRETCHING SURFACE WITH DIFFERENT NANOPARTICLES SHAPE EFFECTS	24
4.1	Mathematical Formulation	25
4.2	Numerical Stratagem	28
4.3	Graphical Analysis and Discuusion	29
5	IMPACT OF MAGNETOHYDRODYNAMIC AND THERMAL RADIATION ON HYBRID NANOFUID OVER CURVE STRETCHABLE SURFACE	39
5.1	Problem Formulation	39
5.2	Numerical Stratagem	44
5.3	Graphical Results and Discuusion	45
6	CONCLUSION AND FUTURE WORK	59
6.1	Conclusion Remarks	59
6.2	Future Work	60
7	REFERNCES	61

LIST OF TABLES

TABLE NO.	TITLE	PAGE
4.1	Thermo physical properties considered nanofluid and hybrid nanofluid	27
4.2	Thermo physical properties of hybrid nanofluid (Al_2O_3 , Cu and H_2O)	27
5.1	Thermo physical properties considered nanofluid and hybrid nanofluid	42
5.2	Thermophysical properties of hybrid nanofluid ($Al_2O_3 - Cu/H_2O$)	42
5.3	Nano particle shape factor	42
5.4	Comparison table of temperature gradient $\theta'(0)$ for different λ when $\phi_1 = 0.05$ and $\phi_2 = 0$.	58

LIST OF FIGURES

FIGURE NO.	TITLE	PAGE
3.1	Applications of Newtonian fluids	14
3.2	Applications of Non Newtonian fluids	15
4.1	Flow configuration model	24
4.2	Influence of curvature parameter (B) on velocity profile $f'(\xi)$	32
4.3	Influence of Forchheimer parameter (Fr) on velocity profile $f'(\xi)$	32
4.4	Influence of porosity parameter (λ) on velocity profile $f'(\xi)$	33
4.5	Influence volume fraction (ϕ_2) on velocity profile $f'(\xi)$	33
4.6	Influence of temperature exponent (A) on temperature profile $\theta(\xi)$	34
4.7	Influence of curvature parameter (B) on temperature profile $\theta(\xi)$	34
4.8	Influence of Forchheimer parameter (Fr) on temperature profile $\theta(\xi)$	35
4.9	Influence of porosity parameter (λ) on temperature profile $\theta(\xi)$	35
4.10	Influence of volume fraction (ϕ_2) on temperature profile $\theta(\xi)$	36
4.11	Influence of Forchheimer parameter (Fr) on Skin friction	36
4.12	Influence of porosity parameter (λ) on Skin friction	37
4.13	Influence of temperature exponent (A) on Nusselt number	37
4.14	Influence of curvature parameter (B) on Nusselt number	38
4.15	Influence of porosity parameter (λ) on Nusselt number	38

5.1	Flow configuration model	41
5.2	Influence of curvature parameter (B) on velocity profile $f'(\xi)$	49
5.3	Influence of Forchheimer parameter (Fr) on velocity profile $f'(\xi)$	49
5.4	Influence of porosity parameter (λ) on velocity profile $f'(\xi)$	50
5.5	Influence of magnetic parameter (M) on velocity profile $f'(\xi)$	50
5.6	Influence of volume fraction (ϕ_2) on velocity profile $f'(\xi)$	51
5.7	Influence of temperature exponent (A) on temperature profile $\theta(\xi)$	51
5.8	Influence of curvature parameter (B) on temperature profile $\theta(\xi)$	52
5.9	Influence of Forchheimer parameter (Fr) on temperature profile $\theta(\xi)$	52
5.10	Influence of porosity parameter (λ) on temperature profile $\theta(\xi)$	53
5.11	Influence of volume fraction (ϕ_2) on temperature profile $\theta(\xi)$	53
5.12	Influence of Eckert number (Ec) on temperature profile $\theta(\xi)$	54
5.13	Influence of magnetic parameter (M) on temperature profile $\theta(\xi)$	54
5.14	Influence of radiation parameter (Rd) on temperature profile $\theta(\xi)$	55
5.15	Influence of Forchheimer parameter (Fr) on Skin friction	55
5.16	Influence of porosity parameter (λ) on Skin friction	56
5.17	Influence of magnetic parameter (M) on Skin friction	56
5.18	Influence of Eckert number (Ec) on Nusselt number	57
5.19	Influence of radiation parameter (Rd) on Nusselt number	57
5.20	Influence of curvature parameter (B) on Nusselt number	58

LIST OF ABBREVIATIONS

Al_2O_3	-	Aluminum oxide
Bvp4c	-	Boundary Value Problem for 4 th Order Collocation
CNT	-	Carbon nanotubes
Cu	-	Copper
C_f	-	Skin Friction Coefficient
FEM	-	Galerkin finite element method
H_2O	-	Water
MWCNTs	-	Multiple wall carbon nanotubes
MHD	-	Magnetohydrodynamics
MCHS	-	Micro channel heat sink
MATLAB	-	Matrix Laboratory
Nu_s	-	Local Nusselt Number
ODEs	-	Ordinary differential equations
PDEs	-	Partial differential equations
PCM	-	Parametric continuation method
PPY	-	Polypyrrole
SWCNTs	-	Single wall carbon nanotubes

LIST OF SYMBOLS

u, v	-	Components of velocity
s, r	-	Curvilinear Coordinates
R^*	-	Radius of curvature
ρ_{hnf}	-	Density of hybrid nanofluid
ϑ_{hnf}	-	Kinematics viscosity of hybrid nanofluid
μ_{hnf}	-	Dynamic viscosity of hybrid nanofluid
α_{hnf}	-	Thermal diffusivity of hybrid nanofluid
k_{hnf}	-	Thermal conductivity of hybrid nanofluid
$(C_p)_{hnf}$	-	Specific heat of hybrid nanofluid
$(\rho C_p)_{hnf}$	-	Heat capacity of hybrid nanofluid
σ_{hnf}	-	Electric conductivity of hybrid nanofluid
ρ_{nf}	-	Density of nanofluid
ϑ_{nf}	-	Kinematics viscosity of nanofluid
μ_{nf}	-	Dynamic viscosity of nanofluid
α_{nf}	-	Thermal diffusivity of nanofluid
k_{nf}	-	Thermal conductivity of nanofluid
$(C_p)_{nf}$	-	Specific heat of nanofluid
$(\rho C_p)_{nf}$	-	Heat capacity of nanofluid
σ_{nf}	-	Electric conductivity of nanofluid
ρ_f	-	Density of base fluid
ϑ_f	-	Kinematics viscosity of base fluid
μ_f	-	Dynamic viscosity of base fluid
α_f	-	Thermal diffusivity of base fluid
k_f	-	Thermal conductivity of base fluid
$(C_p)_f$	-	Specific heat of base fluid
$(\rho C_p)_f$	-	Heat capacity of base fluid
σ_f	-	Electric conductivity of base fluid
P	-	Pressure

\mathcal{F}	-	Non-uniform inertia coefficient
C_b	-	Drag coefficient
A	-	Temperature exponent
q_r	-	Radiative heat flux
B_0	-	Magnetic field strength
T_w	-	Wall Temperatures
T_∞	-	Environmental Temperatures
Fr	-	Forchheimer parameter
λ	-	Porosity parameter
Rd	-	Radiation parameter
K^*	-	Porosity permeability
ϕ_1	-	Volume fraction of 1 st nanoparticle Al_2O_3
ϕ_2	-	Volume fraction of 2 nd nanoparticle Cu
θ	-	Dimensionless temperature
ξ	-	Dimensionless variable
\mathcal{H}	-	Dimensionless pressure
B	-	Dimensionless curvature
M	-	Magnetic parameter
Pr	-	Prandtl number
Ec	-	Eckert number
Re	-	Local Reynolds number
C_f	-	Skin friction coefficient
Nu_s	-	Nusselt number
q_w	-	Heat transfer
τ_{rs}	-	Wall friction

ACKNOWLEDGMENT

I bow my head before Him, who is worth of all praise, The Creator of the universe and offer countless Darood and Salaams to my beloved Holy Prophet Hazrat Muhammad (PBUH), for whom this universe has been manifested. I would like to thank Allah Almighty, whose benediction bestowed upon me talented teachers, provided me sufficient opportunities and enabled me to undertake and execute this research work.

My heartfelt appreciation goes to my affectionate, sincere, kind and most respected supervisor Asst. Prof. Dr. Anum Naseem for so patiently bearing, guiding invaluable suggesting and continuously encouraging me with his precious contributions in completing this thesis. I am grateful for the constructive criticism as well as his encouraging comments.

It is a little sad that I could not spare time for my old parents; though their long lasting prayers have opened new horizons for my success. I pay special thanks and tribute to my beloved parents who loved me a lot and have been taking since my childhood and I cannot pay the reward for such kind and care. The completion of my education was not possible without their prayers and supports. I gratefully acknowledgment the Department of Mathematics, National University of Modern language, Islamabad for providing such wonderful facilities that made my work possible. In the end I would like to thank to all my research fellows and those people who directly and indirectly helped me during my research work.

DEDICATION

This work is a tribute to the two most influential people in my life, my beloved mother and my departed father. I dedicate this to my mother, who was always there for me, even on the tough days. Dad, your belief in the power of education and your unwavering encouragement has been the driving force behind my academic journey. Your sacrifices, both seen and unseen, have allowed me to pursue knowledge and fulfill my educational aspirations. Though you are no longer with us in the physical sense, your spirit and the values you instilled in me are ever present in my heart. This thesis represents not only my hard work and dedication but also a tribute to the unwavering love and guidance that both of you have provided. Your sacrifices and the values you taught in me have paved the way for my academic achievement

CHAPTER 1

INTRODUCTION

Overview

Nature and the technological world both depend on flows for their continued existence. Science's study of the motion of gases and liquids, the way they interact with solids, and the forces behind these phenomena is known as fluid dynamics. Fluid dynamics is imperative to every aspect of our daily lives.

1.1 Hybrid Nanofluid

The terminology ‘nanofluids’ was conceptualized by Choi and Eastman [1]. Nanoparticles with diameters usually varying from 1 to 100 nanometers are dispersed into a host fluid like water, oil or ethylene glycol to form nanofluids. Several processes, including chemical synthesis, precipitation and sol-gel procedures, can be used to create the nanoparticles. Once the nanoparticles have been extracted, they are mixed with the base fluid to form nanofluid using ultra sonication, stirring or other methods. In the same way, a hybrid nanofluid is a specific type of designed liquid mixture that blends a base fluid with nanoparticles and other functional additives. It is essential to suspend two or more different types of nanoparticles which may be metallic, polymeric or non-metallic in the base fluid in order to synthesis a hybrid nanofluid [2]. Numerous researchers have demonstrated through experimental and numerical investigations that the incorporation of nanoparticles can improve heat conduction and heat transfer through convection. As a result, in a variety of applications, hybrid nanofluids often exhibit improved rate of heat

transfer than pure fluids. For manifold reasons, hybrid nanofluids will eventually replace mono nanofluids, including low pressure-drop, lower extinction, high thermal conductivity, reduced frictional losses, wide absorption range and pumping power. In order to better understand the key aspects that affect hybrid nanofluids, various studies have concentrated on investigating rheological and thermo-physical properties. With hybrid nanofluids, numerous applications have been explored, including photovoltaic thermal management, solar collectors, machine cutting, electronic component, photovoltaic thermal applications and automobile cooling. In order to create hybrid nanofluids, different approaches can be utilized. Initially the idea of hybrid nanofluids which have even better increased thermal characteristics than conventional nanofluids was put out by Turcu *et al.* [3]. The study centered on the synthesis and characterization of new hybrid materials comprised of multi-wall carbon nanotubes (MWCNTs). Since hybrid nanofluids were developed, researchers have been investigating the characteristics of hybrid nanofluids. By mixing water with two different types of nanofillers, CNT-*Au* and CNT-*Cu* nanoparticles, Jana *et al.* [4] formed hybrid nanofluids. For the same reason, Al_2O_3 and CuO nanofluid's thermal conductivity raised the temperature range, respectively, from 9.8% to 17.89% for Al_2O_3 and from 15.6% to 24.56% for CuO nanofluids experimentally [5]. Correspondingly Madhesh and Kalaiselvam [6] performed an investigational study that examined the characteristics of a hybrid nanofluid flow used as a cooling agent in a tubular heat exchanger. Using a tubular heat exchanger, Madhesh *et al.* [7] investigated the rheological properties and heat transfer potential of copper-titanium hybrid nanofluids.

1.2 Magnetohydrodynamics (MHD)

The field of magnetohydrodynamics (MHD) studies the motion of electrical conducting fluids including plasmas and liquid metals. Hannes Alfven [8] first presented the fundamental equations of magnetohydrodynamics after realizing the significance of the electric currents carried by plasma and the magnetic field they generate. By incorporating the principles of fluid dynamics with Faraday's and Ampere's laws of electrodynamics, Alfven developed an innovative mathematical framework. It also clarified the physics governing the sun, solar wind and stellar atmospheres. This theory

has proven beneficial in understanding space plasmas within Earth's and other planets' magnetospheres. The electromagnetic force term is added to the fluid's momentum equation to address the fluid dynamical features of MHD. On that account, Ghadikolaei *et al.* [9] focused on the effect of a magnetic field on the stagnation flow of a $TiO_2 - Cu$ /water hybrid nanofluid on a stretching sheet. In the presence of a transverse magnetic field, Das *et al.* [10] examined the MHD flow of aluminum/water nanofluid and copper-aluminum/water hybrid nanofluid across a permeable tube. The lattice Boltzmann technique methodology was used by Ashorynejad and Shahriari [11] to analyze the natural convection heat transport of MHD flow involving hybrid nanofluid (Al_2O_3-Cu /water) in an open wavy cavity. Moreover, Aly and Pop [12] investigated heat transfer in MHD flow of a hybrid nanofluid with suction or injection and convective boundary conditions on a permeable stretching and shrinking sheet. Usman *et al.* [13] intently focused on improving energy and mass transfer in a hybrid nanofluid flow around a rotating disc. They investigated the impacts of SWCNTs and MWCNTs and how these materials are influenced by magnetic and electric fields.

1.3 Thermal Radiation

The term "thermal radiation" signifies electromagnetic radiation which a substance emits as consequence of its heat and the properties of this radiation rely on the medium's temperature. Thermal radiation is produced due to heat from the movement of charges in the substance (electrons and protons in conventional forms of matter) that modifies into electromagnetic radiation [14]. Because it has a direct relation to the thermal state of materials, this phenomenon is known as thermal radiation. The application of thermal radiation can be seen in numerous processes like in cooling appliances, medical imaging and therapy, solar energy harvesting, electronic cooling, aerospace engineering and many others. The infrared radiation produced by an electric heater or typical home radiator is an example of thermal radiation. Due to this cause Mahmoud [15] considered the two-dimensional non Newtonian, time dependent, boundary layer flow on a continuously expanding surface in the existence of thermal radiation and magnetohydrodynamics due to the importance of thermal radiation in many fields. The investigation of the thermally radiative Maxwell nanofluid flow induced by a stretched surface was carried out by Madhu

et al. [16]. The characteristics of the fluid under consideration were examined while taking magnetohydrodynamics and thermal radiation into account. In several fluid flow applications, accurate analysis and design need careful consideration of radiation [17]. The impacts of thermal radiation and Joule heating inside a rotating system comprising two surfaces have been taken into consideration by the researchers as they examined the heat transport and magneto-hydrodynamic flow properties of a hybrid nanofluid [18]. In their research on the phenomenon of mass and heat transfer in three dimensional MHD radiative flow of a hybrid nanofluid (water-based) across an expanding sheet, Sohaib *et al.* [19] took into account the phenomena of heat flow induced by thermal radiation effects. In a study by Zainal *et al.* [20], across a permeable moving surface, the researchers inquired about the flow as well as the heat transfer properties of a hybrid nanofluid ($CuO-Al_2O_3/H_2O$) in the midst of magnetohydrodynamics and thermal radiation.

1.4 Viscous dissipation

Due to internal friction in a moving fluid, a process named viscous dissipation causes mechanical energy to be converted into thermal energy. The impact of viscous dissipation in natural convection was investigated initially by Gebhart [21]. It is a prominent phenomenon in fluid mechanics, especially when there are considerable viscous effects on the flow. Due to viscous forces, a fluid that flows through a channel or across a surface exhibits resistance. There are velocity gradients within the fluid as a result of these forces, which come from interactions between adjacent fluid layers. Because of the work that these viscous forces accomplish, heat gets generated. Higher flow rates and fluids with higher viscosities tend to result in greater viscous dissipation. Many applications like magnetic resonance imaging, food processing, printing processes, polymer processing, heat exchangers and lot more rely on the phenomenon of viscous dissipation. For this reason, Vajravelu and Hadjinicolaou [22] focused on the properties of heat transport in a viscous fluid with a laminar boundary layer through a linearly stretched-out continuous surface with assorted wall temperature in the presence of viscous dissipation and suction/blowing. The combined effects of thermal radiation, convection flow, slip boundary conditions and viscous dissipation induced by a stretched cylinder in a porous media were examined by Pandey and Kumar [23]. The boundary layer flow of hybrid nanofluid across a nonlinear

radially expanding porous disc was investigated by Farooq *et al.* [24] to determine the impacts of suction, injection and viscous dissipation on entropy generation. A research by Swain *et al.* [25] on stretched sheet engulfed in a porous medium, investigated the magnetohydrodynamics (MHD) flow of a Newtonian fluid. Furthermore Mallikarjuna *et al.*'s [26] main objective was to develop a stable mathematical model that would demonstrate the way; a two-phase dusty hybrid nanofluid would behave as it flowed over a stretched sheet in a porous media. Several variables were taken into account in the model, including Darcy-Forchheimer flow, heat transfer, viscous dissipation and the melting heat transfer.

1.5 Thesis Organization

This section provides a brief summary of our six-chapter analysis.

Chapter. 1 serves as an introduction and covers the foundations for several concepts.

In Chapter. 2, an extensive and comprehensive assessment of the literature based on recent research is provided.

Chapter. 3 comprises all the underlying terminology and concepts needed to facilitate an investigation of the recommended work.

Chapter. 4 addresses the hybrid nanofluid's Darcy Forchheimer flow on a curved stretching surface. The flow is driven by stretching the curved surface. Additionally considered the major persuasion of varied shape factors on the process of heat transfer and the flow of fluids. The problem is modeled mathematically as a system of partial differential equations (PDEs) that transform a system of ordinary differential equations (ODEs) using compatible transformations. Bvp4c approach, a numerical method, assists in evaluating the resultant equations. Graphical plots have been utilized to analyze the velocity, temperature, drag force and Nusselt number.

Chapter. 5 reports the MHD and Darcy Forchheimer flow of a hybrid nanofluid driving across a curved surface stretching exponentially. The repercussions of thermal radiation and viscous dissipation are also considered. The whole problem is modeled for different shape factors. With the assistance of the appropriate transformations, the momentum and energy equations translate into ODEs. Then, this model system containing ODEs is solved incorporating the bvp4c approach. The influence of pertinent parameters on velocity,

temperature, skin friction coefficient and Nusselt number has been evaluated by employing a graphical approach.

Chapter. 6 constitutes the findings of the concluded study effort and recommends further projects.

CHAPTER 2

LITERATURE REVIEW

2.1 Hybrid Nanofluid

Several researchers have demonstrated experimentally and numerically that the presence of nanoparticles can enhance thermal conductivity and convective heat transfer, due to which hybrid nanofluids typically have a greater heat transfer rate compared to pure fluids in various applications. Abbas *et al.* [27] addressed the flow of hybrid nanofluid passing over a nonlinear permeable stretched curved surface. Using bvp4c MATLAB, tables and graphs serve for showing the ramifications of relevant physical variables for temperature and velocity profiles. Based upon the findings from the study, in the case of injection, the temperature profile showed falling behavior with improving solid nanoparticle concentration values, whereas in the case of suction, the temperature profile enhances towards greater values of solid nanoparticle concentration. Adopting the Buongiorno model, Mishra and Upreti [28] scrutinized the effects of heat and mass transport of $Fe_3O_4 - CoFe_2O_4$ /water-ethylene glycol hybrid nanofluid and $Ag-MgO$ /water hybrid nanofluid with the effects of heat generation/heat absorption, viscous dissipation and chemical reaction. It has been noticed that when the values of the heat generation/absorption, viscous dissipation and thermophoresis parameters increase, the temperature profiles for both hybrid nanofluids escalate. In experimental investigation from Vinoth *et al.* [29], the heat transfer features of an oblique finned curved micro channel heat sink (MCHS) were investigated, utilizing multiple types of working fluids, specifically deionized water, nanofluid and hybrid nanofluid. The hydrothermal attributes of hybrid nanofluid ($Ag - MgO$) flow over an expanding curved Darcy surface have been studied by Alrabaiah *et al.* [30]. The permeable surface provides the nanofluid flow through the Darcy-Forchheimer effect. The results demonstrated that the temperature decreases but the

velocity curve rises when the curvature component is taken into consideration. The analysis by Mandal and Pal [31] focused on the two dimensional, steady, MHD and Darcy-Forchheimer flow and heat transfer behavior of a non-Newtonian hybrid nanofluid comprised of Go /Kerosene oil and $Go + Ag$ /Kerosene oil passing through the permeable medium on a stretched sheet. The effects of quadratic thermal radiation, Ohmic heating and convective boundary conditions were imposed on heat transfer. Reddy *et al.* [32] contemplated the mass and heat transfer of an unsteady MHD hybrid nanoliquid flow across a shrinking/stretching surface incorporating slip effects, suction effects, chemical reaction and thermal radiation. The finite element method was employed for evaluating the numerical solution. A number of significant parameters' influences on the velocity, concentration and temperature profile of fluids were appraised and the findings were laid out through graphs. The primary objective of Yahaya *et al.* [33] work was to evaluate the stagnation point flow of a $(Cu-Al_2O_3/H_2O)$ hybrid nanofluid over a radially shrinking disk under the presence of magnetic field, viscous-Ohmic dissipation and convective boundary conditions. Using various types of regulating parameters, the flow of hybrid nanofluid and heat transfer characteristics were investigated using the `bvp4c` approach. Along with the impact of viscous dissipation and Joule heating over a porous shrinking sheet, Rasool *et al.* [34] examined the steady MHD flow of $(Cu+Al_2O_3/water)$ hybrid nanofluid. The set of nonlinear ODEs was solved by MATLAB `bvp4c` method numerically. Based on the result, duality exists within a particular range of suction parameters. Lone *et al.* [35] investigated the mixed convective MHD micro polar hybrid nanofluid flow across a flat surface. Additionally, consideration was given to the impact of viscous dissipation, thermal radiation and Joule heating over a vertically positioned plate in a permeable medium together with suction and injection effects.

2.2 Magnetohydrodynamics (MHD)

Keeping in view, the industrial applications of magnetohydrodynamics (MHD), many researchers have contributed towards the research based on MHD. The characteristics of magnetohydrodynamics flow involving viscous fluids were studied by Ullah *et al.* [36]. While contemplating the impacts of viscous dissipation and Joule heating, they investigated the behavior of the fluid flow. Firstly using the shooting method,

nonlinear first-order ODEs were reduced and then a numerical solution was obtained by the RK-4 method. For steady flow and heat transfer, Waini *et al.* [37] evaluated the nonlinearly stretching/shrinking hybrid nanofluid influenced by thermal radiation, MHD and suction. Bvp4c was adopted to solve the governing equations. Dual solutions occurred and the stability study revealed that the first solution was steady. Considering an exponentially expanding porous surface, Nandi *et al.* [38] evaluated the unsteady, MHD, radiative-dissipative and free convective stagnation flow of a hybrid nanofluid through quadratic regression. To stimulate the flow of fluid, copper and alumina nanoparticles were incorporated to the base fluid (water). For a mixed convective 2D flow that consists of (EG (30%) + H₂O (70%), CuO and MgO) hybrid nanofluid flowing across a curve stretched sheet, Sakkaravarthi *et al.* [39] inspected the effects of magnetohydrodynamics, heat generation, thermal radiation, Joule heating and viscous dissipation effects. Heat transfer rates can be improved when hybrid nanofluids were used in MHD flow over a stretched surface with variable viscosity. The investigation focusing on heat transfer characteristics and flow of (Cu – Ti₆Al₄V/H₂O) hybrid nanofluid across a slick surface was conducted by Qureshi [40] with the focus on the shape factor of nanoparticles. The porous media, Cattaneo-Christov, magnetohydrodynamics (MHD), and thermal radiative heat flux were the additionally considered impacts. The Galerkin finite element method (FEM) was implemented to compute the constitutive equations numerically. Patel *et al.* [41] studied the MHD flows induced by a hybrid nanofluid (TiO-Ag/water) sheet, expanding or contracting exponentially due to heat transfer. Dual solutions were found by employing the numerical problem-solving method named as the MATLAB bvp4c tool. Dawar *et al.* [42] considered the flow of magnetically influenced and chemically reactive hybrid nanofluid over a curved surface. Additionally, the influence of the non-Newtonian heating, heat source, thermophoretic, Brownian motion and activation energy were also deliberated. Alqahtani *et al.* [43] assessed a spinning flow of electrically conducting hybrid nanofluid involving silver and gold nanoparticles while the fluid was flowing across two parallel surfaces. The first order set of differential equations were computed by employing a numerical approach referred as the parametric continuation method (PCM). It had been ascertained that the suction factor had an increasing impact on the radial velocity curve. Ouri *et al.* [44] examined the phase change processes and convective heat transmission for a hybrid nanofluid convection system with an L-shaped vented cavity having an inner rotating cylinder and a phase change material-packed bed (PCM-PB) system. An unsteady free convection flow of a hybrid nanofluid through a stretched porous sheet driven to a

uniform magnetic field was investigated in terms of heat transmission analysis by Mathew *et al.* [45]. Based on numerical findings from MATLAB bvp4c, it was noticed that the free convection parameter boosted the fluid temperature and velocity within both the nanofluid and hybrid nanofluid problems. Rafique *et al.* [46] investigated three-dimensional hybrid nanofluid with variable viscosity while flowing over a stretched sheet under the effects of the Smoluchowski temperature and Maxwell velocity slip boundary conditions. On increasing velocity slip parameter, flow rate increased and when the temperature slip parameter was increased, the temperature profile decreased.

2.3 Thermal Radiation

The study of thermal radiation has its own major role in the literature. Abbasi *et al.* [47] performed comparative energy inspection of the stagnation point flow of three type of nanoparticles including titanium aluminum oxide, silicon dioxide nanoparticles and titanium dioxide with the base fluid (ethylene glycol) and the fluid flowed over a curved surface. The model is moreover modified by utilizing the thermal radiation impact. The numerical findings for the Keller box were obtained using the defined set of equations. Considering the significance of thermal radiation study, Alqahtani *et al.* [48] analyzed the friction drag, pressure gradient and heat transfer for the hydromagnetic, thermally radiative and 2D flow of a hybrid nanofluid centered on the viscous dissipation and Joule heating effects while the flow was over a curved surface. It was discovered that raising the radiation parameter and the Hartmann number leads to the decreasing and increasing rate of heat transfer, respectively. Sulochana and Prasanna Kumar [49] investigated boundary layer flow of hybrid nanofluid across a stretched surface having zero mass flux boundary condition. Investigating the effect of thermal radiation and electromagnetohydrodynamic of hybrid nanofluid involving silver and molybdenum disulfide nanoparticles was the major objective. Imran *et al.* [50] addressed the influence of velocity and thermal slip conditions on a hydromagnetic hybrid nanofluid flow across an oscillating stretched curved surface, in addition to thermal radiation impact. For obtaining the analytical solution of the derived flow equations by mean of convergent series solution, the Homotopy analysis technique (HAM) was utilized. In another study, Kho *et al.* [51] investigated the magnetohydrodynamic hybrid nanofluid flow ($Ag - TiO_2/H_2O$) over a permeable wedge.

The study considered the impact of viscous dissipation, thermal radiation and heat dissipation in the analysis. Aminuddin *et al.* [52] examined the hybrid nanofluid (non-Newtonian) flow and heat transfer that incorporates GO, Fe_2O_3 particles and ethylene glycol (EG) as base fluid. The study took into account the magnetic influence and effects of thermal radiation. The significance of the parameters on the temperature profile, velocity profile, the local Nusselt number, measurement of skin friction and the generation of entropy are elucidated and examined. The radially stretchable rotating disk induced incompressible flow of thermally radiative hybrid nanofluid and was investigated computationally by Vijay and Sharma [53] using entropy generation analysis. They also addressed the viscosity dependence on temperature of the hybrid nanofluid, chemical reaction, Joule heating and viscous dissipation effects. The two-dimensional flow of the hybrid nanofluid with thermal radiation and injection/suction effect over two horizontally placed parallel plates was inspected by Farooq *et al.* [54]. The findings showed that the temperature profile increased as the thermal radiation parameter's values were increased. Rashad *et al.* [55] aimed to build a mathematical MHD Eyring-Powell hybrid nanofluid model with mixed convection flow in the presence of heat source and thermal radiation for a porous medium. It has been found that on improving heat generation and thermal radiation, the transfer of heat was augmented. Saupi *et al.* [56] conducted a thorough analysis for the thermal radiation impact on the MHD hybrid copper-alumina nanofluid flow towards a permeable stretched sheet embedded in porous media.

2.4 Viscous Dissipation

To evaluate the impact of higher order chemical reaction parameter on the radiative hybrid nanofluid flow across a shrinking curved sheet including viscous dissipation, Veeram *et al.* [57] accomplished a study. Using the appropriate similarity transformations, governing equations of flow were converted into nonlinear ODEs, and were then solved implementing the built-in MATLAB `bvp4c` solver tool. The major findings of the investigation were that fluid velocity alleviates with the curvature parameter and the Eckert number enhances temperature of the fluid. Alshehri and Shah [58] conducted a computational analysis to demonstrate the effects of the Darcy Forchheimer flow of single nanofluid and hybrid nanofluid over a slick nonlinear, non-uniform stretching surface. In

addition, the heat source/sink, thermal radiation and viscosity dissipation effects were given consideration as well. The effects of radiative flux and Cattaneo-Christov (C-C) heat flow were also reviewed. Taking advantages of the computational MATLAB's bvp4c solver, the shooting approach for nonlinear system was numerically computed. To analyze the relative thermal efficiency of magnetic field flow of nanofluid and hybrid nanofluid synthesized by Cu, Al_2O_3 and water, Khan *et al.* [59] considered viscous dissipation and combined convection over a stretching ($\lambda > 0$) and shrinking ($\lambda < 0$) wedge. The numerical analysis and mathematical representation for the hybrid nanofluid flow past a stretched curved surface with heat source and mixed convection was investigated by Haq *et al.* [60]. For a stretchy surface, velocity slip and convective conditions were implied. Following the analysis, elevating the base fluid's volume fraction enhanced the fluid's speed and temperature. The analysis by Lund *et al.* [61] was based on the 3D stable axisymmetric hybrid nanofluid boundary layer flow made of binary distinct nanoparticles and water as a base liquid with magnetohydrodynamics. The bvp4c MATLAB solver illustrated the effects of an escalating physical parameter on profiles of velocity and temperature with heat transfer rate parallel with skin friction in graphs. A study to investigate the viscous dissipation and thermal radiation effects on the MHD couple stress hybrid nanofluid flow over porous sheets was done by Mahesh *et al.* [62]. Hyper geometric functions were utilized to ascertain the analytical solutions of the modeled problem. Hayat *et al.* [63] discussed hybrid nanofluid ($TiO_2 - Pb$ /water) flowing between two coaxial cylinders with a constant magnetic field. Heat transfer analysis was characterized by viscous dissipation and thermal radiation. Yang *et al.* [64] research's investigated the examination of heat transfer induced by a hybrid nanofluid ($TiO_2 - Al_2O_3/C_2H_6O_2$) with a variety of shape forms namely blade, platelets and cylinder. The findings revealed that the heat rate for blade-shaped titanium oxide-ethylene glycol decomposition was enhanced. For blade structure TiO_2 nanoparticles, the wall shear force was minimized. In the presence of a heat source, magnetohydrodynamics and slip conditions and viscous dissipation, Jamaluddin *et al.* [65] focused on the heat transfer and flow properties of a ($Cu - TiO_2/H_2O$) hybrid nanofluid. Ghazwani [66] analyzed the time-dependent mixed convection flow with the effects of viscous dissipation, radiative heat flux and stagnation point and the fluid flowed by a moving Riga surface. The results of the calculations revealed that both the skin drag force and Nusselt number the declined in response to escalating unstable variable estimations.

The prior deliberate attempts and prominence of Darcy Forchheimer's hybrid nanofluid flow provides an inspiration for the researchers as they continue to investigate the fluid characteristics under different assumptions. To the author best understanding, no research has been conducted on the of Darcy Forchheimer flow of a hybrid nanofluid with various shape variables under the influence of MHD, viscous dissipation and thermal radiation where the flow is stimulated by a curved surface that stretches exponentially. The obtained governing equations are reduced into nonlinear ODEs through similarity transformations, and the `bvp4c` approach is then employed to numerically solve the fluid problem. The same approach is utilized for displaying the velocity and temperature profile graphs. It is anticipated that the current investigation will lead to beneficial outcomes with industrial and technical applications.

CHAPTER 3

FUNDAMENTAL CONCEPTS AND BASIC LAWS

The following chapter describes the explanation of a few fundamental laws, concepts, terminologies and definitions.

3.1 Fluid Mechanics

The discipline of physical sciences known as fluid mechanics examines the behavior of fluids in static or dynamic conditions. It has separated into two branches that explore various fluid properties and the effects of different forces on them [67].

3.2 Newtonian and Non-Newtonian Fluid

Newtonian fluid is a real fluid in which the shear stress and shear strain rate are directly proportional to each other [67].



Figure 3.1: Applications of Newtonian Fluids

A real fluid is a non-Newtonian fluid in which the shear stress and shear strain rate are not directly proportional to each other [67].



Figure 3.2: Applications of Non Newtonian Fluids

3.3 Types of Flow

Fluid flow is characterized as "the motion of a fluid under the direction of unequal forces or stresses, given that the unbalanced force are applied and the motion continues."

3.3.1 Laminar and Turbulent flow

Laminar flow is demonstrated by fluid particles proceeding in a parallel line, but not always with the same velocity along each line. In a turbulent flow, the fluid's particle forces are no longer straight instead they are interfering, sinuous and crossing each other [68].

3.3.2 Steady and Unsteady Flow

Steady flow is the rate of flow at which the fluid's physical characteristics, such as density, velocity and pressure remain constant over time at a specific point. On contrary, an unsteady flow is one whose flow does not change with time [68].

3.3.3 Incompressible and Compressible Flow

Flow is considered to be incompressible if density variations are negligible; otherwise it is referred as compressible. The transport of gases is the most prevalent example of compressible flow, whereas the flow of liquids is generally regarded as incompressible [68]. Mathematically for incompressible flows,

$$\frac{D\rho}{Dt} = 0, \quad (3.1)$$

where ρ donates the fluid density and $\frac{D}{Dt}$ the material derivatives given by

$$\frac{D}{Dt} = \frac{\partial}{\partial t} + \mathbf{V} \cdot \nabla. \quad (3.2)$$

In the previously mentioned equation, \mathbf{V} dominates the flow velocity and ∇ is differential operator. For compressible flows

$$\frac{D\rho}{Dt} \neq 0. \quad (3.3)$$

3.4 Some Thermo-physical Properties of Fluid

3.4.1 Density

Density is expressed as the ratio of mass to one unit of volume. It is symbolized by ρ and mathematically, expressed as

$$\rho = \frac{m}{V}. \quad (3.4)$$

The dimensions and SI unit of density are $[ML^{-3}]$ and kg/m^3 [68].

3.4.2 Pressure

The most dynamic variable in fluid mechanics is pressure (P). The normal force produced by a fluid per unit area is generally referred to as pressure. Mathematically,

$$P = \frac{F}{A}, \quad (3.5)$$

where applied force and area of surface is symbolized by F and A , respectively. The SI unit is kg/s^2m or pascal [68].

3.4.3 Shear Stress

Stress is referred to as "the amount of force per unit area with a body due to shear force. Stress becomes shear stress when a force acts parallel to unit area of the surface. It is symbolized by τ . It is expressed as τ and mathematically defined as

$$\tau = \frac{V}{A}, \quad (3.6)$$

where V and A are shear load and unit area of surface, respectively. The SI unit of stress is N/m^2 [68].

3.4.4 Normal Stress

The normal stress is a force acting normally to a material surface. It is expressed by σ and mathematically defined as

$$\sigma = \frac{P}{A}, \quad (3.7)$$

where P is the axial force and A is the cross-section area and SI unit is N/m^2 [68].

3.4.5 Dynamic Viscosity

The resistance to moving one layer of a fluid over another is known as dynamic viscosity. Mathematically:

$$\mu = \frac{\tau}{\left(\frac{\partial u}{\partial y}\right)}, \quad (3.8)$$

where μ is known as the coefficient of dynamic viscosity, shear stress is labeled as τ and $\left(\frac{\partial u}{\partial y}\right)$ be regarded as the rate of shear deformation. Its SI unit is kg/ms and dimension is $[ML^{-1}T^{-1}]$ [68].

3.4.6 Kinematic Viscosity

Kinematic viscosity is referred to as the viscosity-to-density ratio of a fluid, denoted by Greek letter ν . Thus, mathematically,

$$\nu = \frac{\mu}{\rho}. \quad (3.9)$$

The SI unit of kinematics viscosity is m^2/s and dimension is $[L^2T^{-1}]$ [68].

3.5 Newton Law of Viscosity

Shear stress varies linearly with deformation rate by Newton law of viscosity. Mathematically, it can be represented as

$$\tau \propto \frac{\partial u}{\partial y}, \quad (3.10)$$

$$\tau = \mu \frac{\partial u}{\partial y}, \quad (3.11)$$

where τ is shear stress acting on fluid element and μ is viscosity and $\left(\frac{\partial u}{\partial y}\right)$ is deformation rate. Newtonian fluids are defined as those that follow the previous relation, while non-Newtonian fluids are defined as those that do not [68].

3.6 Specific Heat

It evaluates the thermal energy per unit mass expected to increase the temperature by one degree Celsius. The heat capacity of a material is the product (ρC_p) , which is frequently seen in heat transfer studies. The energy storage potential of a substance can be expressed by the specific heat (C_p) and the heat capacity (ρC_p) . But C_p elucidate it per unit mass, whereas (ρC_p) expresses it per unit volume.”

Mathematically,

$$C_p = \frac{\Delta Q}{\Delta t}, \quad (3.12)$$

where ΔQ is quantity of heat added to increase temperature by ΔT . The SI unit and dimensions of specific heat is $J/kg.K$ and $[M^0L^2T^{-2}L^{-1}]$ [68].

3.7 Thermal Conductivity

The heat transmission rate across a material of a certain thickness having unit surface area per unit temperature difference is thermal conductivity. Mathematically,

$$k = \frac{q\Delta l}{A\Delta T}, \quad (3.13)$$

where q is the heat flow through surface area A causing a temperature difference over a distance of ΔT . The SI unit is W/mK and dimension is $[M^1L^1T^{-3}\theta^{-1}]$ [68].

3.8 Thermal Diffusivity

Thermal diffusivity is ratio of thermal conductivity divided by density and volumetric heat capacity at constant pressure. Mathematically,

$$\alpha = \frac{k}{\rho C_p}, \quad (3.14)$$

where k is thermal conductivity, C_p is specific heat capacity and ρ is density. The SI unit is m^2/s and dimension are $[M^{-2}T^{-1}]$ [68].

3.9 Radiative Heat Flux

In contrast to convection and heat conduction, the radiative heat flow is a flux of electromagnetic radiation and can happen through a vacuum if there is no intervening material. The Stefan-Boltzmann law of radiation governs the rate of heat transfer by radiation emitted:

$$\frac{\partial Q}{\partial t} = \sigma eAT^4, \quad (3.15)$$

where A , T and $\sigma = 5.67 \times 10^{-8} J/s \cdot m^2$ is surface area of the object, surface area of the object the Stefan-Boltzmann constant. The object's emissivity, which is a measurement of the efficiency with which it radiates, is denoted by the sign " e ." The SI unit is W/m^2 [68].

3.10 Dimensionless Number

3.10.1 Prandtl Number

The Prandtl number shed light on how momentum diffusion (ν) (also known as viscous effects) and thermal diffusion (α) (also known as heat conduction) are relative to one another in a fluid. Mathematically,

$$\text{Pr} = \frac{\nu}{\alpha} \Rightarrow \frac{\mu/\rho}{k/C_p} \Rightarrow \frac{\mu C_p}{k}, \quad (3.16)$$

where μ , C_p and k represents dynamic viscosity, specific heat and thermal conductivity [69].

3.10.2 Reynolds Number

The Reynolds number indicates how important inertial forces (influenced by the fluid's density and velocity) are in comparison to viscous forces (which are influenced by the fluid's viscosity). Mathematically,

$$\text{Re} = \frac{UL}{\nu}. \quad (3.17)$$

It aids in identifying the flow regime, whether laminar or turbulent, and analyses the transition between these flows [69].

3.10.3 Nusselt Number

The Nusselt number tells us how much better convective effects affect heat transport than pure conductive effects. It is ratio of conductive heat transfer to convective heat transfer over a boundary layer. Mathematically, it is expressed as:

$$\text{Nu} = \frac{hL}{k}, \quad (3.18)$$

where k , h , L are the thermal conductivity, convective heat transfer coefficient and characteristic length of the fluid respectively [69].

3.10.4 Skin Friction Coefficient

The dimensionless skin friction coefficient is a measurement of the degree of frictional drag that a fluid flow experiences along a solid boundary, like the surface of a body or a wall. Mathematically,

$$C_f = \frac{\tau_w}{\frac{1}{2}\rho U^2}, \quad (3.19)$$

where ρ stands for density, U^2 for surface velocity and τ_w for wall shear stress [69].

3.10.5 Eckert Number

The significance of kinetic energy with convective heat transfer is expressed using the Eckert number. It conveys the kinetic energy ratio to a change in thermal energy. Mathematically,

$$E_c = \frac{u^2}{C_p \Delta T}, \quad (3.20)$$

where fluid flow velocity far from body is u^2 , C_p is specific heat capacity of fluid, ΔT is the temperature difference [69].

3.11 Some Basic Laws

3.11.1 Continuity Equation

The conservation of mass for a fluid flow is given by the continuity equation, which is a fundamental principle of physics [70]. It can be shown mathematically as:

$$\nabla \cdot (\mathbf{V}\rho) + \frac{\partial \rho}{\partial t} = 0. \quad (3.21)$$

For incompressible fluids,

$$(\nabla \cdot \mathbf{V}) = 0, \quad (3.22)$$

where \mathbf{V} is velocity profile and ρ is fluid's density.

3.11.2 Momentum Equation

The momentum equation, which is a fundamental equation in fluid mechanics, determines how momentum is conserved for a fluid flow.

Mathematically,

$$\rho(\mathbf{V} \cdot \nabla)\mathbf{V} = -\nabla p + \mu \nabla^2 \mathbf{V} + \mathbf{b}, \quad (3.23)$$

where \mathbf{V} is velocity profile, p is pressure, \mathbf{b} is body force, ρ is fluid's density and μ viscosity of fluid [70].

3.11.3 Energy Equation

The conservation of energy in a system is described by the energy equation, commonly referred to as the conservation of energy equation [70].

$$(\rho C_p)(\mathbf{V} \cdot \nabla)T = -\nabla \cdot \mathbf{q} + Tr(\boldsymbol{\tau} \cdot \mathbf{L}), \quad (3.24)$$

where

$$\mathbf{q} = -k \text{grad} T. \quad (3.25)$$

The Cauchy stress tensor $\boldsymbol{\tau}$ for incompressible, viscous fluid denoted by

$$\boldsymbol{\tau} = -p\mathbf{I} + \mu \mathbf{A}_1, \quad (3.26)$$

where T , k , \mathbf{q} , \mathbf{L} , \mathbf{A}_1 and \mathbf{I} stands for temperature, thermal conductivity, rate at which heat is generated, rate of strain tensor of fluid, first Rivlin Erickson tensor and identity matrix respectively.

3.12 MATLAB bvp4c

The MATLAB bvp4c function, which stands for "boundary value problem 4th order, is a built-in solver. The bvp4c tool is a three-stage Lobatto IIIa computing approach. It is used to solve boundary value problems (BVPs) for fourth order systems of ordinary differential equations (ODEs). The bvp4c is a versatile approach that can handle a variety of boundary value problems for systems of ODEs. It can solve problems that involve multiple equations, thus being useful for a wide range of technical and scientific applications [71]. To make use of this approach, operators must provide a set of initial estimations that includes the precise value of the border layer thickening parameter ξ_{∞} . Assuming that the boundary conditions are satisfied asymptotically and that the MATLAB program has no errors, the desired outcomes can be generated with the required level of accuracy. The bvp4c utilizes adaptive mesh refinement to develop an appropriate mesh for solving the BVP. Having a lesser requirement for manual mesh specification and adjustment makes bvp4c very beneficial. Like all other programs, bvp4c also has some restrictions. While bvp4c is flexible, it may not be most appropriate for highly nonlinear systems or constantly shifting solutions. Accurate and sufficient initial and boundary conditions are required for the solver to converge and provide meaningful results.

Chapter 4

Darcy Forchheimer Flow of Hybrid Nanofluid across a Curved Stretching Surface with Different Nanoparticles Shape Effects

Hybrid nanofluids are an emerging category of fluids that have appropriate thermal conductivity. This chapter investigates the incompressible, steady, two-dimensional flow of hybrid nanofluid for multiple shape effects across a curved stretched surface. It is assumed that the surface is porous and stretching exponentially. Darcy Forchheimer phenomena have been regarded as an influencing factor in heat transfer. The non-linear coupled differential equations with curvilinear coordinates are represented mathematically as the fluid flow problem. Employing the pertinent similarity transformations, the system of PDEs are transformed into a set of ODEs. The `bvp4c` approach is used to graphically inspect the velocity profile, temperature profile, skin friction coefficient and Nusselt number.

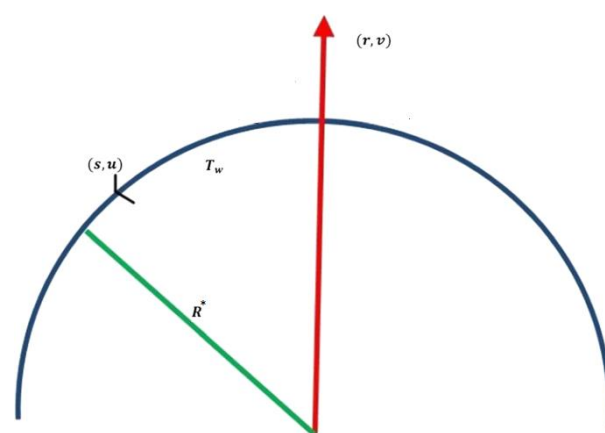

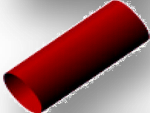
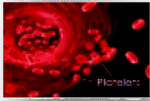
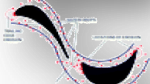


Figure 4.1: Flow Configuration Model

Shape of nanoparticle	Visual representation	Shape factor
Brick		3.7
Cylinder		4.9
Platelet		5.7
Blade		8.6

4.1 Mathematical Formulation

The current model is based on the Darcy Forchheimer flow of a hybrid nanofluid containing aluminum oxide (Al_2O_3) and copper (Cu) with base fluid as water. The flow across a stretching curved surface is assumed to be two dimensional, viscous, incompressible and steady. While the fluid is developing a boundary layer, the surface is stretched along the s -direction having exponential velocity ($u = U_w(s) = a_o e^{\frac{s}{l}}$) where a_o is a constant ($a_o > 0$). The contour of a curved surface is determined by the distance of surface from the origin, R^* . Therefore, for large values of R^* , the surface tends to be flat. Let T_w be surface temperature and is held constant at $T_w(s) = \frac{As}{l}$ where A is a constant, T_∞ being the fluid's ambient temperature, such that $T_\infty < T_w$. The Navier Stokes equations, continuity equations, and energy equation respectively, constitute the governing equations for a steady incompressible flow and are expressed as follows:

$$\nabla \cdot \mathbf{V} = 0, \quad (4.1)$$

$$\rho_{hnf}(\mathbf{V} \cdot \nabla)\mathbf{V} = \nabla \cdot \boldsymbol{\tau} + \mathbf{b}, \quad (4.2)$$

$$(\rho C_p)_{hnf}(\mathbf{V} \cdot \nabla)T = -\nabla \cdot \mathbf{q} + Tr(\boldsymbol{\tau} \cdot \mathbf{L}), \quad (4.3)$$

where

$$\mathbf{q} = -k \text{grad}T. \quad (4.4)$$

In above expressions, density is noted by ρ , velocity field by \mathbf{V} , ρ_{hnf} indicates hybrid nanofluid density, T symbolizes temperature of fluid, \mathbf{q} stands for the heat flux, $\boldsymbol{\tau}$ characterizes Cauchy stress tensor, thermal conductivity is represented by k .

The constitutive equations in curvilinear coordinates have been reduced by employing boundary layer approximation [72].

$$\frac{\partial}{\partial r} [(r + R^*)v] + R^* \frac{\partial u}{\partial s} = 0, \quad (4.5)$$

$$\frac{u^2}{r+R^*} = \frac{1}{\rho_{hnf}} \frac{\partial p}{\partial r^2} \quad (4.6)$$

$$v \frac{\partial u}{\partial r} + \frac{R}{r+R^*} u \frac{\partial u}{\partial s} + \frac{uv}{r+R^*} = -\frac{1}{\rho_{hnf}} \frac{R^*}{r+R^*} \frac{\partial p}{\partial s} + v_{hnf} \left(\frac{\partial^2 u}{\partial r^2} + \frac{1}{r+R^*} \frac{\partial u}{\partial r} - \frac{u}{(r+R^*)^2} \right) - \frac{v_{hnf}}{K^*} u - \mathcal{F}u^2, \quad (4.7)$$

$$v \frac{\partial T}{\partial r} + \frac{R^*}{r+R^*} u \frac{\partial T}{\partial s} = \alpha_{hnf} \left(\frac{\partial^2 T}{\partial r^2} + \frac{1}{r+R^*} \frac{\partial T}{\partial r} \right). \quad (4.8)$$

According to the problem, the corresponding boundary conditions are

$$u = U_w(s) = a_o e^{\frac{s}{l}}, v = 0, T = T_w = T_\infty + T_o e^{\frac{As}{2l}} \text{ when } r = 0, \quad (4.9)$$

$$u \rightarrow 0, \frac{\partial u}{\partial r} \rightarrow 0, T \rightarrow T_\infty \text{ when } r \rightarrow \infty.$$

The velocity components are represented by u and v in the s and r directions, respectively, R^* is denoted by curvature radius, p refers to pressure, ρ_{hnf} denotes for hybrid nanofluid's density, K^* is for porosity permeability and $\mathcal{F} = \frac{C_b}{L\sqrt{K^*}}$ is the uniform inertia coefficient, where C_b is the drag coefficient. The similarity transformation is

$$u = U_w(s) = a_o e^{\frac{s}{l}} f'(\xi), v = \frac{-R^*}{r+R^*} \sqrt{\frac{a_o v_f e^{\frac{s}{l}}}{2L}} (f(\xi) + \xi f'(\xi)), \quad (4.10)$$

$$T = T_\infty + T_o e^{\frac{As}{2l}} \theta(\xi), \quad \xi = r \sqrt{\frac{e^{\frac{s}{l}} a_o}{2v_f L}}, \quad p = \rho_f a_o^2 e^{\frac{2s}{l}} \mathcal{H}(\xi).$$

For the continuity equation, Eq. (4.5) is instantly valid. The nonlinear PDEs in Eqs. (4.6) to (4.8) along with Eq. (4.9) which are the boundary conditions are subjected to Eq. (4.10), the similarity transformation. As a result, following ODEs have transformed as:

$$\frac{1}{\omega_1} \mathcal{H}'(\xi) = \frac{1}{\xi+B} f'^2, \quad (4.11)$$

$$\frac{1}{\omega_2} \left(f'''' + \frac{1}{\xi+B} f''' - \frac{1}{(\xi+B)^2} f'' - 2\lambda f'^2 \right) - \frac{\xi+2B}{(\xi+B)^2} B(f'^2) + \frac{B}{(\xi+B)^2} f f' \quad (4.12)$$

$$+ \frac{B}{\xi+B} f f'' - 2Fr f'^2 = \left(\frac{1}{\omega_1} \right) \frac{B}{\xi+B} (4\mathcal{H} + \xi \mathcal{H}'),$$

$$\frac{1}{Pr} \left(\frac{1}{\omega_3} \right) \frac{k_{hnf}}{k_{bf}} \left(\theta'' + \frac{1}{\xi+B} \theta' \right) + \frac{B}{\xi+B} (f\theta' - Af'\theta) = 0, \quad (4.13)$$

where

$$\omega_1 = \frac{\rho_{hnf}}{\rho_f} = (1 - \phi_2) \left[(1 - \phi_1) + \phi_1 \frac{\rho_{s1}}{\rho_f} \right] + \phi_2 \frac{\rho_{s2}}{\rho_f}, \quad (4.14)$$

$$\omega_2 = \frac{v_f}{v_{hnf}} = (1 - \phi_1)^{2.5} (1 - \phi_2)^{2.5} \left[(1 - \phi_1)(1 - \phi_2) + \phi_1 \frac{\rho_{s1}}{\rho_f} \right] + \phi_2 \frac{\rho_{s2}}{\rho_f}, \quad (4.15)$$

$$\omega_3 = \frac{(\rho C_p)_{hnf}}{(\rho C_p)_f} = (1 - \phi_2) \left[(1 - \phi_1) + \phi_1 \frac{(\rho C_p)_{s1}}{(\rho C_p)_f} \right] + \phi_2 \frac{(\rho C_p)_{s2}}{(\rho C_p)_f}. \quad (4.16)$$

Pressure can be calculated employing Eq. (4.12), as follows:

$$\frac{\omega_1(\xi+B)}{4B} \left[\frac{1}{\omega_2} \left(f'''' + \frac{1}{\xi+B} f'''' + \frac{1}{(\xi+B)^2} f'' - 2\lambda f'^2 \right) - \frac{\xi+2B}{(\xi+B)^2} B(f'^2) + \frac{B}{(\xi+B)^2} f f' + \frac{B}{\xi+B} f f'' - 2Fr f'^2 \right] = \mathcal{H}(\xi). \quad (4.17)$$

Table 4.1: Thermo physical properties considered nanofluid and hybrid nanofluid [73].

Properties	Nanofluid	Hybrid Nanofluid
Density	$\rho_{nf} = (1 - \phi) + \phi\rho_s$	$\rho_{hnf} = (1 - \phi_2)[(1 - \phi_1)\rho_{bf} + \phi_1\rho_{s1}] + \phi_2\rho_{s2}$
Heat capacity	$(\rho C_p)_{nf} = (1 - \phi)(\rho C_p)_f + \phi(\rho C_p)_s$	$(\rho C_p)_{hnf} = (1 - \phi_2)[(1 - \phi_1)(C_p\rho)_f + \phi_1(\rho C_p)_{s1}] + \phi_2(\rho C_p)_{s2}$
Viscosity	$\mu_{nf} = \frac{\mu_f}{(1-\phi)^{2.5}}$	$\mu_{hnf} = \frac{\mu_f}{(1-\phi_1)^{2.5}(1-\phi_2)^{2.5}}$
Thermal Conductivity	$\frac{k_{nf}}{k_f} = \frac{k_s+(n-1)k_f-(n-1)\phi(k_f-k_s)}{k_s+(n-1)k_f+\phi(k_f-k_s)}$	$\frac{k_{hnf}}{k_{bf}} = \frac{k_{s2}+(n-1)k_{bf}-(n-1)(k_{bf}-k_{s2})\phi_2}{k_{s2}+(n-1)k_{bf}+\phi_2(k_{bf}-k_{s2})}$ where $\frac{k_{bf}}{k_f} = \frac{k_{s1}+(n-1)k_f-(n-1)(k_f-k_{s1})\phi_1}{k_{s1}+(n-1)k_f+\phi_1(k_f-k_{s1})}$

Table 4.2: Thermo physical properties of hybrid nanofluid (Al_2O_3 , Cu and H_2O)[74].

Properties	Water	Al_2O_3	Cu
ρ (kg/m^3)	997.0	3970	8933
C_p (J/KgK)	4180	765	385
k (W/mK)	0.6071	40	400
Pr	6.2	-	-

By computing the derivative of Eq. (4.12) w.r.t. ξ and utilizing Eq. (4.11), we may remove pressure from Eq. (4.12) and get,

$$\frac{1}{\omega_2} \left(f'''' + \frac{2}{\xi+B} f'''' - \frac{1}{(\xi+B)^2} f'' + \frac{1}{(\xi+B)^3} f' - 2\lambda \left(f'' + \frac{1}{\xi+B} f' \right) \right) - \frac{B}{(\xi+B)^2} f f'' + \frac{B}{\xi+B} f f'' - \frac{B}{(\xi+B)^3} f f' - \frac{3B}{(\xi+B)^2} f'^2 - \frac{3B}{\xi+B} f' f'' - 2Fr(2f' f'' + \frac{1}{\xi+B} f'^2) = 0. \quad (4.18)$$

The boundary conditions after utilizing transformations are

$$\begin{aligned} f = 0, f' = 1, \theta = 1 \text{ at } \xi = 0, \\ f' \rightarrow 0, f'' \rightarrow 0, \theta \rightarrow 0 \text{ when } \xi \rightarrow \infty. \end{aligned} \quad (4.19)$$

In the relationship discussed above, Pr , λ , Fr and B refers to the Prandtl number, porosity parameter, Forchheimer constant and curvature parameter. The dimensionless quantities include the variables mentioned as

$$Pr = \frac{\nu_f}{\alpha_f}, \quad \lambda = \frac{\nu_f L}{BU_w}, \quad Fr = \frac{C_b}{\sqrt{B}}, \quad B = \left(\frac{a_0 e^{s/l}}{2\nu_f L} \right)^{\frac{1}{2}} R^*. \quad (4.20)$$

The physical quantity that relates the friction drag and role of heat transfer is the skin friction coefficient C_f and local Nusselt number Nu_s .

$$C_f = \frac{\tau_{rs}}{\rho_{hnf} U_w^2}, \quad Nu_s = \frac{Sq_w}{k_{hnf} (T_w - T_\infty)}. \quad (4.21)$$

The heat transfer q_w and wall friction τ_{rs} [75] along s direction is defined as:

$$q_w = -k_{hnf} \left(\frac{\partial T}{\partial r} \right) + q_r \Big|_{r=0}, \quad (4.22)$$

$$\tau_{rs} = \mu \left(\frac{\partial u}{\partial r} - \frac{u}{r+R^*} \right) \Big|_{r=0}, \quad (4.23)$$

utilizing the terms defined in Eq. (4.22) and Eq. (4.23) in Eq. (4.21).

$$C_f (Re)^{\frac{1}{2}} = \frac{1}{(1-\phi_1)^{2.5} (1-\phi_2)^{2.5}} \left(f''(0) - \frac{1}{B} f'(0) \right), \quad (4.24)$$

$$Nu_s (Re)^{-\frac{1}{2}} = -\frac{k_{hnf}}{k_f} \left(1 + Rd \frac{k_f}{k_{hnf}} \right) \theta'(0), \quad (4.25)$$

where local Reynolds number is represented by $Re_s = \frac{a_0 s^2}{\nu_f}$.

4.2 Numerical Stratagem

Making use of `bvp4c` package in MATLAB software, the governing flow equations (ODEs) are sorted out. As a norm the acquired equations are higher order differential equations (DE). The primary phase involves the reduction of these higher order differential equations into first-order differential equations. Then to work out on these arising first-order differential equations `bvp4c` is implemented.

$$f_1 = f, \quad (4.26)$$

$$f_2 = f_1' = f', \quad (4.27)$$

$$f_3 = f_2' = f'', \quad (4.28)$$

$$f_4 = f_3' = f''', \quad (4.29)$$

$$f_5 = f_4' = \left(-\frac{2}{\xi+B} f'''' + \frac{1}{(\xi+B)^2} f'''' - \frac{1}{(\xi+B)^3} f'' + 2\lambda(f'' + \frac{1}{\xi+B} f') \right) + \omega_2 \left[\begin{array}{l} \frac{B}{(\xi+B)^2} f f'' - \frac{B}{\xi+B} f f'''' + \frac{B}{(\xi+B)^3} f f' + \frac{3B}{(\xi+B)^2} f'^2 + \frac{3B}{\xi+B} f' f'' \\ + 2Fr(2f' f'' + \frac{1}{\xi+B} f'^2) \end{array} \right], \quad (4.30)$$

$$f_6 = \theta, \quad (4.31)$$

$$f_7 = f_6' = \theta', \quad (4.32)$$

$$f_8 = f_7' = -\left(\frac{1}{\xi+B} \theta' \right) - Pr \omega_3 \frac{k_{bf}}{k_{hnf}} \frac{B}{\xi+B} (f\theta' - Af'\theta), \quad (4.33)$$

with boundary conditions

$$f_a(1) = 0, f_a(2) = 1, f_a(6) = 1, f_b(2) \rightarrow 0, f_b(3) \rightarrow 0, f_b(6) \rightarrow 0. \quad (4.34)$$

4.3 Graphical Analysis and Discussion

Concerning different parameters, the graphical findings for velocity, temperature, drag force and Nusselt number are attended to in this portion of the chapter. With the aid of a hybrid nanofluid applied to a surface that is curved, the influence of multiple range of spherical nanoparticle shape is observed. The essential flow characteristics in the r and s directions together with the heat transfer are obtained numerically. Graphical plots are developed for spherical nanoparticles featuring different shape variables including bricks, cylinder, platelets and blades. A comparison of spherical nanoparticles for various shape factors is one of the key area of concentration in the study. The variation in velocity profile $f'(\xi)$ for particular values of B , Fr , λ and ϕ_2 over stretchable surface are illustrated in Figure 4.2 to Figure 4.5. Figure 4.2 depicts the influence of the curvature parameter (B) on the velocity profile $f'(\xi)$. It shows that when the curvature parameter increases, the fluid flow improves correspondingly. Physically, the curve surface facilitates in the fluid

movement overhead. As the value of B rises, radius of the curved surface decreases which reduces the area of contact between the solid surface and fluid. Thus the fluid flow improves correspondingly. Figure 4.3 illustrates the Forchheimer parameter (Fr) impact on $f'(\xi)$. This phenomenon takes place due to the inertial effect that drags the fluid backward. Due to this inertial force, the fluid's speed decreases, leading to a decline in the velocity profile. Any modification to the fluid's characteristics on the stretched surface assists in decreasing the fluid's flow. Turning attention to this figure additionally reveals that for certain variables relative to others, the velocity decline is considerably more apparent. Figure 4.4 exhibits that the velocity reduces when the local porosity parameter (λ) escalates. This is generally due to the local porosity field that increases fluid flow resistance. From this figure, it is assumed that $f'(\xi)$ declines in prominently for shape factors. Figure 4.5 illustrated graphically the impact of volumetric fraction ϕ_2 on velocity when different shapes factors are observed. The velocity curve displays a decline in behavior as the value of ϕ_2 increases. The subject of stretching channels emphasizes the effect of A , Fr , ϕ_2 , B and λ for temperature profile which is clearly demonstrated in Figure 4.6 to Figure 4.10. Moreover each graph illuminates four distinct shape factors. Figure 4.6 investigates the impact of temperature exponent (A) on $\theta(\xi)$. As illustrated in the figure, the increase in A on the stretching surface leads the fluid to decelerate, resulting in the reduction of the temperature profile. Figure 4.7 shows the impact of the curvature parameter (B) on temperature profile $\theta(\xi)$. The fluid is decelerated by the curvature parameter which diminishes the temperature profile. As curvature parameter B increases, the fluid's temperature falls. As B increases, the stretching surface becomes more flat. Increasing the flatness of the stretching surface leads to increase in flow velocity and lowers temperature profile due to reduced resistance between fluid layers. This behavior is observed for different shape effects of the nanoparticles. The blade shaped nanoparticles shows increasing behavior in temperature profile as compared to cylinder, platelets and bricks shaped nanoparticles as shown in Figure 4.6 and Figure 4.7. Figure 4.8 shows the Forchheimer parameter (Fr) influence on temperature profile $\theta(\xi)$. The aforementioned results indicate that when Fr raises, the temperature rises simultaneously. The greater conduction causes raised temperature and conduction effects are greatly related to values of Fr . Similarly, blade shaped nanoparticles have the greatest temperature while bricks shaped nanoparticles develop the temperature distribution at the lowest. Figure 4.9 represent the impacts of local porosity parameter (λ) on temperature distribution $\theta(\xi)$.

When the surface temperature exceeds the ambient temperature, a greater amount of heat from the surrounding air travels towards the fluid, thus expanding the thickness of the thermal boundary layer and the temperature as a consequence trends to enhance. Figure 4.10 illustrates the manner in which volumetric fractions (ϕ_2) impacts the temperature. It is to be noted that the thickness of thermal layers and temperature rise by rising the values of ϕ_2 . This is because ϕ_2 slows fluid movement, which indirectly raises temperature. Equally noteworthy is that the brick-shaped nanoparticles preserve lower temperature than the blade-shaped hybrid nanofluid nanoparticles, which exhibit higher temperature.

The study of friction drag is needed in many industrial purposes. Stretching channels induce the C_f to move rapidly over the surface. Figure 4.11 and Figure 4.12 highlights the specified patterns for skin friction. Figure 4.11 is drawn to understand the effect of Fr and ϕ_2 on the friction drag and it represents the decreasing manner in which Forchheimer parameter (Fr) affects skin friction coefficients. Similar decreasing behavior is experienced for ϕ_2 . With raising porosity parameter (λ), a reverse relation is shown in Figure 4.12 for skin friction which is plotted for the influence of λ and ϕ_2 . In Figure 4.13–4.15, the effects of distinct factor values on the local Nusselt number Nu_s are evaluated as functions of various considered parameters. The increasing values of ϕ_2 are labeled along the horizontal axis. Figure 4.13 is displayed to observe the Nusselt number for influencing values of temperature exponent (A) along with ϕ_2 . Nusselt number may be demonstrated to be decreasing with expanding values of A and an improvement was observed with ϕ_2 . Furthermore, the rate of heat transfer for blade shaped nanoparticles seemed to be highest. The effect of curvature parameter B and nanoparticle volume fraction ϕ_2 on the Nusselt number is illustrated through Figure 4.14. The curvature parameter and the volume fraction presents opposite trend for Nusselt number. Figure 4.15 represents the varied values of porosity parameter (λ) and depicts decreasing behavior with rising λ but shows elevated trend for ϕ_2 . Recurrently, it has been verified that blade shaped nanoparticles can transmit heat far better than nanoparticles composed of platelets, cylinders or bricks.

Table 4.1 and Table 4.2 are displayed for the thermo-physical characteristics of the nanofluids and hybrid nanofluids. The data shown in these tables are used to perform the analysis for the considered fluid model.

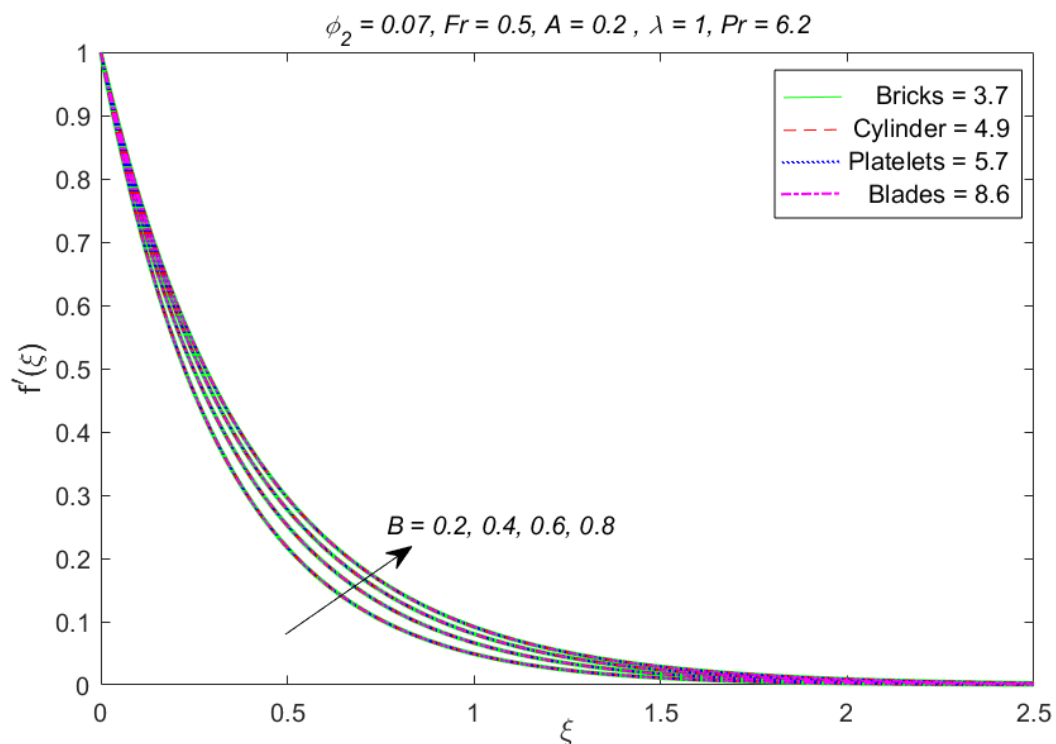


Figure 4.2: Influence of curvature parameter (B) on velocity profile $f'(\xi)$.

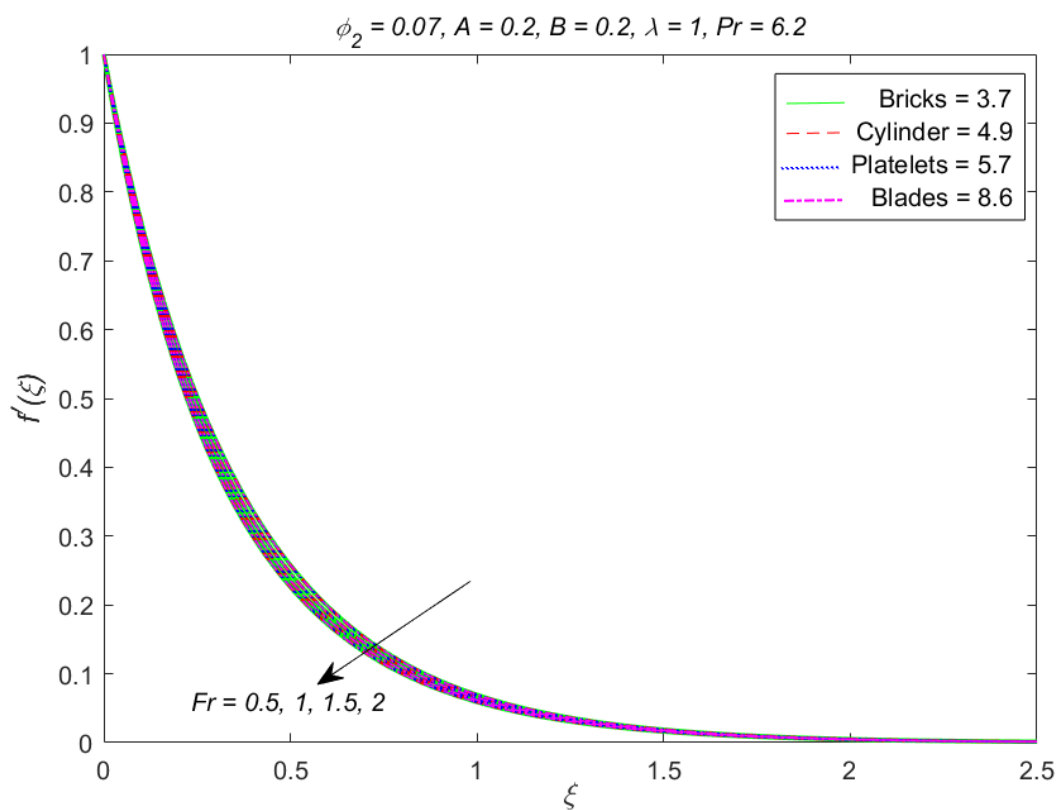


Figure 4.3: Influence of Forchheimer parameter (Fr) on velocity profile $f'(\xi)$.

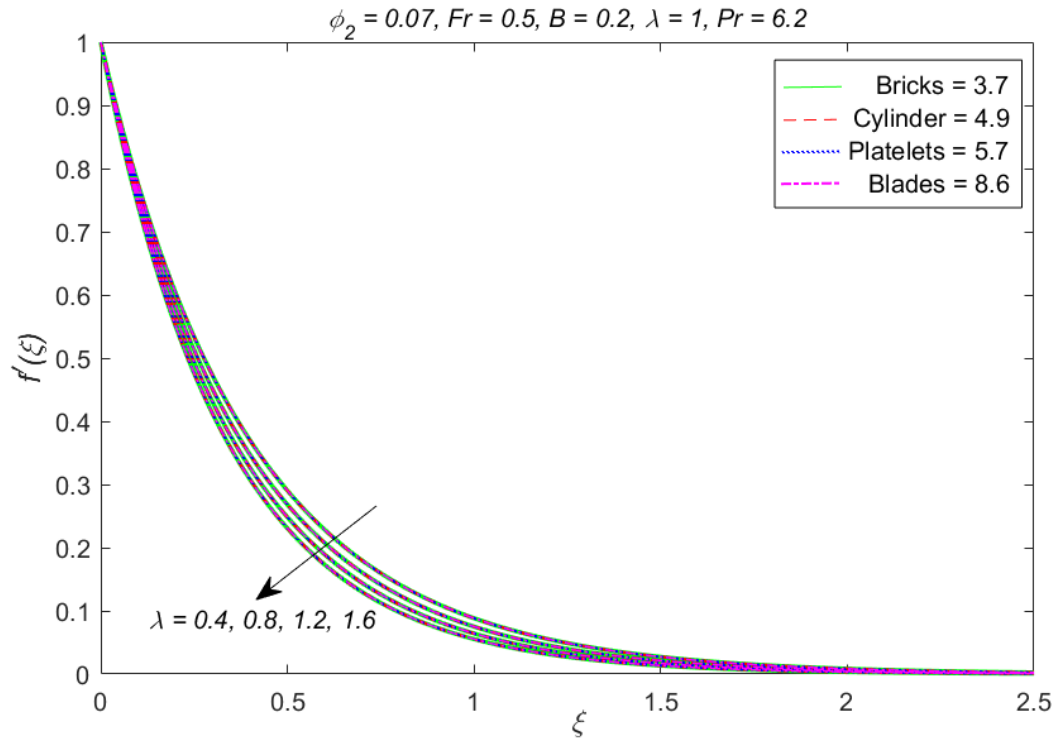


Figure 4.4: Influence of porosity parameter (λ) on velocity profile $f'(\xi)$.

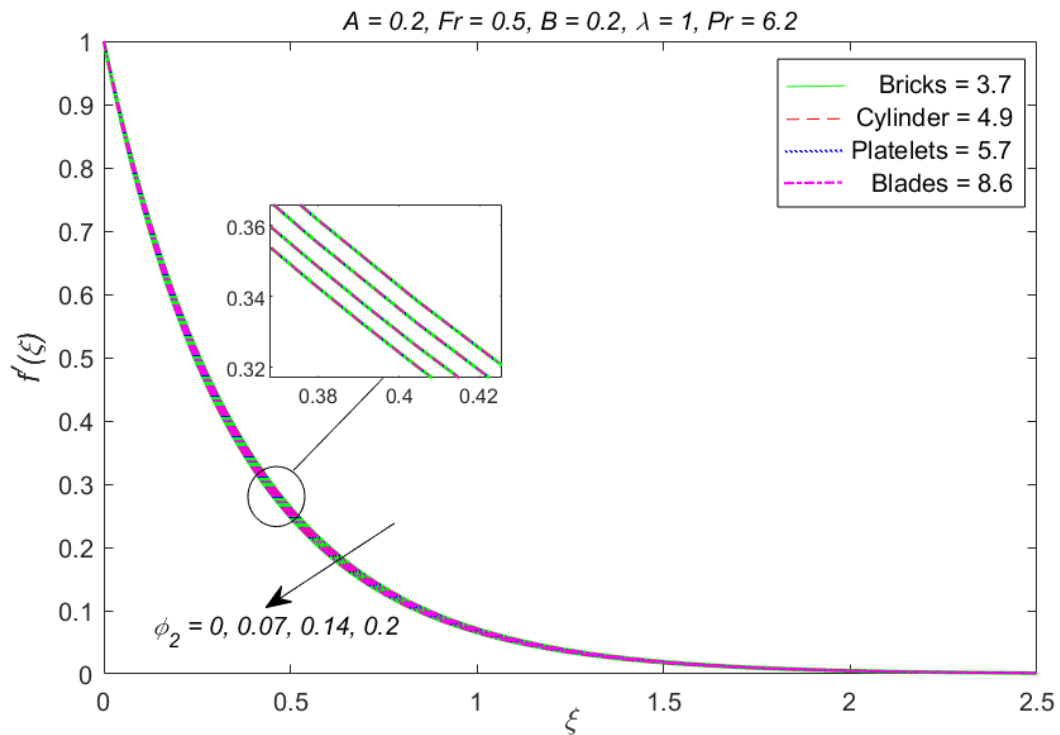


Figure 4.5: Influence of volume fraction (ϕ_2) on velocity profile $f'(\xi)$.

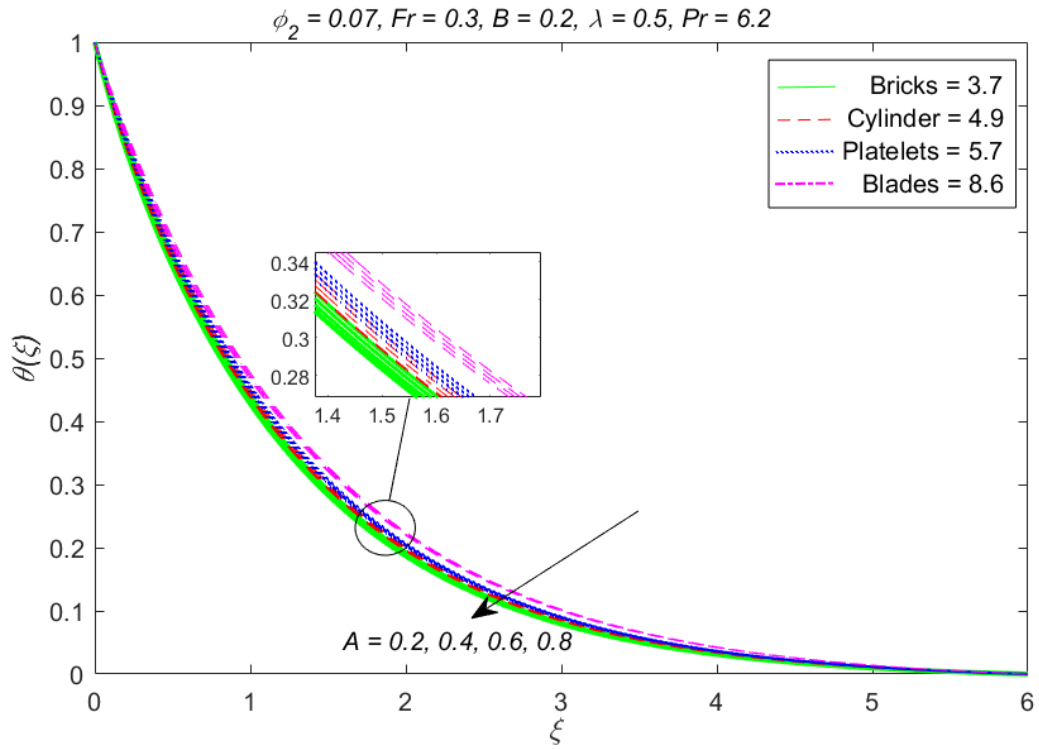


Figure 4.6: Influence of temperature exponent (A) on temperature profile $\theta(\xi)$.

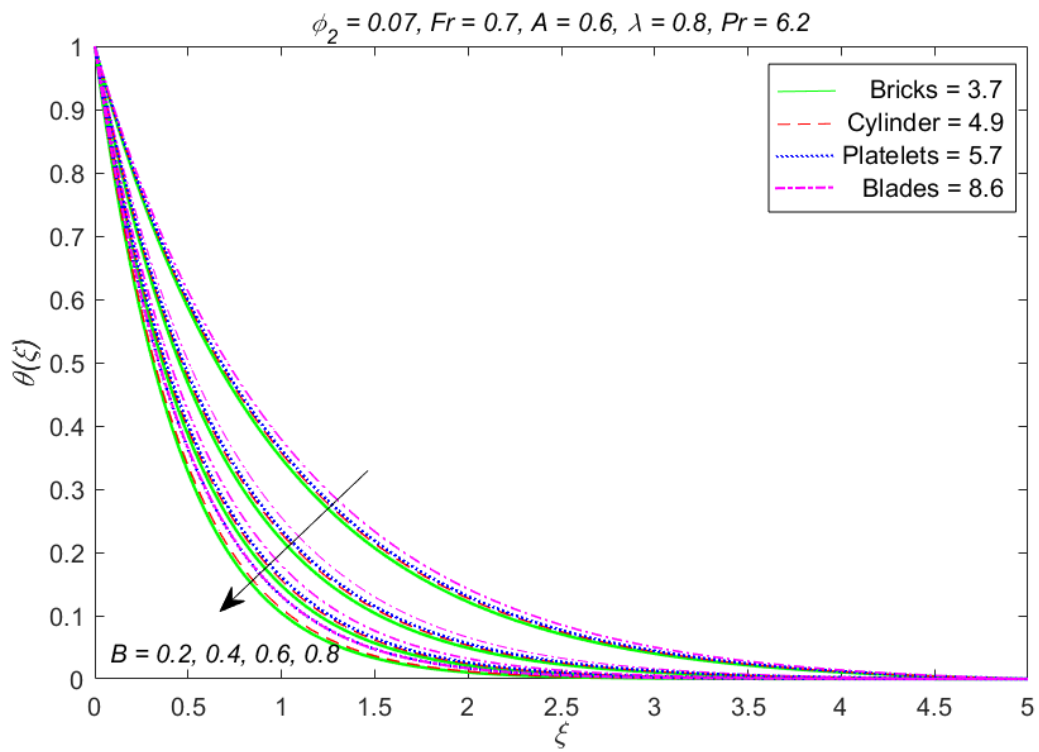


Figure 4.7: Influence of curvature parameter (B) on temperature profile $\theta(\xi)$.

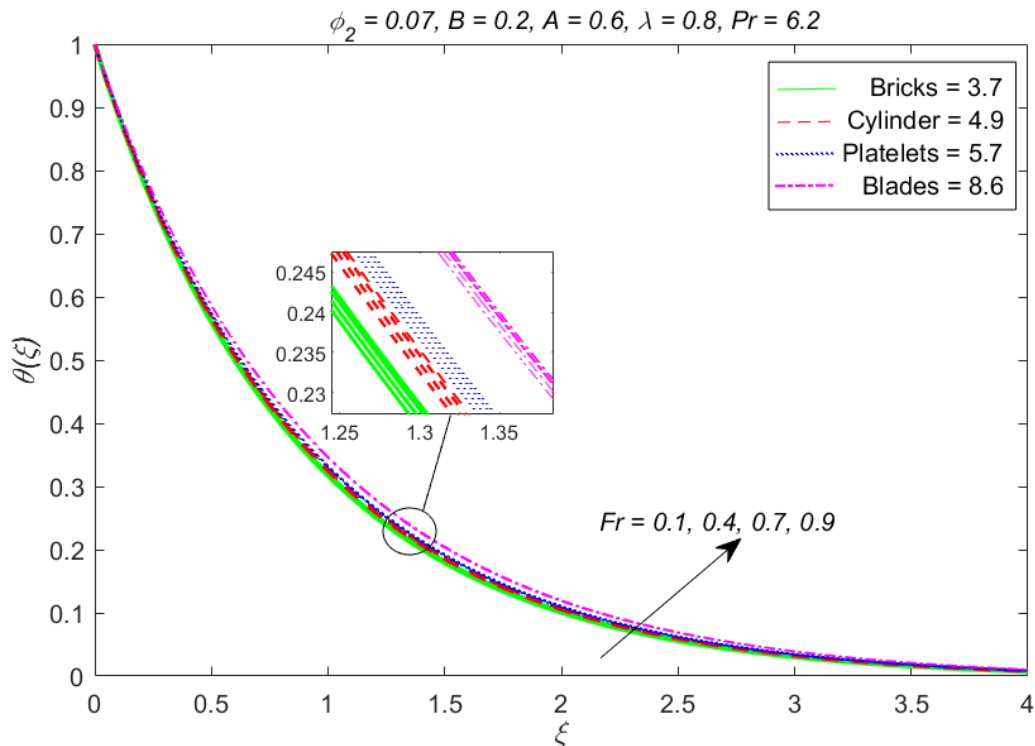


Figure 4.8: Influence of Forchheimer parameter (Fr) on temperature profile $\theta(\xi)$.

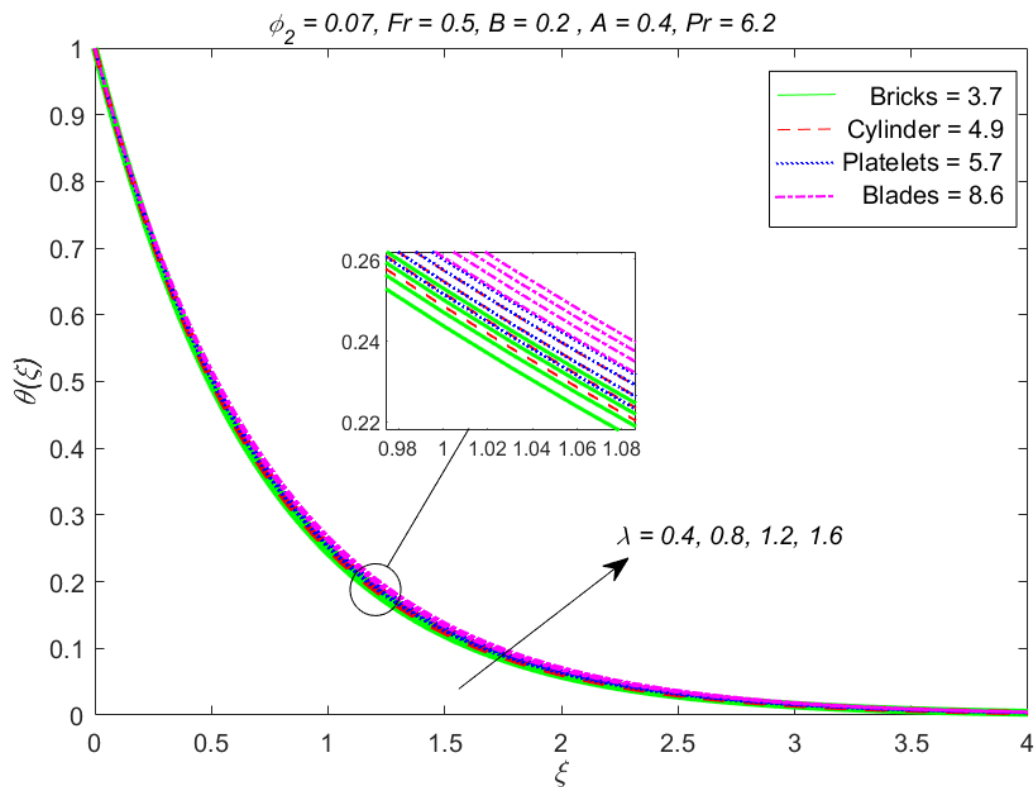


Figure 4.9: Influence of porosity parameter (λ) on temperature profile $\theta(\xi)$.

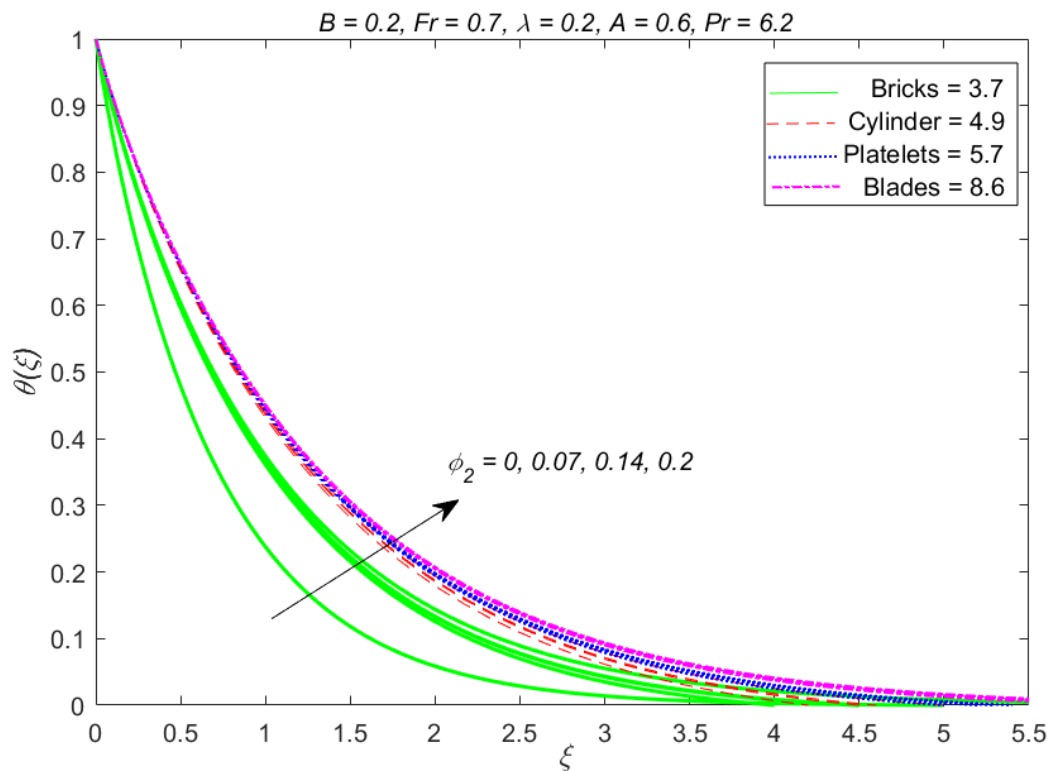


Figure 4.10: Influence of volume fraction (ϕ_2) on temperature profile $\theta(\xi)$.

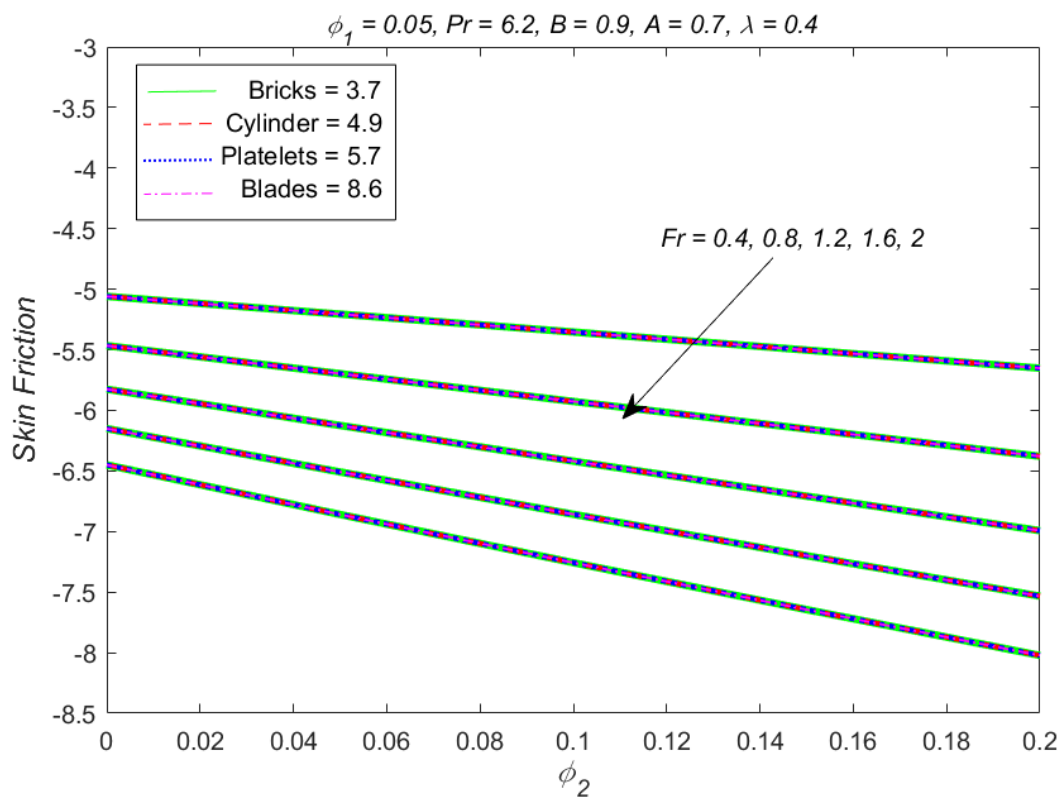


Figure 4.11: Influence of Fr and ϕ_2 on Skin friction.

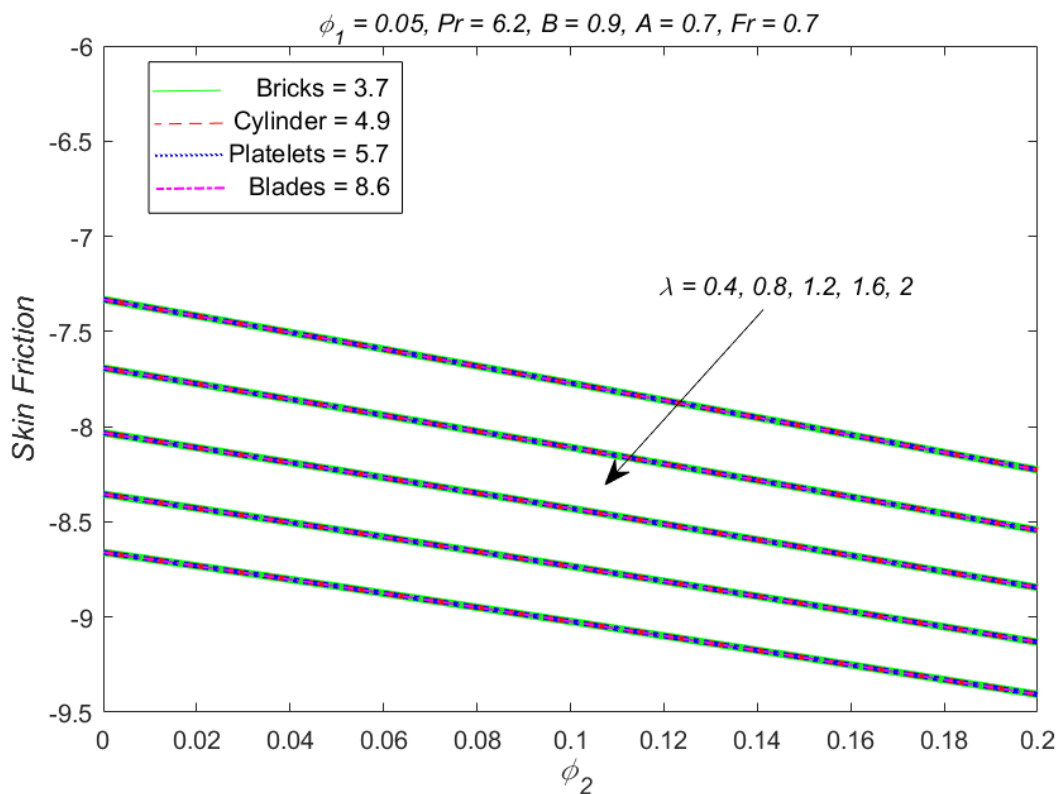


Figure 4.12: Influence of λ and ϕ_2 on Skin friction.

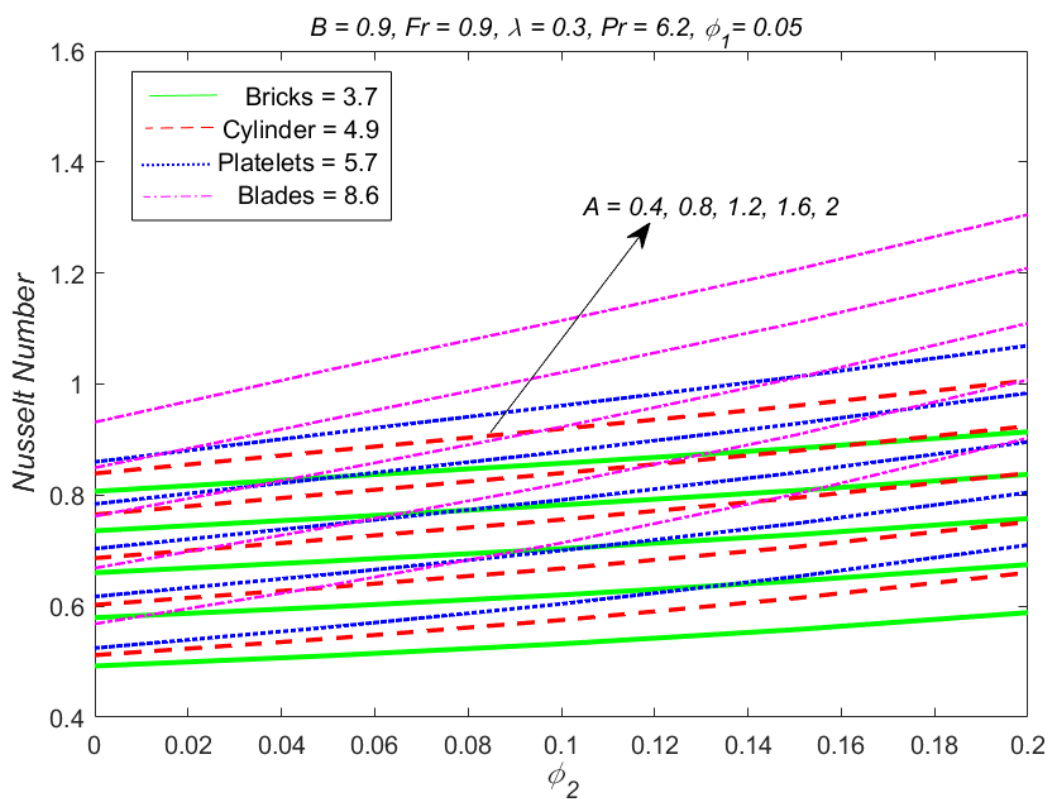


Figure 4.13: Influence of A and ϕ_2 on Nusselt number.

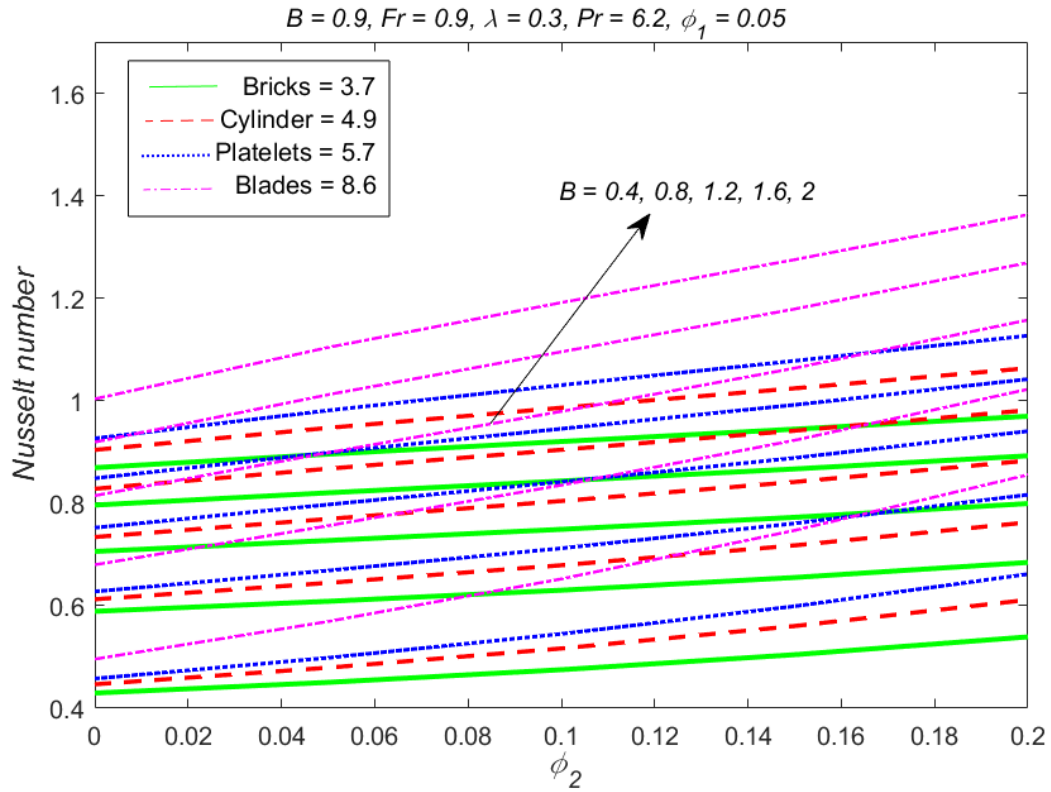


Figure 4.14: Influence of B and ϕ_2 on Nusselt number.

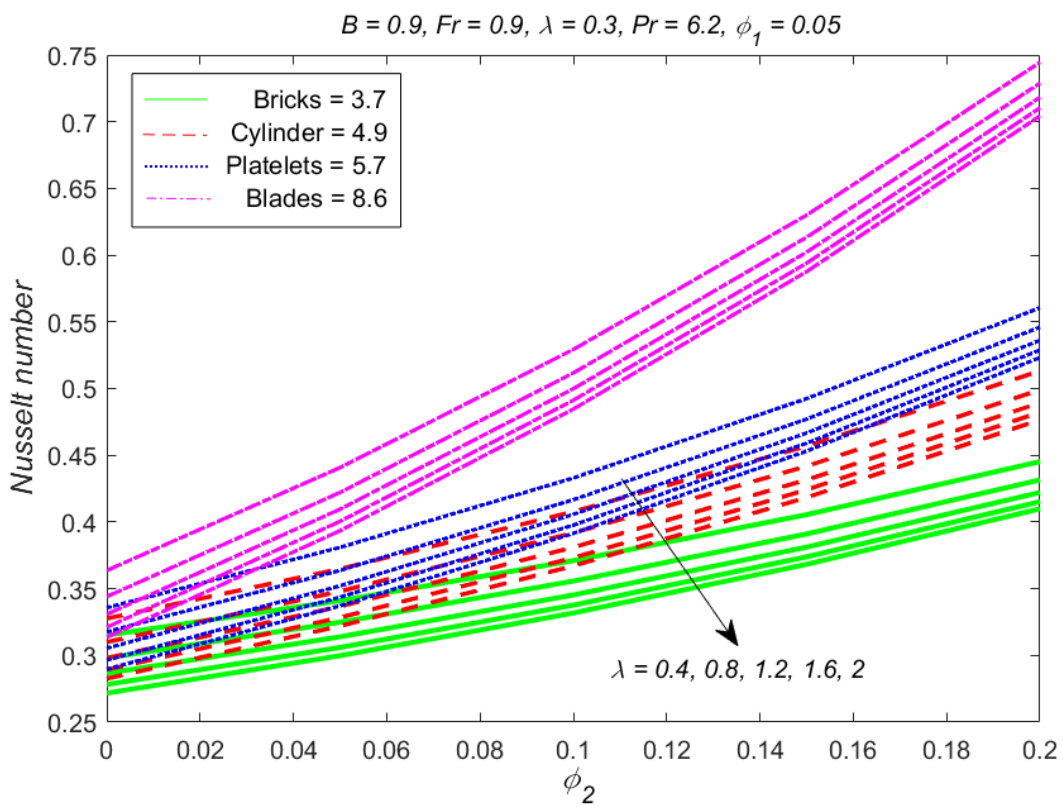


Figure 4.15: Influence of λ and ϕ_2 on Nusselt number.

Chapter 5

Impact of Magnetohydrodynamic and Thermal Radiation on Hybrid Nanofluid Flow over a Curved Stretchable Surface

This chapter deals with the hybrid nanofluid ($Al_2O_3 - Cu/H_2O$) flow over a curved surface that is stretched. The study is performed for containing multiple shape factors when Darcy Forchheimer effect is implicated. In the fluid model, the flow is investigated with the substantial effects of magnetohydrodynamics, viscous dissipation and thermal radiation. By implementing appropriate similarity transformations, the system of nonlinear partial differential equations are transfigured into a system of nonlinear ordinary differential equations. The resultant equations can be solved computationally with the bvp4c approach, and variations in notable parameters have impact on the temperature and velocity profiles in conjunction with the skin friction and Nusselt number.

5.1 Problem Formulation

The current model is built up on the flow of a hybrid nanofluid containing copper and aluminum oxide, with water serving as the base fluid while multiple shape factors are considered. It is assumed that the curved surface undergoes exponential stretching for a two dimensional, steady, viscous, incompressible and MHD flow. The curved surface is stretched with velocity ($u = U_w(s) = a_o e^{\frac{s}{l}}$), in which a_o is a constant ($a_o > 0$). The s represents the arc length coordinate in the direction of a sheet and the coordinate r is taken normal to any tangent on the s -axis. The distance of the surface from the origin, R^* , specifies the radius of a curved surface. The radial direction receives exposure to a constant magnetic flux, resulting in electrically conducted fluid having magnetic field strength B_o .

By taking into account the low magnetic Reynolds number, the induced magnetic field's impact can be evaded. Let $T_w = \frac{As}{l}$ be the temperature of curved surface with a constant A and $T_\infty < T_w$. Along with the Darcy Forchheimer flow, the consequences arising from viscous dissipation and thermal radiation are also emphasized and considered. The governing flow equations for the flow employing the boundary layer approximation are [72]:

$$\frac{\partial}{\partial r} [(r + R^*)v] + R^* \frac{\partial u}{\partial s} = 0, \quad (5.1)$$

$$\frac{u^2}{r+R^*} = \frac{1}{\rho_{hnf}} \frac{\partial p}{\partial r}, \quad (5.2)$$

$$v \frac{\partial u}{\partial r} + \frac{R^*}{r+R^*} u \frac{\partial u}{\partial s} + \frac{uv}{r+R^*} = -\frac{1}{\rho_{hnf}} \frac{R^*}{r+R^*} \frac{\partial p}{\partial s} + \nu_{hnf} \left(\frac{\partial^2 u}{\partial r^2} + \frac{1}{r+R^*} \frac{\partial u}{\partial r} - \frac{u}{(r+R^*)^2} \right) - \frac{\nu_{hnf}}{K^*} u - \mathcal{F}u^2 - \frac{\sigma_{hnf}}{\rho_{hnf}} B_0^2 u, \quad (5.3)$$

$$v \frac{\partial T}{\partial r} + \frac{R^*}{r+R^*} u \frac{\partial T}{\partial s} = \alpha_{hnf} \left(\frac{\partial^2 T}{\partial r^2} + \frac{1}{r+R^*} \frac{\partial T}{\partial r} \right) - \frac{1}{r+R^*} \frac{\partial}{\partial r} [(r + R^*)q_r] + \frac{\mu_{hnf}}{(C_p \rho)_{hnf}} \left[\frac{\partial u}{\partial r} - \frac{u}{r+R^*} \right]^2. \quad (5.4)$$

The nonlinear radiative heat flow, q_r in Eq. (5.4), may be determined employing Rossland's approximation [76] and is given as

$$q_r = \frac{-4\sigma^*}{3k^*} \frac{\partial T^4}{\partial r}, \quad (5.5)$$

where σ^* and k^* is the Stefan Boltzmann coefficient and the mean absorption coefficient. By omitting higher order terms and employing Taylor's expansion of T^4 about T_∞ given by

$$T^4 = 4TT_\infty^3 - 3T_\infty^4. \quad (5.6)$$

Differentiating Eq. (5.6)

$$\frac{\partial T^4}{\partial r} = 4T_\infty^3 \frac{\partial T}{\partial r}. \quad (5.7)$$

Putting Eq. (5.7) in Eq. (5.5), we obtain

$$q_r = \frac{-16\sigma^*}{3k^*} T_\infty^3 \frac{\partial T}{\partial r}, \quad \text{where } \frac{-16\sigma^*}{3k^*} T_\infty^3 = Rd. \quad (5.8)$$

Thus Eq. (5.4) become

$$v \frac{\partial T}{\partial r} + \frac{R^*}{r+R^*} u \frac{\partial T}{\partial s} = \frac{k_{hnf}}{(C_p \rho)_{hnf}} \left[1 + Rd \frac{k_f}{k_{hnf}} \right] \left(\frac{\partial^2 T}{\partial r^2} + \frac{1}{r+R^*} \frac{\partial T}{\partial r} \right) + \frac{\mu_{hnf}}{(C_p \rho)_{hnf}} \left[\frac{\partial u}{\partial r} - \frac{u}{r+R^*} \right]^2. \quad (5.9)$$

The sufficient boundary conditions are as follows in the problem:

$$\begin{aligned} u = U_w(s) = a_o e^{\frac{s}{l}}, \quad v = 0, \quad T = T_w = T_\infty + T_o e^{\frac{As}{2l}} \quad \text{when } r = 0, \\ u \rightarrow 0, \quad \frac{\partial u}{\partial r} \rightarrow 0, \quad T \rightarrow T_\infty \quad \text{when } r \rightarrow \infty. \end{aligned} \quad (5.10)$$

In the above expression, u and v are represented for velocity components in the s and r directions, respectively, pressure signified as p , ρ_{hnf} is denoted by hybrid nanofluid density, R^* for curvature radius, $\mathcal{F} = \frac{C_b}{L\sqrt{K^*}}$ is the uniform inertia coefficient, C_b is the drag coefficient and K^* for porosity permeability.

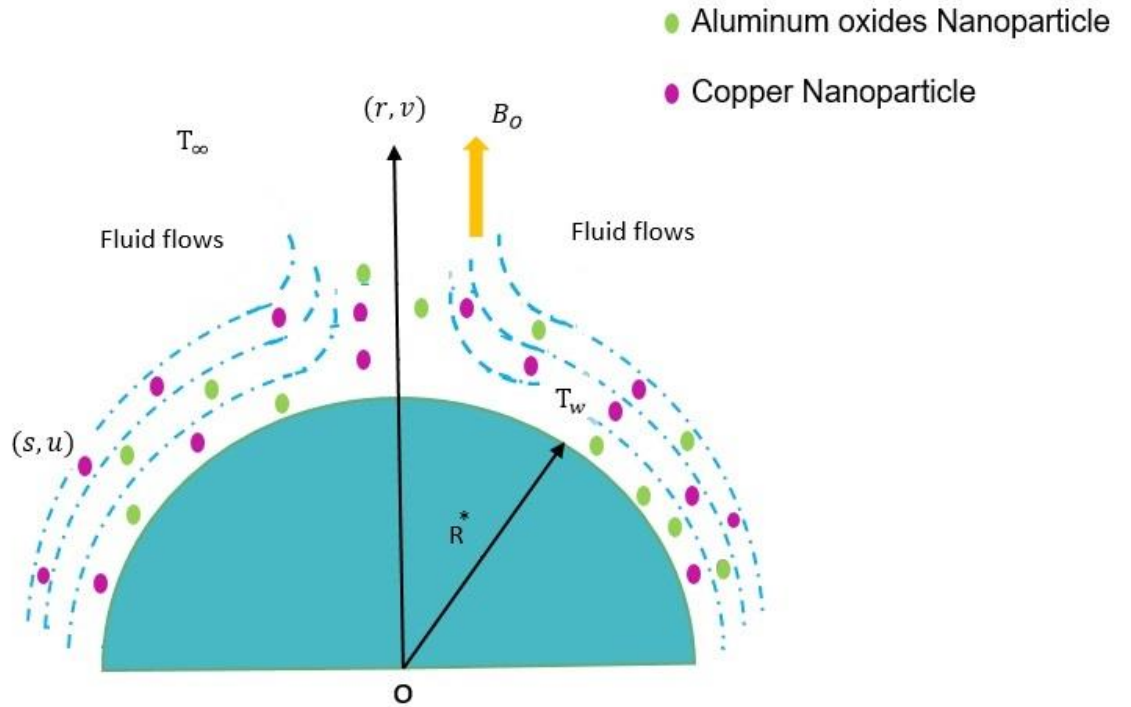


Figure 5.1: Flow Configuration Model

The suitable similarity transformations for the above mentioned system is

$$\begin{aligned} u = U_w(s) = a_o e^{\frac{s}{l}} f'(\xi), \quad v = \frac{-R^*}{r+R^*} \sqrt{\frac{a_o v_f e^{\frac{s}{l}}}{2L}} (f(\xi) + \xi f'(\xi)), \quad T = T_\infty + T_o e^{\frac{As}{2l}} \theta(\xi), \\ \xi = r \sqrt{\frac{a_o e^{\frac{s}{l}}}{2v_f L}}, \quad p = \rho_f a_o^2 e^{\frac{2s}{l}} \mathcal{H}(\xi). \end{aligned} \quad (5.11)$$

Table 5.1: Thermo physical properties considered of nanofluid and hybrid nanofluid [77].

Properties	Nanofluid	Hybrid Nanofluid
Density	$\rho_{nf} = (1 - \phi) + \phi\rho_s$	$\rho_{hnf} = (1 - \phi_2)[(1 - \phi_1)\rho_{bf} + \phi_1\rho_{s1}] + \phi_2\rho_{s2}$
Heat capacity	$(\rho C_p)_{nf} = (1 - \phi)(\rho C_p)_f + \phi(\rho C_p)_s$	$(\rho C_p)_{hnf} = (1 - \phi_2)[(1 - \phi_1)(C_p\rho)_f + \phi_1(\rho C_p)_{s1}] + \phi_2(\rho C_p)_{s2}$
Viscosity	$\mu_{nf} = \frac{\mu_f}{(1-\phi)^{2.5}}$	$\mu_{hnf} = \frac{\mu_f}{(1-\phi_1)^{2.5}(1-\phi_2)^{2.5}}$
Thermal Conductivity	$\frac{k_{nf}}{k_f} = \frac{k_s+(n-1)k_f-(n-1)\phi(k_f-k_s)}{k_s+(n-1)k_f+\phi(k_f-k_s)}$	$\frac{k_{hnf}}{k_{bf}} = \frac{k_{s2}+(n-1)k_{bf}-(n-1)(k_{bf}-k_{s2})\phi_2}{k_{s2}+(n-1)k_{bf}+\phi_2(k_{bf}-k_{s2})}$ where $\frac{k_{bf}}{k_f} = \frac{k_{s1}+(n-1)k_f-(n-1)(k_f-k_{s1})\phi_1}{k_{s1}+(n-1)k_f+\phi_1(k_f-k_{s1})}$
Electrical Conductivity	$\sigma_{nf} = \frac{\sigma_{s1}+(n-1)\sigma_f-(n-1)\phi_{s1}(\sigma_f-\sigma_{s1})}{\sigma_{s1}+(n-1)\sigma_f+\phi_{s1}(\sigma_f-\sigma_{s1})} (\sigma_f)$	$\sigma_{hnf} = \frac{\sigma_{s2}+(n-1)\sigma_{nf}-(n-1)\phi_{s1}(\sigma_{nf}-\sigma_{s2})}{\sigma_{s2}+(n-1)\sigma_{nf}+\phi_{s1}(\sigma_{nf}-\sigma_{s2})} (\sigma_{nf})$

Table 5.2: Thermophysical properties of nanofluid and hybrid nanofluid ($Al_2O_3 - Cu/H_2O$)

Properties	Water	Al_2O_3	Cu
$\rho (kg/m^3)$	997.0	3970	8933
$C_p (J/KgK)$	4180	765	385
$k (W/mK)$	0.6071	40	400
$\sigma (\Omega/m)^{-1}$	5.5×10^{-6}	36×10^6	59.6×10^6
Pr	6.2	-	-

Table 5.3: Nano particle shape factor [78].

Type of Nanoparticle	Shape Factor
Bricks	$n = 3.7$
Cylinder	$n = 4.9$
Platelets	$n = 5.7$
Blades	$n = 8.6$

Eq. (5.1) is instantly verified by Eq. (5.11). While the Eqs. (5.2), (5.3) and (5.9) together with Eq. (5.10) are reduced to the following expressions via use of (5.11) similarities.

$$\frac{1}{\omega_1} \mathcal{H}'(\xi) = \frac{1}{\xi+B} f'^2, \quad (5.12)$$

$$\frac{1}{\omega_2} \left(f'''' + \frac{1}{\xi+B} f''' - \frac{1}{(\xi+B)^2} f'' - 2\lambda f' \right) - \frac{\xi+2B}{(\xi+B)^2} B(f'^2) + \frac{B}{(\xi+B)^2} f f' \quad (5.13)$$

$$+ \frac{B}{\xi+B} f f'' - 2Fr f'^2 - \omega_4 M f' = \left(\frac{1}{\omega_1} \right) \frac{B}{\xi+B} (4\mathcal{H} + \xi \mathcal{H}'),$$

$$\left(\frac{1}{\omega_3} \right) \left(\frac{k_{hnf}}{k_f} + Rd \right) \left(\theta'' + \frac{1}{\xi+B} \theta' \right) + Pr. \frac{B}{\xi+B} (f \theta' - A f' \theta) \quad (5.14)$$

$$+ Ec. Pr. \left(\frac{\omega_5}{\omega_3} \right) \left(f'' - \frac{1}{\xi+B} f' \right)^2 = 0.$$

In this instance

$$\omega_1 = \frac{\rho_{hnf}}{\rho_f} = (1 - \phi_2) \left[(1 - \phi_1) + \phi_1 \frac{\rho_{s1}}{\rho_f} \right] + \phi_2 \frac{\rho_{s2}}{\rho_f}, \quad (5.15)$$

$$\omega_2 = \frac{v_f}{v_{hnf}} = (1 - \phi_1)^{2.5} (1 - \phi_2)^{2.5} \left[(1 - \phi_1)(1 - \phi_2) + \phi_1 \frac{\rho_{s1}}{\rho_f} \right] + \phi_2 \frac{\rho_{s2}}{\rho_f}, \quad (5.16)$$

$$\omega_3 = \frac{(\rho C_p)_{hnf}}{(\rho C_p)_f} = (1 - \phi_2) \left[(1 - \phi_1) + \phi_1 \frac{(\rho C_p)_{s1}}{(\rho C_p)_f} \right] + \phi_2 \frac{(\rho C_p)_{s2}}{(\rho C_p)_f}, \quad (5.17)$$

$$\omega_4 = \frac{\sigma_{hnf}}{\sigma_f} \cdot \frac{\rho_f}{\rho_{hnf}}, \quad (5.18)$$

$$\omega_5 = \frac{\mu_{hnf}}{\mu_f}. \quad (5.19)$$

From Eq. (5.13), the pressure may be expressed as follows:

$$\frac{\omega_1(\xi+B)}{4B} \left[\frac{1}{\omega_2} \left(f'''' + \frac{1}{\xi+B} f''' - \frac{1}{(\xi+B)^2} f'' - 2\lambda f' \right) - \frac{\xi+2B}{(\xi+B)^2} B(f'^2) \right] = \mathcal{H}(\xi). \quad (5.20)$$

By computing the derivative of Eq. (5.13) w.r.t. ξ and utilizing Eq. (5.12), the pressure from Eq. (5.13) may be removed

$$\begin{aligned} & \frac{1}{\omega_2} \left(f'''' + \frac{2}{\xi+B} f'''' - \frac{1}{(\xi+B)^2} f'' + \frac{1}{(\xi+B)^3} f' - 2\lambda \left(f'' + \frac{1}{\xi+B} f' \right) \right) \\ & + \frac{B}{(\xi+B)^2} f f'' + \frac{B}{\xi+B} f f''' - \frac{B}{(\xi+B)^3} f f' - \frac{3B}{(\xi+B)^2} \xi f'^2 - \frac{3B}{\xi+B} f' f'' \\ & - 2Fr(2f' f'' + \frac{1}{\xi+B} f'^2) - \omega_4 M \left(f'' - \frac{1}{\xi+B} f' \right) = 0. \end{aligned} \quad (5.21)$$

The amended boundary conditions are mentioned as

$$\begin{aligned} f = 0, \quad f' = 1, \quad \theta = 1 \text{ at } \xi = 0, \\ f' \rightarrow 0, \quad f'' \rightarrow 0, \quad \theta \rightarrow 0 \text{ when } \xi \rightarrow \infty. \end{aligned} \quad (5.22)$$

The significant parameters are specified to be the Prandtl number (Pr), porosity parameter (λ), Forchheimer constant (Fr), magnetic parameter (M), curvature parameter (B) and Eckert number (Ec) in the relationships discussed above. The above variables include the following:

$$Pr = \frac{\nu_f}{\alpha_f}, \quad \lambda = \frac{\nu_f L}{B U_w}, \quad Fr = \frac{C_b}{\sqrt{B}}, \quad M = \frac{2L\sigma_f B_0^2}{\rho_f U_w}, \quad B = \left(\frac{a_0 e^{s/l}}{2\nu_f L} \right)^{\frac{1}{2}} R^*, \quad Ec = \frac{(U_w)^2}{(C_p)_f (T_w - T_\infty)}. \quad (5.23)$$

The skin friction coefficient C_f and local Nusselt number Nu_s are the prominent physical attributes and are expressed as

$$C_f = \frac{\tau_{rs}}{\rho_{hnf} U_w^2}, \quad Nu_s = \frac{sq_w}{k_{hnf} (T_w - T_\infty)}, \quad (5.24)$$

where q_w and τ_{rs} are rate of heat transfer and wall shear stress [75].

$$q_w = -k_{hnf} \left(\frac{\partial T}{\partial r} \right) + q_r \Big|_{r=0}, \quad (5.25)$$

$$\tau_{rs} = \mu \left(\frac{\partial u}{\partial r} - \frac{u}{r+R^*} \right) \Big|_{r=0}. \quad (5.26)$$

Thus Eq. (5.24) becomes

$$C_f (Re)^{\frac{1}{2}} = f''(0) - \frac{1}{B} f'(0), \quad (5.27)$$

$$Nu_s (Re)^{-\frac{1}{2}} = -\frac{k_{hnf}}{k_f} \left(1 + Rd \frac{k_f}{k_{hnf}} \right) \theta'(0), \quad (5.28)$$

here local Reynolds number is expressed by $Re_s = \frac{as^2}{\nu_f}$.

5.2 Numerical Stratagem

The governing flow equations are sorted utilizing MATLAB's bvp4c tool. Higher order differential equations are usually acquired. Initially, these higher order partial differential equations can be converted into system of ordinary differential equation. Subsequently bvp4c is implemented to resolve these evolving first-order differential equations.

$$f_1 = f, \quad (5.29)$$

$$f_2 = f_1' = f', \quad (5.30)$$

$$f_3 = f_2' = f'', \quad (5.31)$$

$$f_4 = f_3' = f''', \quad (5.32)$$

$$f_5 = f_4' = \left(-\frac{2}{\xi+B} f'''' + \frac{1}{(\xi+B)^2} f'''' - \frac{1}{(\xi+B)^3} f' + 2\lambda \left(f'' + \frac{1}{\xi+B} f' \right) \right) + \omega_2 \left[-\frac{B}{(\xi+B)^2} f f'' - \frac{B}{\xi+B} f f'''' + \frac{B}{(\xi+B)^3} f f' + \frac{3B}{(\xi+B)^2} f'^2 + \frac{3B}{\xi+B} f' f'' \right] + 2Fr \left(2f' f'' + \frac{1}{\xi+B} f'^2 \right) + \omega_4 M \left(f'' - \frac{f'}{\xi+B} \right), \quad (5.33)$$

$$f_6 = \theta, \quad (5.34)$$

$$f_7 = f_6' = \theta', \quad (5.35)$$

$$f_8 = f_7' = -\left(\frac{1}{\xi+B} \theta' \right) + \frac{\omega_3}{\left(\frac{k_{hnf}}{k_f} + Rd \right)} \left[-Pr \frac{k_{bf}}{k_{hnf}} \frac{B}{\xi+B} (f\theta' - Af'\theta) \right] - Ec \cdot Pr \frac{\omega_5}{\omega_3} \left(f'' - \frac{f'}{\xi+B} \right)^2. \quad (5.36)$$

While the boundary conditions are

$$f(1) = 0, f_a(2) = 1, f_a(6) = 1, f_b(2) \rightarrow 0, f_b(3) \rightarrow 0, f_b(6) \rightarrow 0. \quad (5.37)$$

5.3 Graphical Results and Discussion

The Darcy Forchheimer flow of hybrid nanofluid flowing over a stretching curved surface has been analyzed for multiple shape factors. The fluid model is examined in the presence of magnetohydrodynamics, viscous dissipation and thermal radiation. The effects of several relevant variables concerning heat transfer rate, skin friction, temperature profile and velocity profile are displayed in this section. Figures 5.2–5.6 demonstrate the velocity profile for different shape factors. For each graph, four shape factors including bricks, cylinder, platelets and blades are shown. Figure 5.2 illustrates influence of curvature parameter (B) on the velocity profile. Whenever the curvature parameter is increased, the fluid flow and boundary layer thickness simultaneously expand. As B increases, the radius of the curved surface reduces which corresponds to a reduction in the area of contact between the fluid and the solid surface. Therefore $f'(\xi)$ enlarges. For velocity profile, bricks shaped nanoparticles have high velocity as compared to cylinder,

platelets and blade shaped nanoparticles. Figure 5.3 shows the influence of Forchheimer parameter (Fr) on velocity profile. The increment in Forchheimer parameter decreases fluid velocity because an increase in Forchheimer value signifies a larger nonlinear resistance to fluid flow in porous media. Physically, the Darcy number inhibits the increase in Darcian drag force resulting in improved fluid flow permeability while minimizing fluid velocity. Figure 5.4 displays the velocity profile $f'(\xi)$ with larger assumptions of the local porosity parameter (λ). The Decline in $f'(\xi)$ is induced by higher values of λ . Rising permeability enables the particles' internal resistive force to rise, thus lowering the fluid's velocity. Furthermore, hybrid nanofluid having blade shaped nanoparticles have the lowermost velocity but brick shaped nanoparticles correspond to comparatively higher velocity. Timofeeva *et al.*'s [79] experimental research defends up the aforementioned findings. They discovered that the flow rate of nanofluids is highest when the dispersed nanoparticles are brick shaped, because the flow resistive capacity of nanofluids is least in this situation also brick-shaped hybrid nanofluid possesses a lower dynamic viscosity, it ultimately elevates the momentum boundary layer. Figure 5.5 demonstrates the relationship between magnetic parameter (M) and velocity profile. The velocity of fluid declines as M increases. The Lorentz force becomes more significant as M increases, due to which this force may act against the motion of the fluid causing velocity decline. Figure 5.6 depicts the increasing behavior in velocity profile under the influence of volume fraction ϕ_2 . The reason is that the velocity with hybrid particles is much higher than that of single particles. This is primarily because the density of the nanofluid with hybrid particles is more extensive than the density of the nanofluid with single particles. In this figure, brick shaped nanoparticles once again shows higher velocity than other shape factors. Figures 5.7 to 5.14 depict the temperature profile $\theta(\xi)$ of hybrid nanofluid for numerous parameters like $A, B, Fr, \lambda, \phi_2, Ec, M$ and Rd and for each graph, the four shape factors are also plotted. The variation in the temperature profile with the alterations of temperature exponent (A) is illustrated in Figure 5.7. A declining role of $\theta(\xi)$ for A is seen through the figure and any adjustments in the fluid's temperature exponent (A) on the stretched surface cause the fluid to decrease in velocity. Figure 5.8 depicts that when the curvature (B) of surface grows larger, there is simultaneous decline in temperature profile. The resistance lessens between the fluid layers for increased B . In temperature profile, blade shaped nanoparticles have higher heat transfer rates than bricks, cylinder and platelets shaped nanoparticles. In Figure 5.9, it is perceivable that Forchheimer's term (Fr) causes the temperature field to grow.

The blade shaped nanoparticles have been apparent to be superior in transferring heat than nanoparticles based on platelets, cylinders or bricks shapes. Figure 5.10 illustrates the effects of porosity parameter (λ) on the temperature profile. Basically, the porosity term boosts the extending surface area's length and kinetic viscosity causing increase in fluid's temperature. The relationship between volumetric fractions ϕ_2 and temperature profile is seen in Figure 5.11. With an increase of ϕ_2 , it is anticipated that the thickness of the thermal boundary layer and temperature boundary layer will rise as well. Incorporating nanoparticles with different volume fractions values increases the temperature of the fluid. The base fluid water has considerably greater specific heat capacity than aluminum and copper oxide, thus incorporating nanoparticles to water reduces their ability to absorb heat, causing excessive heat generation in the fluid. This figure additionally demonstrates that hybrid nanofluid based on brick-shaped nanoparticles have the lowest temperature but blade shaped nanoparticles particularly correspond to high temperature. Figure 5.12 demonstrates that when the value of Eckert number (Ec) increases, the fluid's kinetic energy and boundary layer thickness are elevated, reinforcing the thermal field. As a result, higher Ec directly relates to the temperature of the fluid. Highly stable fluid particles are the cause of this phenomenon and blade shaped nanoparticles possess higher heat than other shape factors. Figure 5.13 depicts the variation of the magnetic parameter (M) on temperature profile $\theta(\xi)$. In this case, it is figured out that larger M values lead to a rise in thermal boundary layer. It follows that when the value of M increases, the Lorentz force (resistive force) also increases, causing raise in the temperature of hybrid nanofluid. Brick-shaped nanofluid nanoparticles possess the least temperature magnitude while blade-shaped nanofluid nanoparticles achieve their highest temperature. Figure 5.14 exhibits the effect of the radiation parameter (Rd) on the temperature profile $\theta(\xi)$. The increase in radiation parameter's values maximized the temperature of the hybrid nanofluid. Physically, as Rd expands, the radiative heat flux increased which raised the fluid's temperature.

Figure 5.15-5.17 depicts the impact of Fr , λ and M on skin friction C_f with ϕ_2 . Figure 5.15 illustrates the effect of the Forchheimer parameter (Fr) on C_f in association with ϕ_2 . It has been shown that skin friction decreases with Fr and increasing behavior is seen for ϕ_2 . A rise in the Forchheimer parameter (Fr) may minimize skin friction in some extremely porous media with unique topologies, such as open-cell foams or specific types of filter media. This is because, regardless of the presence of nonlinear effects, the

medium's structure may promote favorable flow patterns or lessen resistance. Figure 5.16 reveals that when the porosity parameter (λ) increases, there is a lower resistance to fluid's movement, leading in reduced C_f . This is due to the fact that there are less solid barriers or surfaces for the fluid to come into contact with a highly porous medium. The reverse behavior is shown for ϕ_2 . The influence of the magnetic parameter (M) on the skin fraction along with ϕ_2 can be observed in Figure 5.17. The skin friction coefficient drops as the magnetic field expands due to the reduced velocity of the flow while increasing behavior is seen for ϕ_2 . Figure 5.18-5.20 demonstrates the relation between Nusselt number Nu_s and different parameters including Ec , Rd and B with variability in ϕ_2 values. Fig 5.18 shows the effect of Eckert number on Nu_s along with ϕ_2 . The Nusselt number and the Eckert number are mutually exclusive. The temperature rises as viscous dissipation expands, while Nu_s declines when Eckert number (Ec) improves and reverse trend is followed for ϕ_2 . The numerical results for the Nu_s for the radiation parameter (Rd) are depicted in Figure 5.19. Nusselt number shows increasing behavior with an increase in Rd and same trend is seen for parameter ϕ_2 . The reason for this is that elevating the values of the radiation parameter helps to improve the rate of heat transfer and as a consequence, a rise in Nu_s is obtained. In Figure 5.20, the curvature parameter (B) improves the Nu_s , and the parameter ϕ_2 experiences a similar behavior. It seems that blade shaped nanoparticles achieve their greatest temperature in contrast to other nanoparticles.

Tables 5.1 and 5.2 show the thermo-physical properties of the nanoparticles and base fluid necessary for the investigation. Table 5.3 displays the shape factor for various nanoparticles under consideration. Table 5.4 spectacles significant coherence between the values obtained for the current investigation on hybrid nanofluid model and the previously found values in the literature.

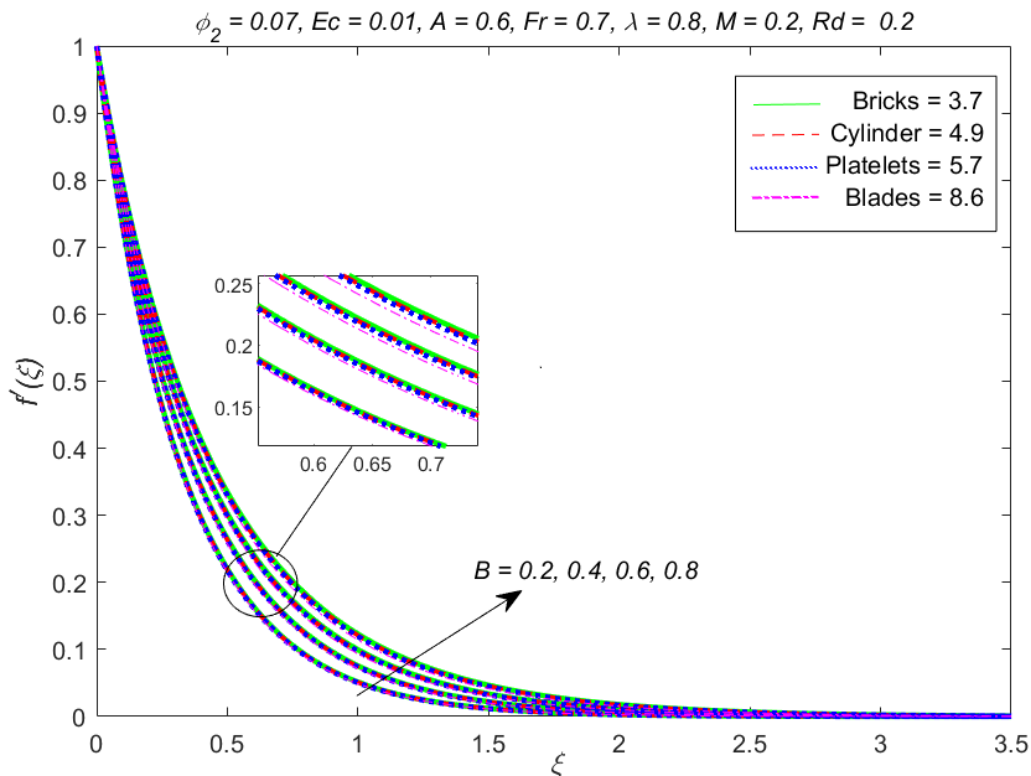


Figure 5.2: Influence of curvature parameter (B) on velocity profile $f'(\xi)$.

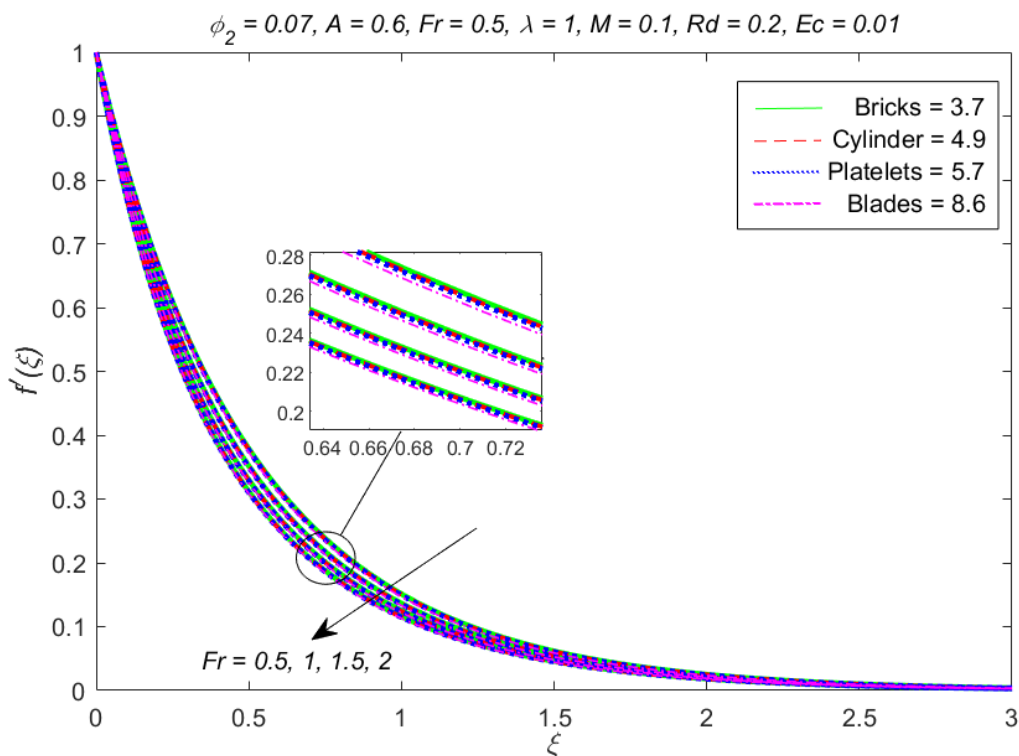


Figure 5.3: Influence of Forchheimer Parameter (Fr) on velocity profile $f'(\xi)$.

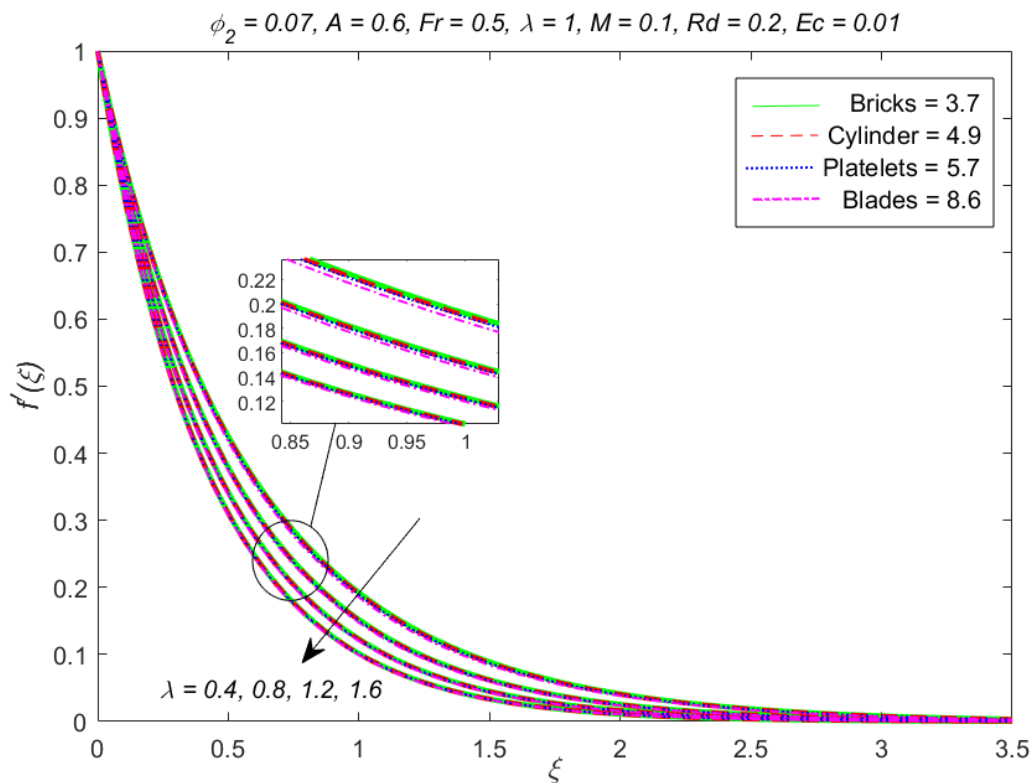


Figure 5.4: Influence of porosity parameter (λ) on velocity profile $f'(\xi)$.

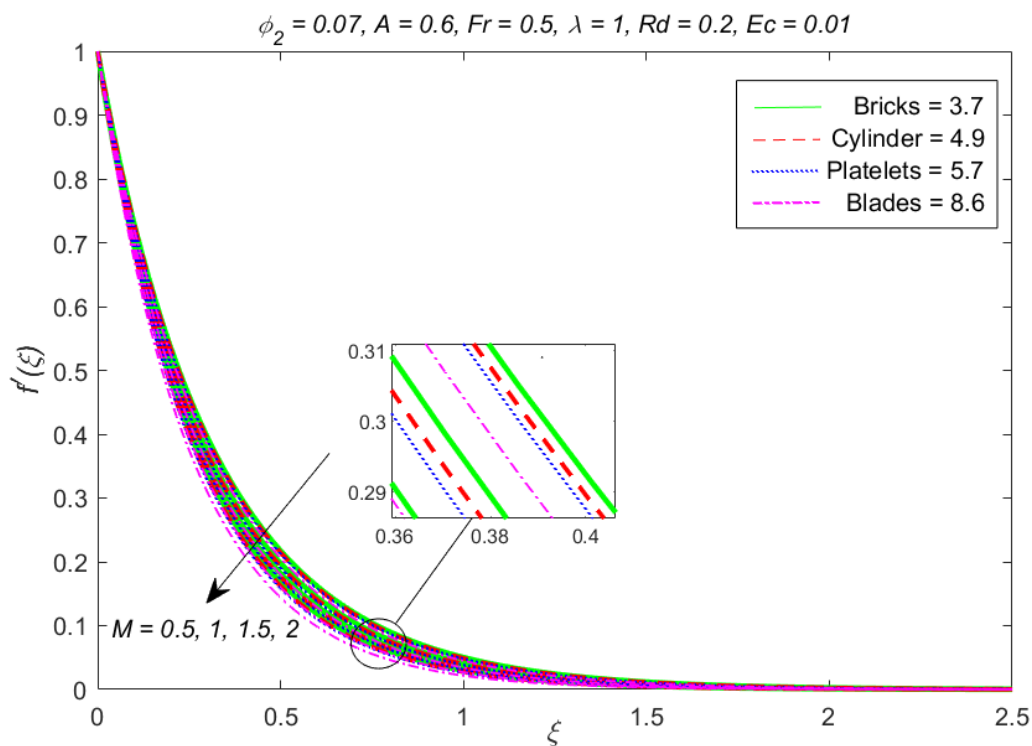


Figure 5.5: Influence of magnetic parameter (M) on velocity profile $f'(\xi)$.

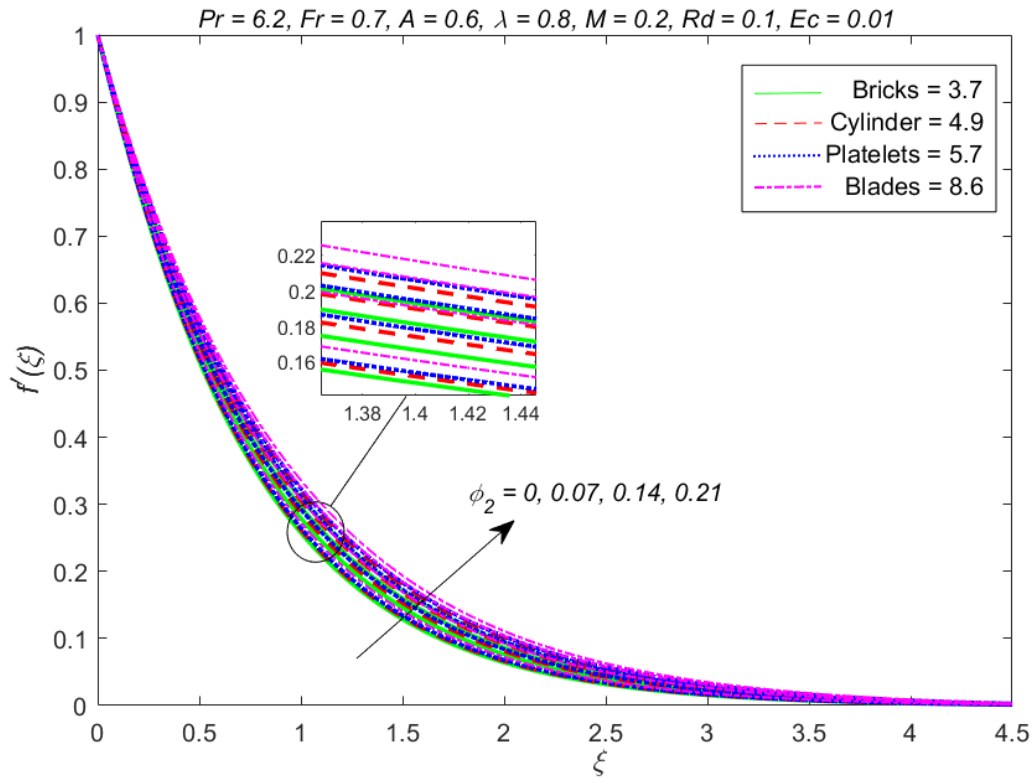


Figure 5.6: Influence of volume fraction (ϕ_2) on velocity profile $f'(\xi)$.

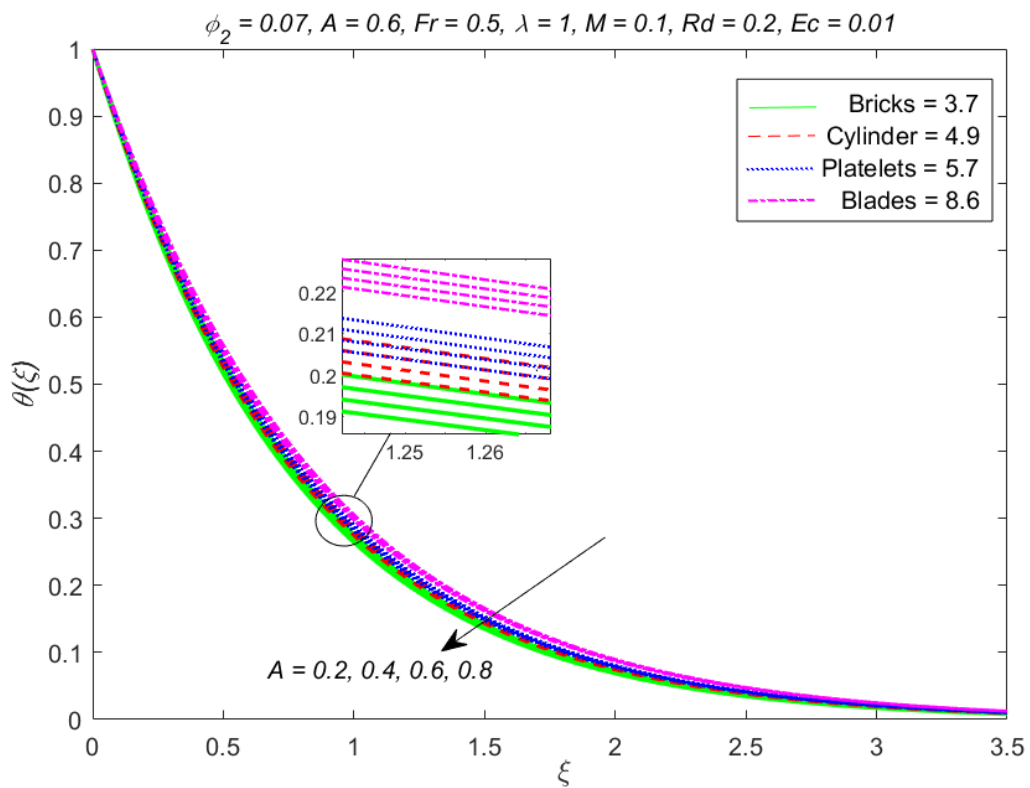


Figure 5.7: Influence of temperature exponent (A) on temperature profile $\theta(\xi)$.

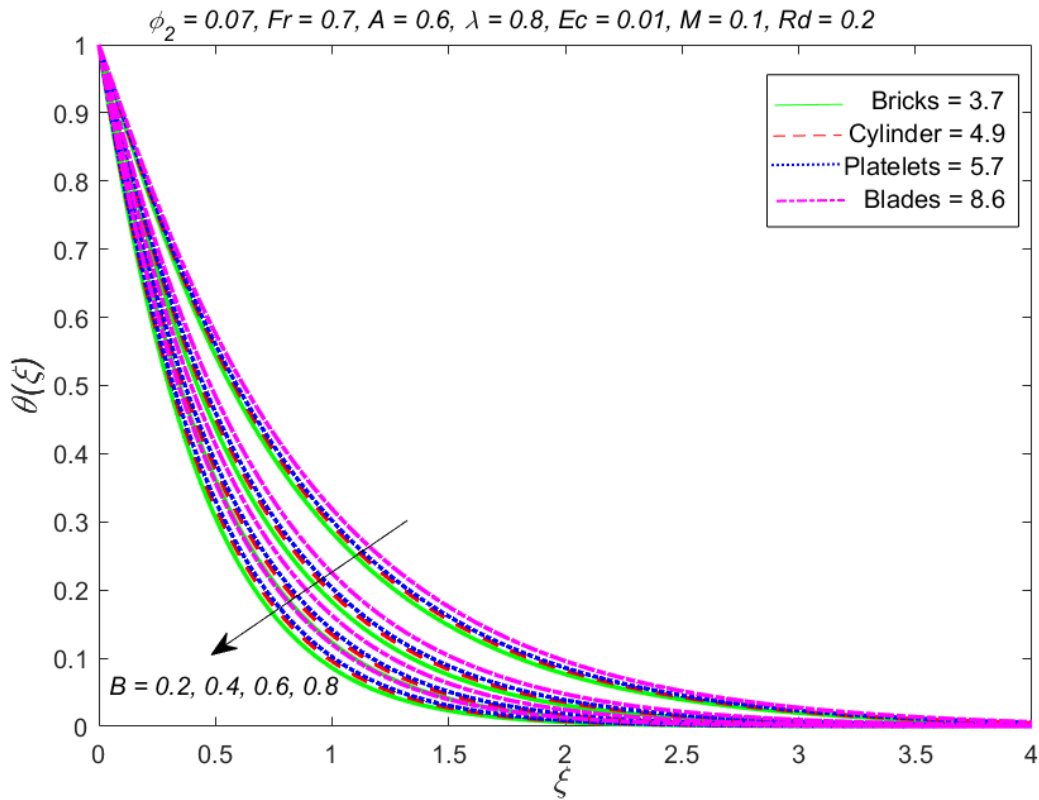


Figure 5.8: Influence of curvature parameter (B) on temperature profile $\theta(\xi)$.

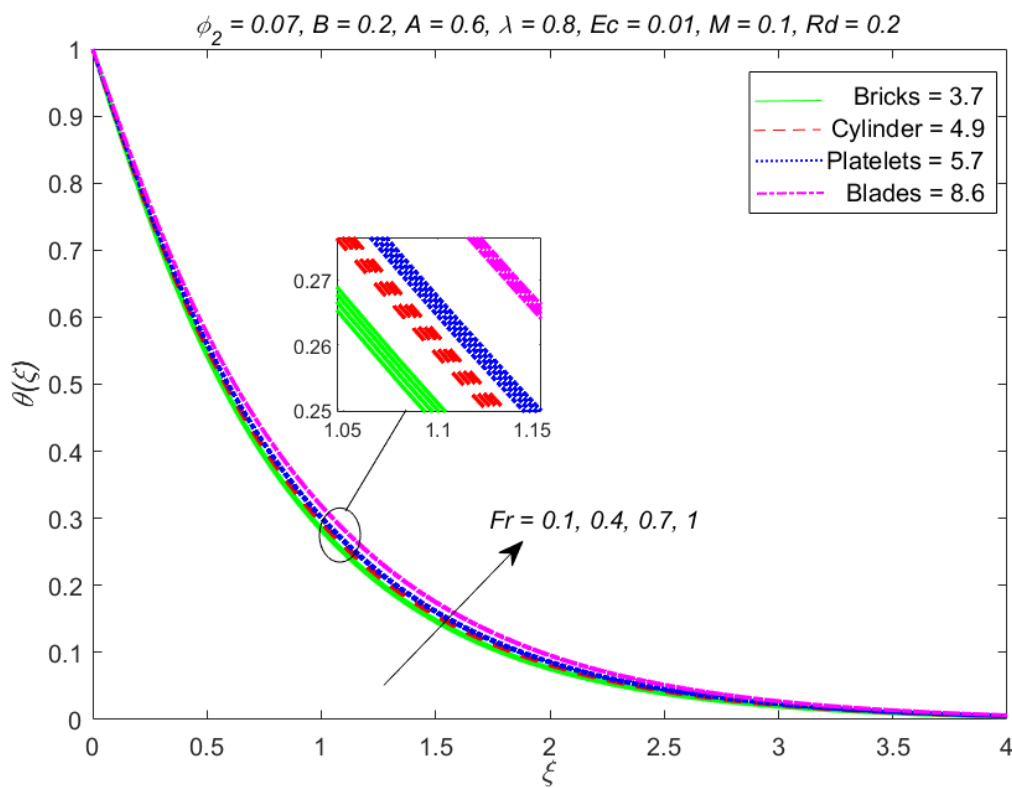


Figure 5.9: Influence of Forchheimer parameter (Fr) on temperature profile $\theta(\xi)$.

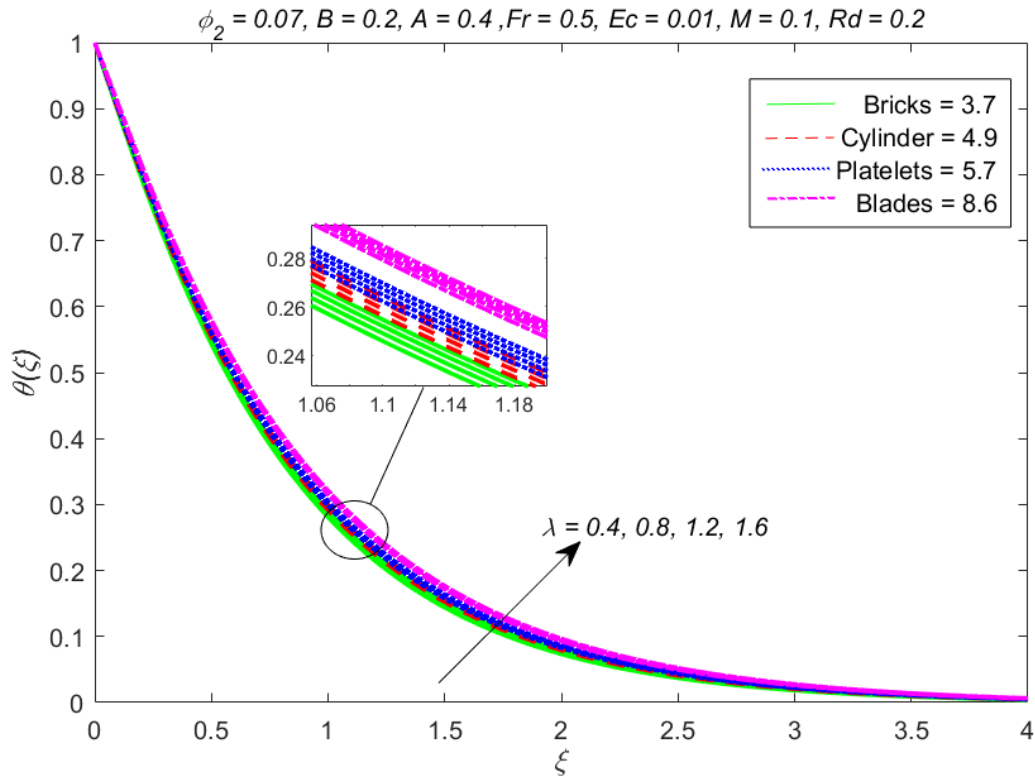


Figure 5.10: Influence of porosity parameter (λ) on temperature profile $\theta(\xi)$.

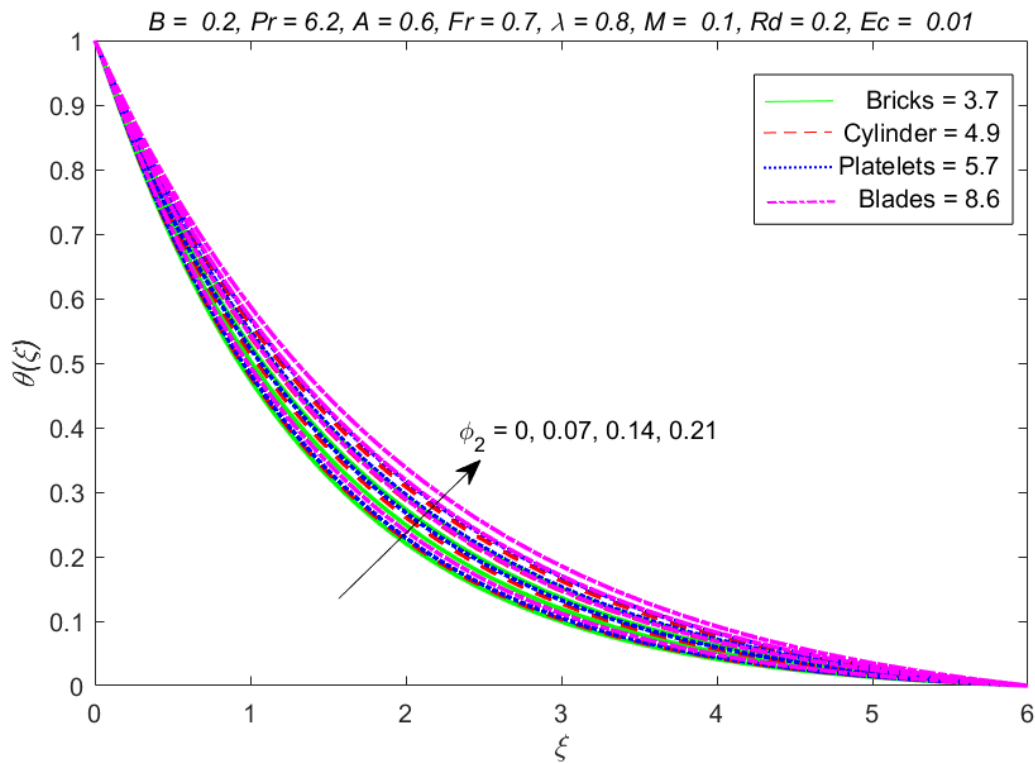


Figure 5.11: Influence of volume fraction (ϕ_2) on temperature profile $\theta(\xi)$.

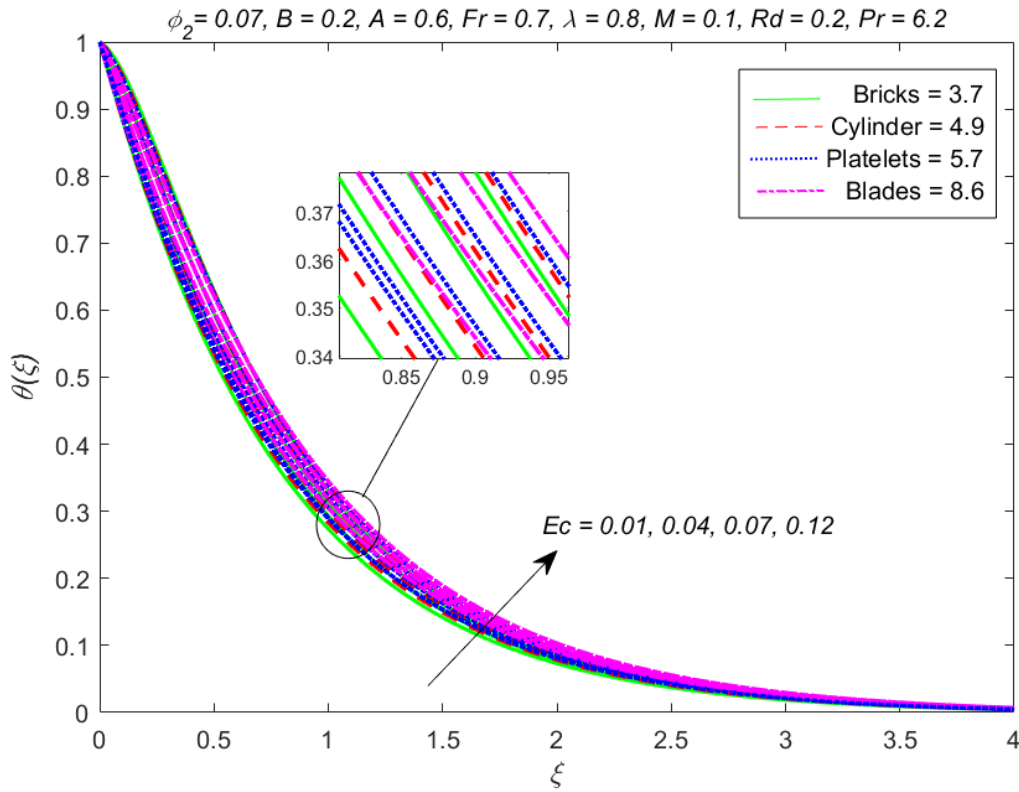


Figure 5.12: Influence of Eckert number (Ec) on temperature profile $\theta(\xi)$.

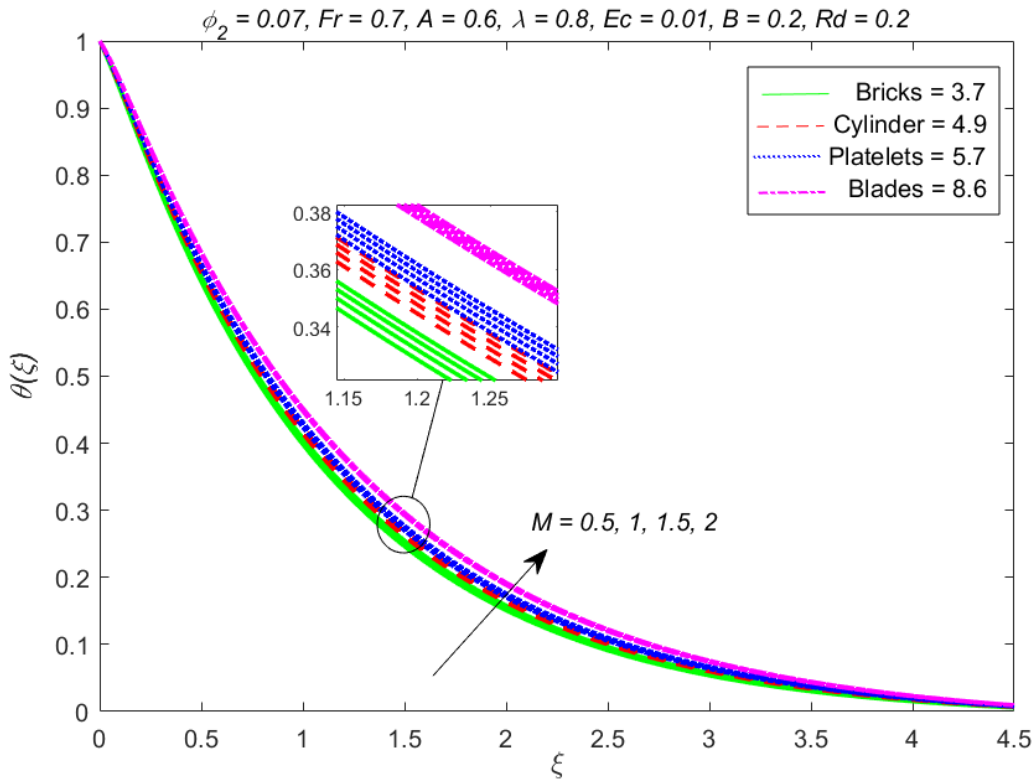


Figure 5.13: Influence of magnetic parameter (M) on temperature profile $\theta(\xi)$.

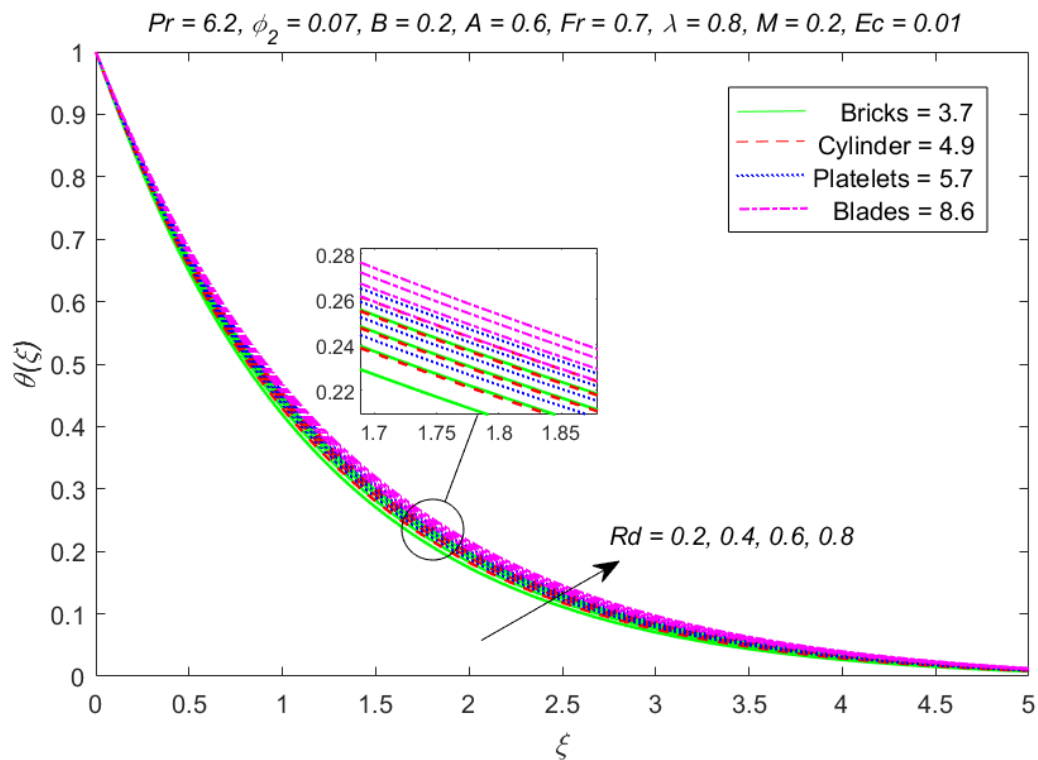


Figure 5.14: Influence of radiation parameter (Rd) on temperature profile $\theta(\xi)$.

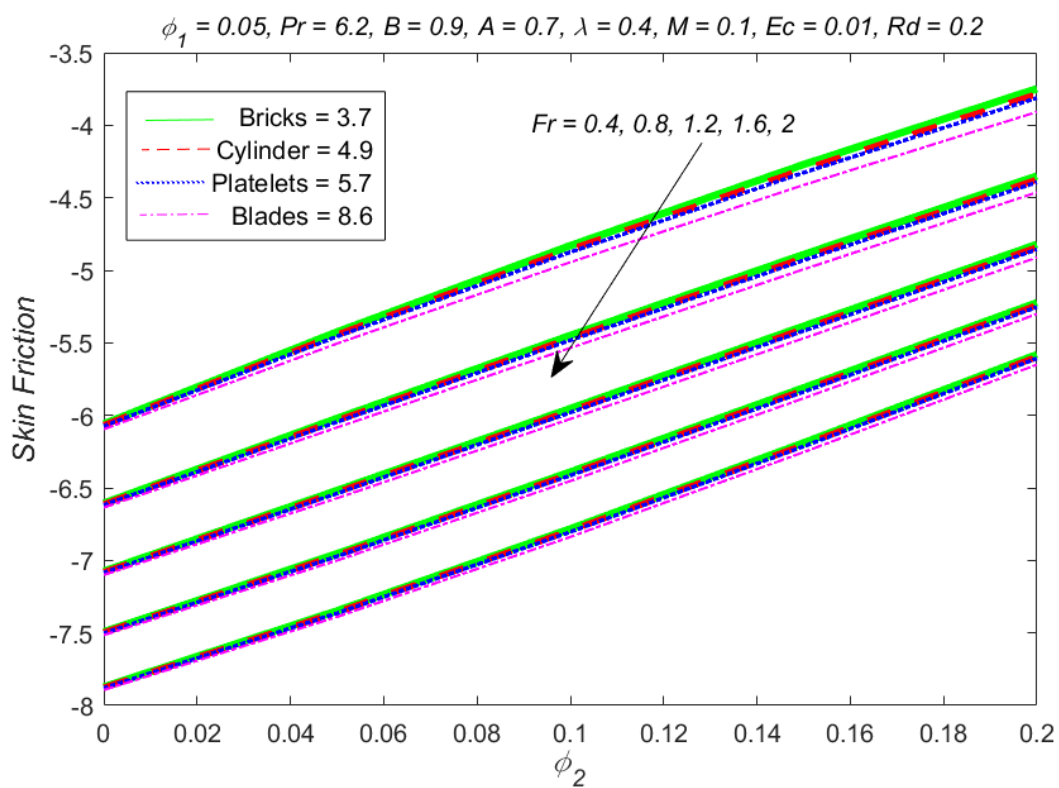


Figure 5.15: Influence of Fr and ϕ_2 on Skin Friction.

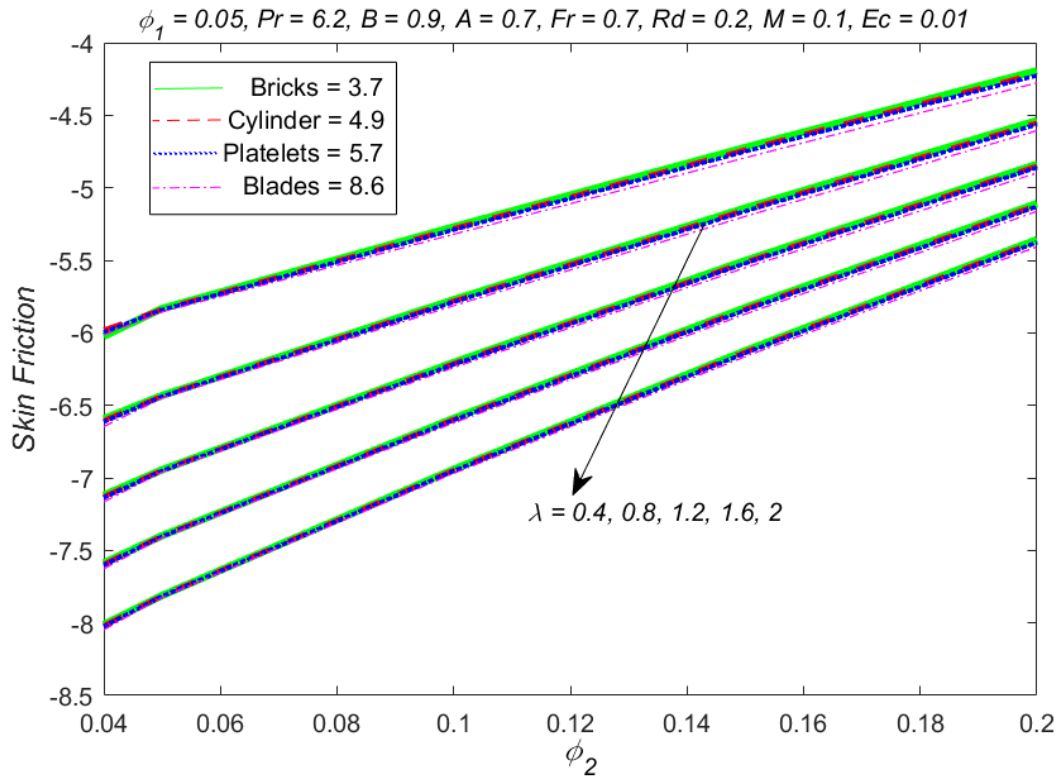


Figure 5.16: Influence of λ and ϕ_2 on Skin friction.

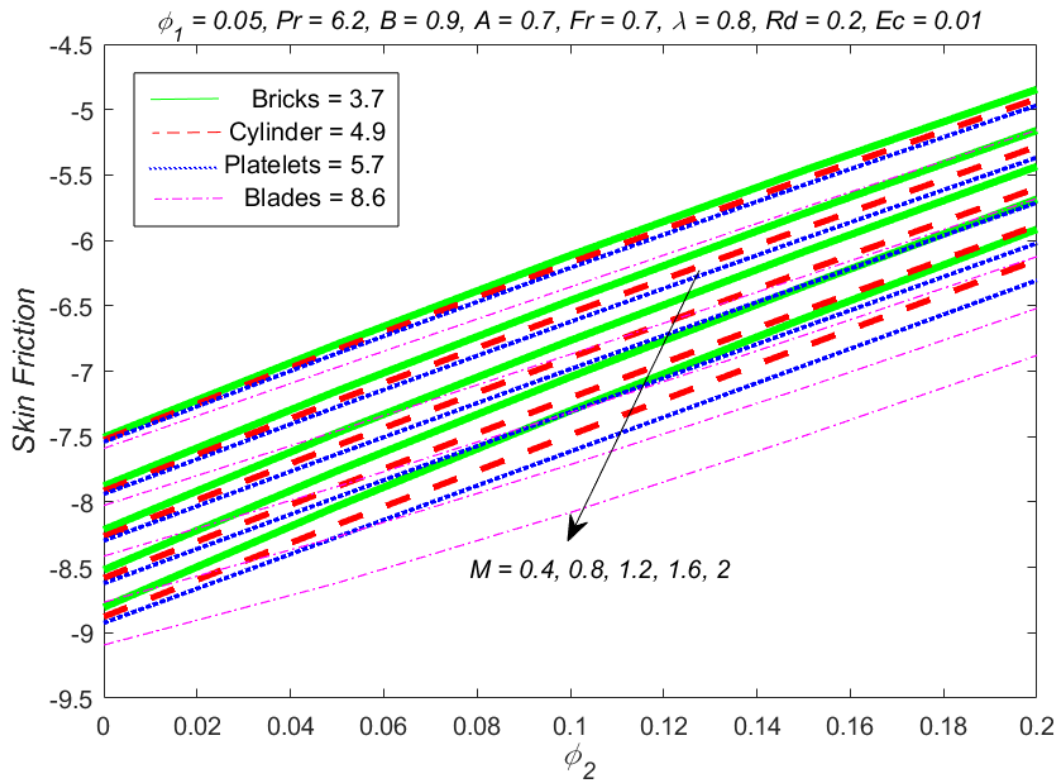


Figure 5.17: Influence of M and ϕ_2 on Skin Friction.

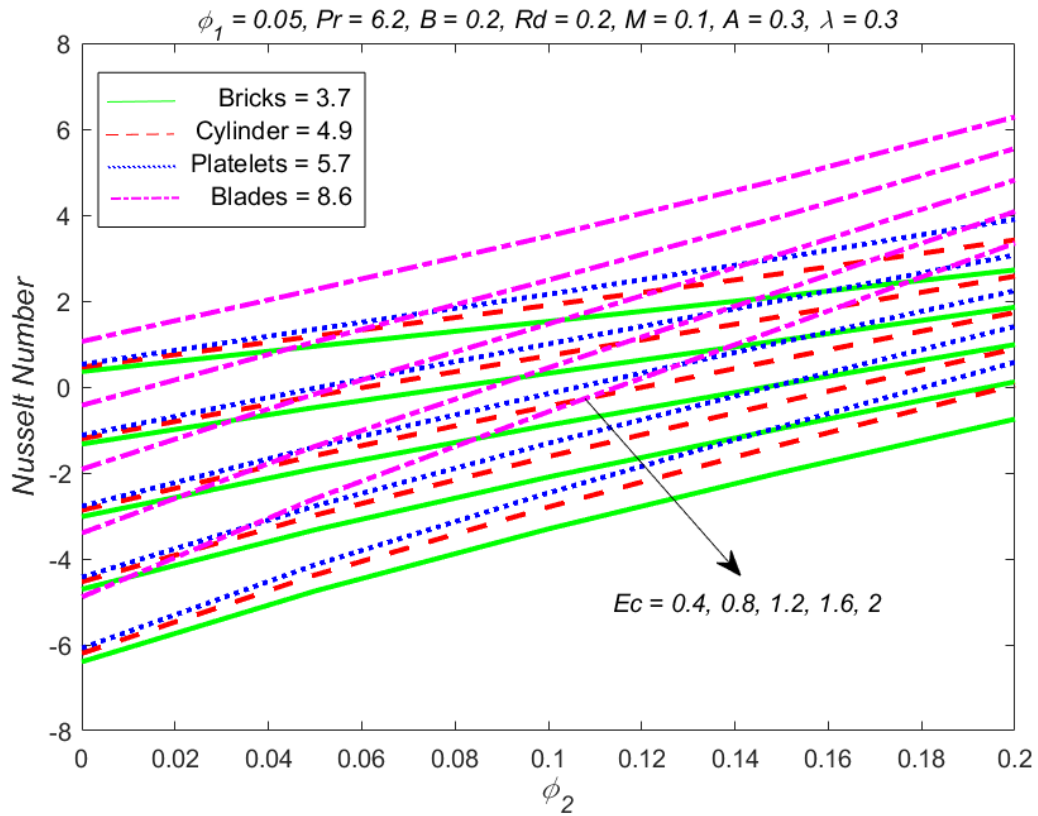


Figure 5.18: Influence of Ec and ϕ_2 on Nusselt number.

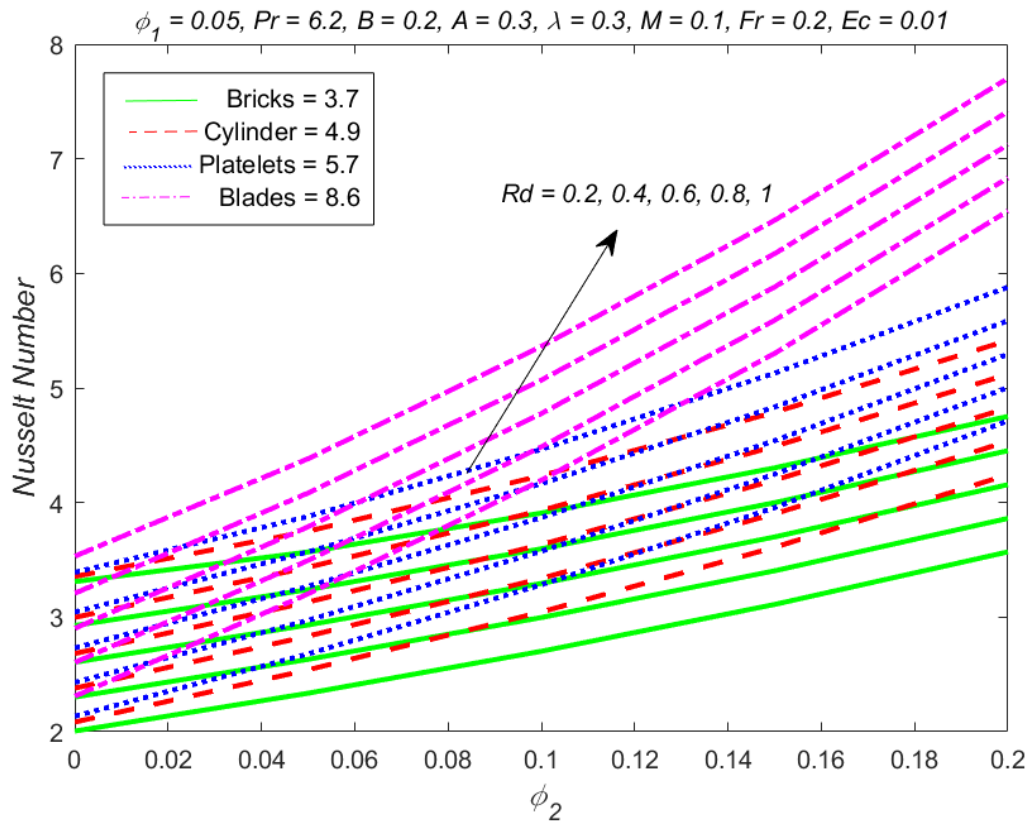


Figure 5.19: Influence of Rd and ϕ_2 on Nusselt number.

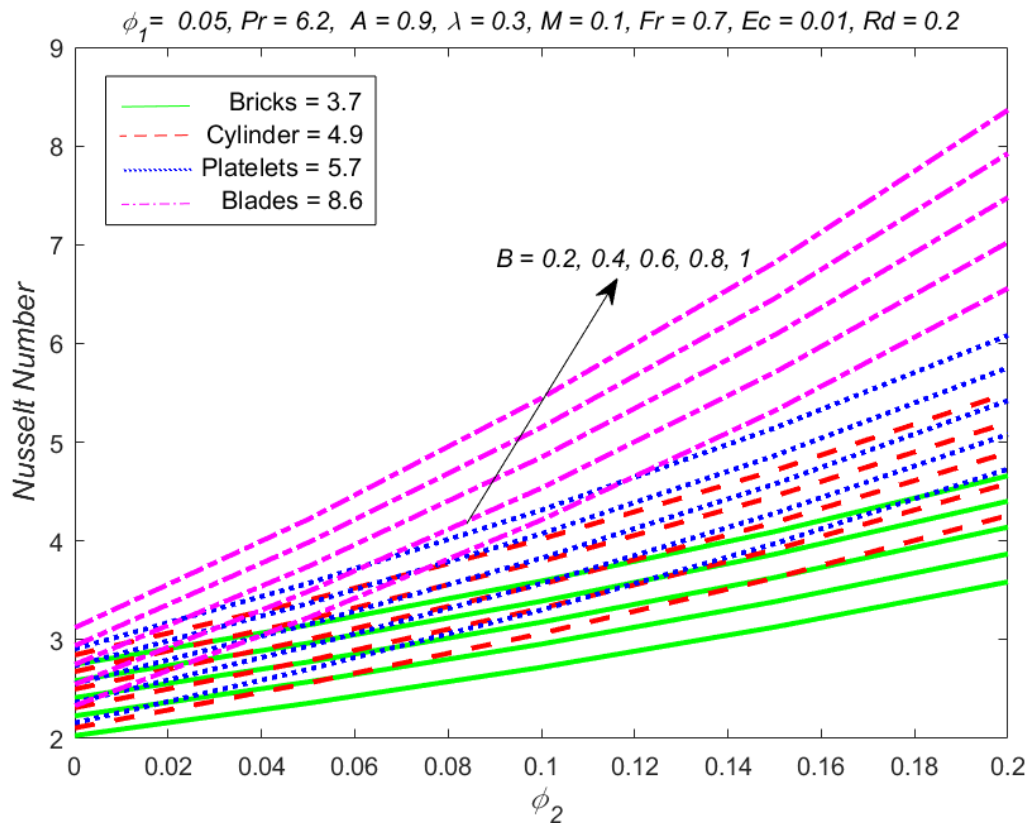


Figure 5.20: Influence of B and ϕ_2 on Nusselt number.

Table 5.4: Comparison table of temperature gradient $\theta'(0)$ for different λ when $\phi_1 = 0.05$ and $\phi_2 = 0$ [80, 81, 82].

λ	Iqbal <i>et al.</i> [80]	Hayat <i>et al.</i> [81]	Ullah <i>et al.</i> [82]	Current results
0.2	0.5673	0.5673	0.56731	0.567316
0.4	0.3403	0.3403	0.34030	0.340302
0.6	0.4413	0.4413	0.44130	0.441307
0.8	0.1282	0.1282	0.1282	0.12825

Chapter 6

Conclusion and Future work

6.1 Conclusion Remarks

In the current investigation, the relationship that exists between Darcy Forchheimer and the magnetohydrodynamics flow of a hybrid nanofluid ($Al_2O_3 - Cu/H_2O$) was addressed. Moreover additionally considered effects are the viscous dissipation and thermal radiation. Hybrid nanofluids have several potential applications in various industries due to their enhanced heat transfer capabilities and improved performance. The considered hybrid nanofluid is flowing over a curved stretching surface and the problem involves multiple shape factors. The systems of equations are shown in terms of PDEs, which are subsequently transformed into ODEs for further simplifications using similarity transformations. The problem's numerical analysis yields the considerable results. The velocity distribution exemplifies a growing drift under the influence curvature parameter. The raise in values of magnetic parameter, Forchheimer constant and porosity parameter induces a decline in velocity of the hybrid nanofluid. The nanoparticles having blade shape have the least velocity, however brick-shaped nanoparticles have unusually high velocity. The temperature distribution reduces down for the improved values of parameters temperature exponent and curvature parameter. Any change in the fluid's curvature on the stretched surface causes the fluid to decelerate and raise temperature. With increasing values of Forchheimer constant, magnetic parameter, porosity parameter and Eckert number, the temperature distribution lifts up. Furthermore, blades shape nanoparticles in hybrid nanofluid have higher thermal conductivity than bricks, cylinder and platelets shape nanoparticles. The Nusselt number rises for higher values curvature parameter and radiation parameter, and similar trend is noticed for ϕ_2 . The Nusselt number is affected by higher values of Eckert number, causing drop in the rate of heat transfer. The skin friction

coefficient is another crucial factor during the study of fluid flow problems. It is imperative in the design and examination of aerodynamic surfaces and its correct assessment is essential for predicting drag forces and boosting the performance of vehicles and other objects moving through fluids. For magnetic parameter, Forchheimer constant and porosity parameter the skin friction lessens and reverse trend is noticed for ϕ_2 .

6.2 Future Work

In the present investigation, with few rigorously examined assumptions, the influence of thermal radiation and viscous dissipation for hybrid nanofluid passing over a curved surface stretching exponentially with a presence of magnetohydrodynamics have been analyzed. Yet, the conducted research paves a path towards further intriguing works. Here are some fascinating studies that hold the potential to be captivating in the future.

- The unsteady hybrid nanofluid flow across a curved surface influenced by inclined magnetohydrodynamics and thermal slip.
- The numerical simulation of hybrid nanofluid flow with mixed convection and Newtonian heating.
- The effect of Arrhenius activation energy on hybrid nanofluid flow over a permeable surface accompanied by viscous dissipation.
- Heat and mass transfer of hybrid nanofluid flow due to nonlinearly stretching surface in the presence of stagnation point.

REFERENCES

1. Choi, S. U., & Eastman, J. A. (1995). *Enhancing thermal conductivity of fluids with nanoparticles* (No. ANL/MSD/CP-84938; CONF-951135-29). Argonne National Lab. (ANL), Argonne, IL (United States).
2. Marquis, F. D. S., & Chibante, L. P. F. (2005). Improving the heat transfer of nanofluids and nanolubricants with carbon nanotubes. *Jom*, *57*, 32-43.
3. Turcu, R., Darabont, A., Nan, A., Aldea, N., Marcovei, D., Bica, D., & Koos, A. (2006). New Polypyrrole-multiwall carbon nanotubes hybrid materials. *Journal of optoelectronics and advanced materials*. *8*(2), 643-647.
4. Jana. S., Salehi-Khojin. A., & Zhong. W. H. (2007). Enhancement of fluid thermal conductivity by the addition of single and hybrid nano-additives. *Thermochimica Acta*. *462*(1), 45-55
5. Sundar, L. S., Farooq, M. H., Sarada, S. N., & Singh, M. K. (2013). Experimental thermal conductivity of ethylene glycol and water mixture based low volume concentration of Al₂O₃ and CuO nanofluids. *International Communications in Heat and Mass Transfer*, *41*, 41-46.
6. Madhesh, D., & Kalaiselvam, S. (2014). Experimental analysis of hybrid nanofluid as a coolant. *Procedia engineering*, *97*, 1667-1675.
7. Madhesh, D., Parameshwaran, R., & Kalaiselvam, S. (2014). Experimental investigation on convective heat transfer and rheological characteristics of Cu–TiO₂ hybrid nanofluids. *Experimental Thermal and Fluid Science*, *52*, 104-115.
8. Falthammar, C. G. (1997). Plasma physics from laboratory to Cosmos-the life and achievements of Hannes Alfvén. *IEEE transactions on plasma science*, *25*(3), 409-414.
9. Ghadikolaei, S. S., Yassari, M., Sadeghi, H., Hosseinzadeh, K., & Ganji, D. D. (2017). Investigation on thermophysical properties of TiO₂–Cu/H₂O hybrid nanofluid transport dependent on shape factor in MHD stagnation point flow. *Powder technology*, *322*, 428-438.

10. Das, S., Jana, R. N., & Makinde, O. D. (2017). MHD flow of Cu-Al₂O₃/water hybrid nanofluid in porous channel: analysis of entropy generation. In *Defect and diffusion forum* (Vol. 377, pp. 42-61). Trans Tech Publications Ltd.
11. Ashorynejad, H. R., & Shahriari, A. (2018). MHD natural convection of hybrid nanofluid in an open wavy cavity. *Results in Physics*, 9, 440-455.
12. Aly, E. H., & Pop, I. (2019). MHD flow and heat transfer over a permeable stretching/shrinking sheet in a hybrid nanofluid with a convective boundary condition. *International Journal of Numerical Methods for Heat & Fluid Flow*, 29(9), 3012-3038.
13. Usman, M., Gul, T., Khan, A., Alsubie, A., & Ullah, M. Z. (2021). Electromagnetic couple stress film flow of hybrid nanofluid over an unsteady rotating disc. *International Communications in Heat and Mass Transfer*, 127, 105562.
14. Martin, J. E. (2006). *Physics for radiation protection: a handbook*. John Wiley & Sons.
15. Mahmoud. M. A. (2007). Thermal radiation effects on MHD flow of a micropolar fluid over a stretching surface with variable thermal conductivity. *Physica A: Statistical Mechanics and its Applications*. 375(2), 401-410.
16. Madhu, M., Kishan, N., & Chamkha. A. J. (2017). Unsteady flow of a Maxwell nanofluid over a stretching surface in the presence of magnetohydrodynamic and thermal radiation effects. *Propulsion and Power research*. 6(1), 31-40.
17. Pandey, K. M., & Chaurasiya, R. (2017). A review on analysis and development of solar flat plate collector. *Renewable and Sustainable Energy Reviews*, 67, 641-650.
18. Chamkha, A. J., Dogonchi, A. S., & Ganji, D. D. (2019). Magneto-hydrodynamic flow and heat transfer of a hybrid nanofluid in a rotating system among two surfaces in the presence of thermal radiation and Joule heating. *AIP Advances*, 9(2), 025103.
19. Shoaib, M., Raja, M. A. Z., Sabir, M. T., Islam, S., Shah, Z., Kumam, P., & Alrabaiah, H. (2020). Numerical investigation for rotating flow of MHD hybrid nanofluid with thermal radiation over a stretching sheet. *Scientific Reports*, 10(1), 18533.
20. Zainal, N. A., Nazar, R., Naganthran, K., & Pop, I. (2021). MHD flow and heat transfer of hybrid nanofluid over a permeable moving surface in the presence of thermal radiation. *International Journal of Numerical Methods for Heat & Fluid Flow*, 31(3), 858-879.
21. Gebhart, B. (1962). Effects of viscous dissipation in natural convection. *Journal of*

- fluid Mechanics*, 14(2), 225-232.
22. Vajravelu, K. & Hadjinicolaou, A. (1993). Heat transfer in a viscous fluid over a stretching sheet with viscous dissipation and internal heat generation. *International Communications in Heat and Mass Transfer*, 20(3), 417-430.
 23. Pandey, A. K., & Kumar, M. (2017). Natural convection and thermal radiation influence on nanofluid flow over a stretching cylinder in a porous medium with viscous dissipation. *Alexandria Engineering Journal*, 56(1), 55-62.
 24. Farooq, U., Afridi, M. I., Qasim, M., & Lu, D. (2018). Transpiration and viscous dissipation effects on entropy generation in hybrid nanofluid flow over a nonlinear radially stretching disk. *Entropy*, 20(9), 668.
 25. Swain, B. K., Parida, B. C., Kar, S., & Senapati, N. (2020). Viscous dissipation and joule heating effect on MHD flow and heat transfer past a stretching sheet embedded in a porous medium. *Heliyon*, 6(10), e05338.
 26. Mallikarjuna, H. B., Nirmala, T., Punith Gowda, R. J., Manghat, R., & Varun Kumar, R. S. (2021). Two-dimensional Darcy–Forchheimer flow of a dusty hybrid nanofluid over a stretching sheet with viscous dissipation. *Heat Transfer*, 50(4), 3934-3947.
 27. Abbas, N., Rehman, K. U., Shatanawi, W., & Malik, M. Y. (2022). Numerical study of heat transfer in hybrid nanofluid flow over permeable nonlinear stretching curved surface with thermal slip. *International Communications in Heat and Mass Transfer*, 135, 106107.
 28. Mishra, A., & Upreti, H. (2022). A comparative study of Ag–MgO/water and Fe₃O₄–CoFe₂O₄/EG–water hybrid nanofluid flow over a curved surface with chemical reaction using Buongiorno model. *Partial Differential Equations in Applied Mathematics*, 5, 100322.
 29. Vinoth, R., Sachuthanathan, B., Vadivel, A., Balakrishnan, S., & Raj, A. G. S. (2023). Heat transfer enhancement in oblique finned curved microchannel using hybrid nanofluid. *International Journal of Thermal Sciences*, 183, 107848.
 30. Alrabaiah, H., Iftikhar, S., Saeed, A., Bilal, M., Eldin, S. M., & Galal, A. M. (2023). Numerical Calculation of Darcy Forchheimer Radiative Hybrid Nanofluid Flow across a Curved Slippery Surface. *South African Journal of Chemical Engineering*.
 31. Mandal, G., & Pal, D. (2023). Estimation of entropy generation and heat transfer of magnetohydrodynamic quadratic radiative Darcy–Forchheimer cross hybrid nanofluid (GO+ Ag/kerosene oil) over a stretching sheet. *Numerical Heat Transfer, Part A: Applications*, 1-24.

32. Reddy, P. S., Sreedevi, P., & Chamkha, A. J. (2023). Hybrid nanofluid heat and mass transfer characteristics over a stretching/shrinking sheet with slip effects. *Journal of Nanofluids*, 12(1), 251-260.
33. Yahaya, R. I., Md Arifin, N., Pop, I., Md Ali, F., & Mohamed Isa, S. S. P. (2023). Dual solutions for MHD hybrid nanofluid stagnation point flow due to a radially shrinking disk with convective boundary condition. *International Journal of Numerical Methods for Heat & Fluid Flow*, 33(2), 456-476.
34. Rasool, G., Wang, X., Yashkun, U., Lund, L. A., & Shahzad, H. (2023). Numerical treatment of hybrid water based nanofluid flow with effect of dissipation and Joule heating over a shrinking surface: Stability analysis. *Journal of Magnetism and Magnetic Materials*, 571, 170587.
35. Lone, S. A., Alyami, M. A., Saeed, A., Dawar, A., Kumam, P., & Kumam, W. (2022). MHD micropolar hybrid nanofluid flow over a flat surface subject to mixed convection and thermal radiation. *Scientific Reports*, 12(1), 17283.
36. Ullah, B., Khan, U., Wahab, H. A., Khan, I., & Alam, M. N. (2022). Entropy generation analysis for MHD flow of hybrid nanofluids over a curved stretching surface with shape effects. *Journal of Nanomaterials*, 2022.
37. Waini, I., Jamaludin, A., Nazar, R., & Pop, I. (2022). MHD flow and heat transfer of a hybrid nanofluid past a nonlinear surface stretching/shrinking with effects of thermal radiation and suction. *Chinese Journal of Physics*, 79, 13-27.
38. Nandi, S., Kumbhakar, B., & Seth, G. S. (2022). Quadratic regression analysis of unsteady MHD free convective and radiative–dissipative stagnation flow of hybrid nanofluid over an exponentially stretching surface under porous medium. *Chinese Journal of Physics*, 77, 2090-2105.
39. Sakkaravarthi, K., & Reddy, P. B. A. (2023). Entropy optimization of MHD hybrid nanofluid flow through a curved stretching sheet with thermal radiation and heat generation: semi-analytical and numerical simulations. *Proceedings of the Institution of Mechanical Engineers, Part E: Journal of Process Mechanical Engineering*, 237(2), 138-148.
40. Qureshi, M. A. (2023). Irreversibility analysis of electromagnetic hybrid nanofluid for Cattaneo–Christov heat flux model using finite element approach. *Scientific Reports*, 13(1), 4288.
41. Patel, V. K., Pandya, J. U., & Patel, M. R. (2023). Testing the influence of TiO₂–Ag/water on hybrid nanofluid MHD flow with effect of radiation and slip conditions

- over exponentially stretching & shrinking sheets. *Journal of Magnetism and Magnetic Materials*, 572, 170591.
42. Dawar, A., Islam, S., Shah, Z., & Mahmud, S. R. (2023). A passive control of Casson hybrid nanofluid flow over a curved surface with alumina and copper nanomaterials: A study on sodium alginate-based fluid. *Journal of Molecular Liquids*, 382, 122018.
 43. Alqahtani, A. M., Bilal, M., Ali, A., Alsenani, T. R., & Eldin, S. M. (2023). Numerical solution of an electrically conducting spinning flow of hybrid nanofluid comprised of silver and gold nanoparticles across two parallel surfaces. *Scientific Reports*, 13(1), 7180.
 44. Ouri, H., Selimefendigil, F., Bouterrea, M., Omri, M., Alshammari, B. M., & Kolsi, L. (2023). MHD hybrid nanofluid convection and phase change process in an L-shaped vented cavity equipped with an inner rotating cylinder and PCM-packed bed system. *Alexandria Engineering Journal*, 63, 563-582.
 45. Mathews, Joel, & T. Hymavathi. "Magnetohydrodynamic stagnation point flow and heat transfer effects of Al₂O₃-Cu/water hybrid nanofluid over a porous stretching surface." *Proceedings of the Institution of Mechanical Engineers, Part E: Journal of Process Mechanical Engineering* 237.3 (2023): 1064-1072.
 46. Rafique, K., Mahmood, Z., & Khan, U. (2023). Mathematical analysis of MHD hybrid nanofluid flow with variable viscosity and slip conditions over a stretching surface. *Materials Today Communications*, 36, 106692.
 47. Abbasi, A., Gul, M., Farooq, W., Khan, S. U., Aydi, A., Ayadi, B., Eladeb, A., & Kolsi, L. (2022). A comparative thermal investigation for modified hybrid nanofluid model (Al₂O₃-SiO₂-TiO₂)/(C₂H₆O₂) due to curved radiated surface. *Case Studies in Thermal Engineering*, 37, 102295
 48. Alqahtani, A. M., Ould Sidi, M., Khan, M. R., Elkotb, M. A., Tag-Eldin, E., & Galal, A. M. (2022). Transport properties of two-dimensional dissipative flow of hybrid nanofluid with Joule heating and thermal radiation. *Scientific Reports*, 12(1), 19374.
 49. Sulochana, C., & Prasanna Kumar, T. (2022). Electromagnetohydrodynamic boundary layer flow in hybrid nanofluid with thermal radiation effect: Numerical simulation. *Heat Transfer*, 51(5), 4485-4503.
 50. Imran, M., Naveed, M., Iftikhar, B., & Abbas, Z. (2023). Heat transfer analysis in a curvilinear flow of hybrid nanofluid across a curved oscillatory stretched surface with nonlinear thermal radiation. *ZAMM-Journal of Applied Mathematics and*

Mechanics/Zeitschrift für Angewandte Mathematik und Mechanik, e202200600.

51. Kho. Y. B., Jusoh. R., Salleh. M. Z., Ariff, M. H., & Zainuddin, N. (2023). Magnetohydrodynamics flow of Ag-TiO₂ hybrid nanofluid over a permeable wedge with thermal radiation and viscous dissipation. *Journal of Magnetism and Magnetic Materials*. 565, 170284.
52. Aminuddin, N. A., Nasir, N. A. A. M., Jamshed, W., Ishak, A., Pop, I., & Eid, M. R. (2023). Impact of Thermal Radiation on MHD GO-Fe₂O₄/EG Flow and Heat Transfer over a Moving Surface. *Symmetry*, 15(3), 584.
53. Vijay, N., & Sharma, K. (2023). Entropy generation analysis in MHD hybrid nanofluid flow: Effect of thermal radiation and chemical reaction. *Numerical Heat Transfer, Part B: Fundamentals*, 1-17.
54. Farooq, U., Waqas, H., Noreen, S., Imran, M., Akgül, A., Baleanu, D., El Din, S.M., Muhammad, T., & Galal, A. M. (2023). Numerical framework of hybrid nanofluid over two horizontal parallel plates with non-linear thermal radiation. *International Journal of Thermofluids*, 18, 100346
55. Rashad, A. M., Nafe, M. A., & Eisa, D. A. (2023). Heat generation and thermal radiation impacts on flow of magnetic Eyring–Powell hybrid nanofluid in a porous medium. *Arabian Journal for Science and Engineering*, 48(1), 939-952.
56. Saupi, S., Abd Ghani, A., Arifin, N. M., Rosali, H., & Wahid, N. S. (2023). An Exact Solution of MHD Hybrid Nanofluid over a Stretching Surface Embedded in Porous Medium in the Presence of Thermal Radiation and Slip with Suction. *CFD Letters*, 15(5), 74-85.
57. Veeram, G., Poojitha, P., Katta, H., Hemalatha, S., Babu, M. J., Raju, C. S., Shah, N.A., & Yook, S. J. (2022). Simulation of dissipative hybrid nanofluid (PEG-Water+ ZrO₂+ MgO) flow by a curved shrinking sheet with thermal radiation and higher order chemical reaction. *Mathematics*, 10(10), 1706.
58. Alshehri, A., & Shah, Z. (2022). Computational analysis of viscous dissipation and Darcy-Forchheimer porous medium on radioactive hybrid nanofluid. *Case Studies in Thermal Engineering*, 30, 101728.
59. Khan, U., Adnan, & Haleema, B. (2022). Thermal performance in nanofluid and hybrid nanofluid under the influence of mixed convection and viscous dissipation: numerical investigation. *Waves in Random and Complex Media*, 1-19

60. Ul Haq, S., Bilal Ashraf, M., & Nawaz, R. (2023). Nonsimilar solution of hybrid nanofluid over curved stretching surface with viscous dissipation: A numerical study. *Numerical Heat Transfer, Part A: Applications*, 1-20.
61. Lund, L. A., Yashkun, U., & Shah, N. A. (2023). Magnetohydrodynamics streamwise and cross flow of hybrid nanofluid along the viscous dissipation effect: Duality and stability. *Physics of Fluids*, 35(2).
62. Mahesh, R., Mahabaleshwar, U. S., Kumar, P. V., Öztop, H. F., & Abu-Hamdeh, N. (2023). Impact of radiation on the MHD couple stress hybrid nanofluid flow over a porous sheet with viscous dissipation. *Results in Engineering*, 17, 100905.
63. Hayat, T., Yazman, M., Muhammad, K., & Momani, S. (2023). Radiative and dissipative flow of hybrid nanofluid between two coaxial cylinders: A comparative numerical study. *Alexandria Engineering Journal*, 71, 79-88.
64. Yang, H., Hayat, U., Shaiq, S., Shahzad, A., Abbas, T., Naeem, M., Khan, S.U., Labidi, T., Kolsi, L., & Zahid, M. A. (2023). Thermal inspection for viscous dissipation slip flow of hybrid nanofluid (TiO₂-Al₂O₃/C₂H₆O₂) using cylinder, platelet and blade shape features. *Scientific Reports*, 13(1), 8316.
65. Jamaludin, A., Nasir, N. A. A. M., Nazar, R., & Pop, I. (2023). MHD opposing flow of Cu- TiO₂ hybrid nanofluid under an exponentially stretching/shrinking surface embedded in porous media with heat source and slip impacts. *Results in Engineering*, 17, 101005.
66. Ghazwani, H. A. (2023). Time-dependent mixed stagnation point hybrid nanofluid flow with radiative heat flux and viscous dissipation effects over a movable EMHD Riga plate. *International Journal of Modern Physics B*, 2450090.
67. R. Bansal, A Textbook of Fluid Mechanics and Hydraulic Machines. Laxmi Publications, 2004.
68. F. M. White and I. Coreld, Viscous Fluid Flow (McGraw-Hill Mechanical Engineering). McGraw-Hill New York, 2006.
69. J. Kunes, Dimensionless Physical Quantities in Science and Engineering. Elsevier, 2012.
70. Huilgol, R. R., & Kefayati, G. H. R. (2018). A particle distribution function approach to the equations of continuum mechanics in Cartesian, cylindrical and spherical coordinates: Newtonian and non-Newtonian fluids. *Journal of Non-Newtonian Fluid Mechanics*, 251, 119-131.

71. Keskin, A. Ü., & Keskin, A. Ü. (2019). Solution of BVPs using bvp4c and bvp5c of MATLAB. *Boundary Value Problems for Engineers: with MATLAB Solutions*, 417-510.
72. Sajid, M., Ali, N., Javed, T., & Abbas, Z. (2010). Stretching a curved surface in a viscous fluid. *Chinese Physics Letters*, 27(2), 024703.
73. Balla, H. H., Abdullah, S., MohdFaizal, W., Zulkifli, R., & Sopian, K. (2013). Numerical study of the enhancement of heat transfer for hybrid CuO-Cu nanofluids flowing in a circular pipe. *Journal of oleo science*, 62(7), 533-539.
74. Waini, I., Ishak, A., & Pop, I. (2019). Hybrid nanofluid flow and heat transfer over a nonlinear permeable stretching/shrinking surface. *International Journal of Numerical Methods for Heat & Fluid Flow*, 29(9), 3110-3127.
75. Ahmed, N., Saba, F., Khan, U., Mohyud-Din, S. T., Sherif, E. S. M., & Khan, I. (2019). Nonlinear thermal radiation and chemical reaction effects on a (Cu-CuO)/NaAlg hybrid nanofluid flow past a stretching curved surface. *Processes*, 7(12), 962.
76. Hassan, M., Marin, M., Ellahi, R., & Alamri, S. Z. (2018). Exploration of convective heat transfer and flow characteristics synthesis by Cu-Ag/water hybrid-nanofluids. *Heat Transfers*. 49(18):1837-48.
77. Ghadikolaie, S. S., Hosseinzadeh, K., & Ganji, D. D. (2018). Investigation on three dimensional squeezing flow of mixture base fluid (ethylene glycol-water) suspended by hybrid nanoparticle (Fe₃O₄-Ag) dependent on shape factor. *Journal of Molecular Liquids*. 262, 376-388.
78. Zari, I., Ali, F., Khan, T. S., & Shafiq, A. (2022). Radiative Hiemenz flow towards a stretching Riga plate in hybrid nanofluid. *International Communications in Heat and Mass Transfer*, 139, 106492.
79. Timofeeva, E. V., Routbort, J. L., & Singh, D. (2009). Particle shape effects on thermophysical properties of alumina nanofluids. *Journal of applied physics*, 106(1).
80. Iqbal, Z., Maraj, E. N., Azhar, E., & Mehmood, Z. (2017). A novel development of hybrid (MoS₂- SiO₂/H₂O) nanofluidic curvilinear transport and consequences for effectiveness of shape factors. *Journal of the Taiwan Institute of Chemical Engineers*, 81, 150-158.
81. Hayat, T., Haider, F., Muhammad, T., & Alsaedi, A. (2019). Numerical treatment for Darcy-Forchheimer flow of carbon nanotubes due to an exponentially stretching curved surface. *Journal of Central South University*, 26(4), 865-872.

82. Ullah, B., Fadhl, B. M., Makhdoum, B. M., Nisar, K. S., Wahab, H. A., & Khan, U. (2022). Heat transfer analysis in Darcy Forchheimer flow of hybrid nanofluid for multiple shape effects over a curved stretching surface. *Case Studies in Thermal Engineering*, 40, 102538.